Nano Energy 113 (2023) 108606

Contents lists available at ScienceDirect

Nano Energy

journal homepage: www.elsevier.com/locate/nanoen

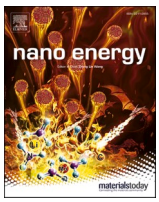

Review

Recent progress in piezotronic sensors based on one-dimensional zinc oxide nanostructures and its regularly ordered arrays: From design to application

Ramesh Ghosh

James Watt School of Engineering, University of Glasgow, Glasgow G12 8QQ, United Kingdom

ARTICLE INFO

Keywords:
Zinc oxide
One-dimensional
Controlled array
Heterostructure
Piezotronics devices
Healthcare devices

ABSTRACT

Piezotronic sensors and self-powered gadgets are highly sought-after for flexible, wearable, and intelligent electronics for their applications in cutting-edge healthcare and human-machine interfaces. With the advantages of a well-known piezoelectric effect, excellent mechanical properties, and emerging nanotechnology applications, one-dimensional (1D) ZnO nanostructures organized in the form of a regular array have been regarded as one of the most promising inorganic active materials for piezotronics. This report intends to review the recent developments of 1D ZnO nanostructure arrays for multifunctional piezotronic sensors. Prior to discussing rational design and fabrication approaches for piezotronic devices in precisely controlled dimensions, well-established synthesis methods for high-quality and well-controlled 1D ZnO nanostructures are addressed. The challenges associated with the well-aligned, site-specific synthesis of 1D ZnO nanostructures, development trends of piezotronic devices, advantages of an ordered array of 1D ZnO in device performances, exploring new sensing mechanisms, incorporating new functionalities by constructing heterostructures, the development of novel flexible device integration technology, the deployment of novel synergistic strategies in piezotronic device performances, and potential multifunctional applications are covered. A brief evaluation of the end products, such as small-scale miniaturized unconventional power sources in sensors, high-resolution image sensors, and personalized healthcare medical devices, is also included. The paper is summarized towards the conclusion by outlining the present difficulties and promising future directions. This study will provide guidance for future research directions in 1D ZnO nanostructure-based piezotronics, which will hasten the development of multi-functional devices, sensors, chips for human-machine interfaces, displays, and self-powered systems.

1. Introduction

Modern healthcare electronics are rapidly deploying for continuous remote monitoring of human health, diagnosis of its abnormal conditions, wellness, invasive medical procedures, and more [1–9]. With the advancement of novel sensing technologies, wearable and portable sensors are gaining significant research focus in an effort to bring healthcare into the house by creating intelligent systems that effectively measure physiological health parameters [1,10–19]. Piezotronics provide a promising approach for designing future electronic devices beyond Moore's law with the potential for developing smart sensors, systems for monitoring the physical health as well as the surrounding environment, components for human-machine interfaces, and other transducers [20–27]. The near-future developments of piezotronics are going to be one of the powerful attentions for the industries as it integrates multipurpose sensors with self-powering technology [28–36]. Piezoelectric harvesting is significantly strengthening alternative energy ways to meet the increasing energy demands of the world, as it can power up small-scale, low-powered devices [37–48]. The modern development in flexible electronics, mechanics, material science, and manufacturing engineering allows the production of piezotronic devices in precise dimensions. Significant progress has been made in the study of piezoelectric materials [49–55], their numerous nanostructures [56–61], piezotronic devices and their ongoing trends [62–71], performance improvement strategies [72–79], hybridization tactics [80–88] to provide synergy [89–94], multi-directionality [95,96], flexible and wearable platforms [97–100], etc. With the advantages of enhanced piezoelectric effect, excellent mechanical properties, and emerging nanotechnology applications, one-dimensional (1D) ZnO nanostructures have been considered as the most promising inorganic piezoelectric nanomaterial [101–105]. Therefore, enormous attention is required in 1D ZnO nanostructures by considering (a) rational design and material engineering, (b) miniaturization of various functional devices, (c) their high specific surface area, (d) easier integration of multifunctionality,

E-mail address: Ramesh.Ghosh@glasgow.ac.uk.

https://doi.org/10.1016/j.nanoen.2023.108606
Received 17 April 2023; Received in revised form 22 May 2023; Accepted 11 June 2023
Available online 15 June 2023

(e) interfacing with flexible, portable and stretchable surfaces, (f) improvement strategies for device performances, (g) reproducible and reliable performance in a long-term basis, and (h) day-to-day nanotechnology applications. This will make them superior building blocks for future piezotronic devices, especially in the field of smart sensing, advanced medical science, portable and wearable personal electronics, and self-powered systems. The existing technology for piezotronic devices, particularly in the case of sensors is mainly focused on the most traditional large-area film and randomly oriented 1D nanostructures of ZnO. This limits the practical application of these sensors because of the difficulties in miniaturization, regular arraying, reproducibility, and reliability in performance.

Integrated systems are anticipated to provide qualitative and quantitative gains in properties by combining physical or chemical attributes that depend on components, size, spacing, and higher-order structure [106]. By incorporating innovative materials with additional functionalities and complexities in a heterostructure (HS) approach, one can modify or enhance the piezoelectric capabilities of the 1D wurtzite materials to meet specific requirements as well as to extend the direction of potential applications [28,66,107–115]. On the other hand, regularly ordered arrays of vertically aligned 1D semiconductor nanostructures have the potential to function as a strong building block for the realization of all-dielectric metamaterials, artificial electromagnetic materials, and piezoelectric materials, whose properties can be tailored to enable novel functions and improved performances in associated devices compared to isolated or randomly organized materials [10,57,116–124]. Therefore, with the advancement in nanofabrication and synthesis techniques, precisely designed and controlled arrays of 1D ZnO nanostructures including their different kinds of HSs are taking enormous research attention nowadays for the fabrication of small and accurate piezotronic devices [125–130]. The regular arrays of controlled 1D nanostructures of ZnO and its HSs are expected to lead the direction of piezotronics toward the rapid development of multifunctional devices, sensors, human-machine interfacing chips, displays, and self-powered systems [68,131–138].

Over the years, a lot of progress has been well-documented on piezotronic devices, particularly in the context of sensors that focus on material synthesis [28,37,65,139,140], integration of materials [66,141,142], piezoelectric properties and its improvement strategies [37,65,95], the design and fabrication approaches [1,37,66,139], their operating principles [23,27,69,95,139], and extensive multifunctional applications [1,39,139,143–145]. Z. L. Wang and co-workers have documented several reviews articles on the research progress of piezotronics and piezo-phototronics by considering the piezoelectric materials [23,30,139,142], mechanism of piezotronics and piezo-phototronics [27,68,69,139], piezotronic devices and device engineering techniques [66,69,95,139], piezoelectric energy harvesting and self-powering technologies [142,144,146], integration strategies of different directions of science [40,69,121,137,139,142], commercial viabilities of devices, and various nanotechnology applications including sensors, displays, light-emitting diodes (LEDs), healthcare devices, wearable electronics, robotics, internet of things (IoT), and many more [30,33,64,70,87]. Recently, a comprehensive review of the piezoelectric nanogenerators (PNGs) for personalized healthcare was presented by W. Deng et al [1]. In this review, a brief overview of the fundamental physical science underlying the piezoelectric effect was presented which was followed by a systematic discussion of material engineering techniques, device structural layouts, and applications for energy harvesting, sensing, and therapies that focus on the human body. Inorganic materials-based piezotronic sensors have been the subject of a few review papers, which are primarily dedicated to various kinds of nanomaterials in different forms of nanostructures, and their individual effects on piezotronics [23,28,69,105,139,143,146]. K. Gupta et al. reviewed the progress in nano/microstructure development of inorganic 1D nanostructures for piezotronics and PNGs [28]. In case of ZnO nanomaterials, reported review articles are restricted within the most conventional large-area film, individually collected nanowires (NWs), NW films, and randomly oriented 1D nanostructure arrays [28,37,103,121,143,146,147]. R. Yu et al. reviewed Schottky-structured NW sensors for the utilization of piezotronic effect in optical, gas, chemical, and biological sensors [95]. The impact of the crystal polarity of ZnO NWs on the performance of piezotronic and piezoelectric devices, as well as the methods to improve their performances, was reviewed by V. Consonni et al [65]. Y. Zhang et al. reviewed the progress made in ZnO NW arrays in using the piezo-phototronic effect for enhancing photodetectors, pressure sensors, light-emitting diodes, and solar cells [121]. The development of hydrothermally grown ZnO nanorods (NRs) as piezoelectric building blocks for low cost, large area electronic skin has been reviewed by A. F. Morgera et al [140]. With a focus towards potential future breakthroughs in the field, they discussed how the growth parameters influence the morphological aspect of the fabricated NRs and how effective pressure/force sensors can be constructed employing so-grown ZnO NRs on various substrates. Using third-generation semiconductor NWs such as ZnO and GaN, C. Pan et al. presented an extensive review of piezotronics and piezo-phototronics [139]. They went over in depth for a comprehensive review on the synthesis of NWs, from randomly organized NW arrays to well-ordered, controlled NW arrays, as well as the designing of piezotronic and piezo-phototronic devices, their fundamental principles of operation, the engineering of various types of device interfaces, and the wide range of applications for these devices ranging from various types of sensors to other photonic and electronic devices. More recently, Y. Wang et al. contributed a review article to the ZnO NW-based piezotronics and piezo-phototronics where they addressed the preparation procedures and structural features of ZnO NWs with various doping types [143]. Theoretical aspects of the piezotronic effect were also covered, as well as its applications in the fields of sensors, biochemistry, energy harvesting, and logic operations. Furthermore, a summary and analysis of the piezo-phototronic effect's impact on photodetectors, solar cells, and LED performances were also provided. There has been rarely found a systematic review in the recent time on the piezotronic devices, particularly sensors and sensor arrays based on well-organized, regularly ordered arrays of 1D ZnO nanostructures. Therefore, a thorough study of the transition of 1D ZnO nanostructures from individually collected and randomly oriented nanostructure arrays to well-organized structures in piezotronics will be quite fascinating. Future research will need to be much more concentrated on a systematic study of the synthesis techniques for high-quality and well-controlled 1D ZnO nanostructures in various forms, as well as the rational design and fabrication techniques for the associated piezotronic devices in precisely controlled dimensions, which are lacking in the earlier published review articles. Beyond ZnO NWs, there has been a lot of progress on various other forms of 1D ZnO nanostructures such as nanotubes (NTs) [125,131,148–151], nanocones/nanoneedles (NNs) [28,152–155], nanobelts (NBs) [156], etc. Therefore, it is also necessary to review how these distinct nanostructures are utilized successfully in various fields of piezoelectrics and piezotronics. From the perspective of applications, a prompt systematic reorganization of the effect of each parameter that significantly influences the piezoelectric properties of well-organized 1D ZnO arrays as well as the associated piezoelectric and piezotronic devices will be a key requirement. The multifunctionalities of devices, the strategies for enhancing device performance, interface engineering, addressing the challenges associated with it, coupling of mechano-electric and optoelectronic properties, and integration strategies for flexible and wearable applications are the additional key factors to take into account. Theoretically and technically, a timely detailed review focused on piezotronics of 1D ZnO nanostructures and their well-organized arrays will be beneficial for forthcoming high-performance piezotronic sensor research, development, and applications.

This paper aims to review the recent developments of 1D ZnO nanostructure arrays for their implementation in multifunctional piezotronic sensors. The report covers the important aspects of 1D ZnO

nanostructures, including their organization in a regular array for considering them as one of the most suitable active components for a multifunctional piezotronic sensor. The evolution of 1D ZnO nanostructures from individually collected and randomly oriented nanostructure arrays to well-organized, uniformly patterned structures are presented for their application in different areas of piezotronics and the associated details are provided as unified discussion as well as in tabulated form. Well-established synthesis methods for high-quality, controllable 1D ZnO nanostructures, rational design, HS strategies, coupling of mechano-electric properties, fabrication of piezotronic devices, and their integration with a flexible substrate/supported matrix for flexible and wearable applications are discussed. By comparing the benefits of well-controlled, individually patterned 1D ZnO nanostructures or patterned bundles over its large-area thinfilm, randomly organized array of 1D ZnO nanostructures, and continuous NW films, a brief review of the device performances, their improvement strategies, and practical applications of the manufactured piezotronic sensors is provided. Miniaturized small-scale unconventional power sources, high-resolution image sensors, and personalized healthcare devices are the end products, which are reviewed briefly. In the end, a summary of the paper is discussed by mentioning the current challenges and future perspectives lying in this field.

1.1. Piezoelectrics and piezotronics

The word "piezoelectric" comes from the Greek word "piezein", which means "to press". Piezoelectricity or literally, "pressing electricity" is the generation of static charges in response to applied mechanical stress on certain kinds of materials. The piezoelectric effect was first discovered by Pierre and Paul-Jacques Curie in 1880. In contrast with the piezoresistance effect, the piezoelectric effect is observed in a crystal having non-central symmetry [20]. The piezoelectric effect is inorganic materials likely limited to the wurtzite family such as ZnO, gallium nitride (GaN), indium nitride (InN), aluminum nitride (AlN), cadmium sulfide (CdS), and zinc sulfide (ZnS) [145,157–162]. Typically, a wurtzite ZnO has a hexagonal structure in which the Zn^{2+} cation is surrounded by four O^{2-} anions and vice versa. This tetrahedral atomic arrangement causes a non-centrosymmetric structure in ZnO crystal. In absence of any mechanical stress, there is no net polarization as centers of mass of the positive and negative ions coincide at the center of the tetrahedron as depicted in Fig. 1(a) [163]. When mechanical stress is applied along the c-axis of the crystal, the centers of mass of the cations and anions are relatively displaced. In this case, the unit cell exhibits a net polarization, indicating the presence of dipole moments inside the crystal. As a result, the crystal exhibits the piezopotential along the direction of the polarization [28]. The distribution of piezopotential has been determined when a ZnO NW is compressed as well as stretched, as displayed in Fig. 1(b) [163]. When a 1D ZnO is bent by some mechanical pressure, the pressure-induced charges are separated along the lateral dimension indicating the formation of a depletion zone as shown in Fig. 1(c) for ZnO NW [131,148,164,165]. Note that the piezoelectric charges in 1D ZnO nanostructures are situated at the ends of the nanostructure, directly influencing the local contacts and the opposite being true (Fig. 1(b)). As a result, contact formation in 1D ZnO-based piezoelectric devices is very crucial. The schematic representation of ZnO NT where gold (Au) was utilized as a contact material, is shown in Fig. 1(d) in both normal (left) and bending (right) conditions. The stress-induced carriers, their relative motion, and the development of the depletion zone are shown in an expanded cross-sectional image of the selected region of the bent ZnO NT. Fig. 1(e, f) shows the energy band diagram for illustrating the effect of piezoelectricity on a Schottky junction [148], while (g, h) is demonstrating the effect of piezoelectricity on a p-n junction [163]. Fig. 1(g) depicts the band diagram at a conventional p-n junction formed by two semiconductors with almost identical bandgaps, whereas Fig. 1(h) shows the band diagram of the p-n junction with the presence of a piezopotential at the p-type side with a polarity of greater potential nearby the junction side [163]. The 1D, vertically aligned ZnO nanostructure-based piezoelectric devices are usually constructed by utilizing the Schottky junction formed between high work-function metal and ZnO. When an external

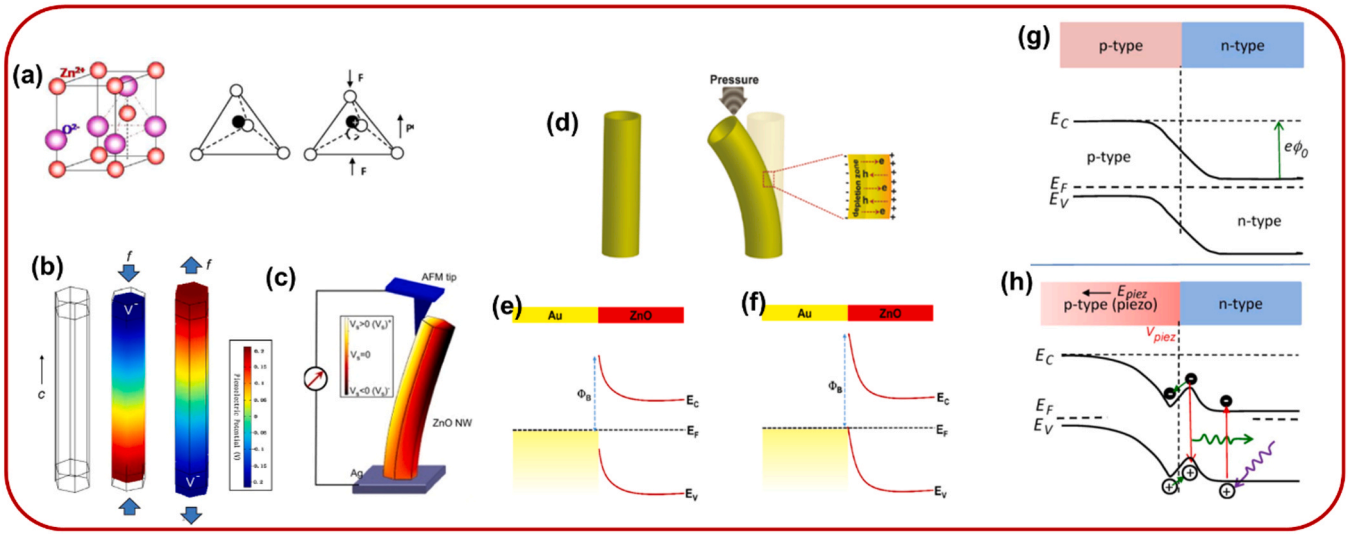

Fig. 1. The structure and band alignment of 1D ZnO in the light of its piezoelectric properties. (a) Schematic illustration of the atomic model of a wurtzite structured ZnO. (b) Numerical calculation of the piezoelectric potential distribution in a ZnO NW under axial strain. Reproduced with permission [163]. Copyright 2010, Elsevier. (c) A numerical calculation of the piezoelectric potential distribution caused by bending in a ZnO NW. Reproduced with permission [164]. Copyright 2012, Elsevier. (d) Schematic representation of a ZnO NT in normal (left) and bent (middle). Right one in the enlarged cross-sectional view of the selective portion of the bent ZnO NT. The formation of stress-induced carriers, their relative motion, and the formation of depletion zone are shown schematically. Reproduced with permission [131]. Copyright 2021, Springer Nature. (e–f) Energy band diagram for illustrating the effect of piezoelectricity on a Schottky junction. Band diagrams at the interface of Au and ZnO in (e) normal, and (f) bent condition. Reproduced with permission [148]. Copyright 2022, Springer Nature. (g–h) Energy band diagram for illustrating the effect of piezoelectricity on a p-n junction. (g) Band diagram at a conventional p-n junction made by two semiconductors with nearly identical bandgap bandgaps. (h) Band diagram of the p-n junction with the presence of a piezopotential at the p-type side with a polarity of higher potential at the junction side. Reproduced with permission [163]. Copyright 2010, Elsevier.

force is applied to the ZnO in this situation, Schottky barrier height (SBH) is built. A positive piezopotential caused by tensile strain at the semiconductor side effectively reduces the SBH, while a negative piezopotential caused by compressive strain increases the local SBH. Therefore, the design parameters influencing the device's performance have a significant impact on the production of piezoelectric devices.

Z. L. Wang and co-workers introduced the concept of piezotronics for the first time during 2006–2007 [20,166–169]. It deals with the coupling of piezoelectric and semiconducting properties of materials. In piezotronics, external mechanical stimuli induce piezopotential in a piezoelectric semiconductor material, and the induced piezopotential further regulates the carrier transport by modifying the effective barrier height at the interface. A simple piezotronic device composed of a 1D piezoelectric nanomaterial is more likely a kind of transistor which differs from the conventional one as the conventional gate is replaced by the deformation induced piezopotential generated inside the piezoelectric semiconducting crystal (inner potential). The fundamental working principle for piezotronic p–n junction and Schottky diode is the generation of deformation-induced piezopotential which effectively controls the width of p–n junction and the height of Schottky barrier. Over the past 15 years, a number of electronic devices have been demonstrated based on piezotronic effects, including pressure/strain/force sensors [72,73,170], smart healthcare devices [1,29,49,171], tactile sensors [10,118,172], image sensors [68,128,173], piezopotential-gated field-effect transistors [69,163,174,175], bio-chemical sensors [21,176,177], gas sensors [95,176], etc. Piezotronics is now classified as a new direction in semiconductor technology as piezotronic devices have promising potentiality for applications in nondestructive medical equipment, touch screens, human-machine interfaces, micro-electro-mechanical systems, nanorobotics, and active flexible electronics [20,23,25,64,69,70,87,139].

1.2. Why ZnO?

Inorganic materials, polymers, and bio-piezoelectric materials are the three primary groups of materials that exhibit piezoelectric effects based on their material composition and structure. Inorganic piezoelectric materials, particularly those with wurtzite families like ZnO, GaN, InN, AlN, CdS and ZnS, have gained enormous attention due to their outstanding properties [145,157–162]. These are (a) long-term stability, (a) superior mechanical quality factor, (c) compatibility with Si-based electronics, and (d) multifunctionality of devices. Furthermore, these environment-friendly materials are advantageous over the lead-based piezoelectric materials. These materials are widely used as a sensing platform for artificial intelligence and medical devices by coupling piezoelectricity with photonics and electronics [20,126–128,133,136]. ZnO has become the most widely used material system in piezotronics in recent years among the known systems of piezoelectric materials. This is particularly true of its 1D nanostructures, which are thought to be highly favorable for piezoelectric devices. Here are the following reasons: (a) higher piezoelectric constants as compared to the other inorganic wurtzite materials;[104] (b) various high-quality and uniaxially oriented variants of ZnO nanostructures with multi-dimensions, including various 1D structures such as NWs, NRs, NBs, NTs, and NNs, etc.; (c) economic growth on crystalline or amorphous substrates those are hard or flexible and compatible with technologically vital materials such as Si or polymers; (d) biologically compatible and environmental-friendly materials; (e) ability to easily tune the optoelectronic properties through doping, surface modification, and the creation of HSs with suitable nanomaterials; (f) ability to easily achieve synergistic effects in device performances by integrating different semiconductor and photonic properties with bare piezoelectric devices; and (g) multi-functionality in device characteristics.

A specific material with a specific structure, however, is unable to satisfy the demand for multiple functionality and performance types. In case of piezotronic sensors, the actual selection of the materials and their appropriate structure is challenging to balance the sensitivity, linearity, working range, multi-functionality, cost-effective fabrication, long-term stability, and commercial viability. The performance characteristics of the piezotronic sensor and the requirements of the application scenario may be utilized to design various nano/microstructures, enabling the best nanomaterials to be chosen.

1.3. Why 1D?

Because of the following factors, ZnO nanostructures in 1D form like NWs, NRs, NTs, and NBs are regarded as the ideal candidates for piezotronics.

- In comparison to their thin film or bulk equivalents, 1D nanostructures are advantageous because they allow for a variety of deformations, including stretching, compression, bending, twisting, etc., at the nanoscale level. Various kinds of deformations in 1D ZnO nanostructure are schematically shown in Fig. 2 (schematics in the inner circle). Both finite element modeling (FEM) and experiments demonstrated that piezoelectric 1D architectures generate stronger piezoelectric potential than planar films [10,178].
- 1D nanostructures offer a higher degree of bending and hence strain under the same external force as compared to its other form of structures. Consequently, it displays a larger piezoelectric coefficient [65,179,180].
- 1D ZnO nanostructures provide an effective strain relaxation from the lateral surfaces [65,181]. The piezopotential can be significantly increased compared to that of a ZnO thin film because surface Fermi level pinning was supposed to be pinned on all 1D ZnO interfaces. Based on arrays of vertical ZnO NWs, the piezopotential created by a piezoelectric PNG was found to be up to nine times greater than that produced by the thin film [182].
- The preferential axis of ZnO growth is the c-axis, which is usually the longitudinal direction of a 1D ZnO [139]. Due to the asymmetric structure, 1D ZnO exhibit strong spontaneous polarization along their longitudinal direction [139]. A strong piezopotential is generated in the direction of the polarization when mechanical stress is applied along the c-axis [28,105]. This provides great simplification and convenience for subsequent development of integrated devices/systems and avoids the challenging and elusive predetermination of the c-axis orientation for 1D ZnO nanostructures [25].
- For closed-packed integration of device arrays for practical applications, 1D nanostructures comprise a very small area. (Ideal for high-resolution tactile imaging)
- Fabricated sensors exhibit better sensitivity as well as a wide range of pressure/force/strain detection [139].
- The large surface area offers opportunities for the creation of various kinds of HSs and the integration of different emerging areas of nanotechnology.
- 1D nanostructures offer a variety of morphologies by integrating different other forms of nanomaterials [183]. Similar to HS approach, the rational design of geometrical structures and homojunctions of 1D ZnO are crucial to the functionality of piezotronic devices, particularly sensors.
- There are numerous well-established methods to fabricate high-quality, c-axis oriented, and well-controlled 1D piezoelectric nanostructures.
- 1D nanostructures incorporated into polymers are preferable for flexible and stretchable electronics because they can resist material delamination and/or cracking in the presence of high mechanical strain [183–185]. Additionally, it has been demonstrated that 1D nanostructures successfully reduce the percolation threshold of conductive fillers [183,186].

Different aspects of ZnO in 1D form are summarized in Fig. 2, which make this material as a superior active component of piezotronic

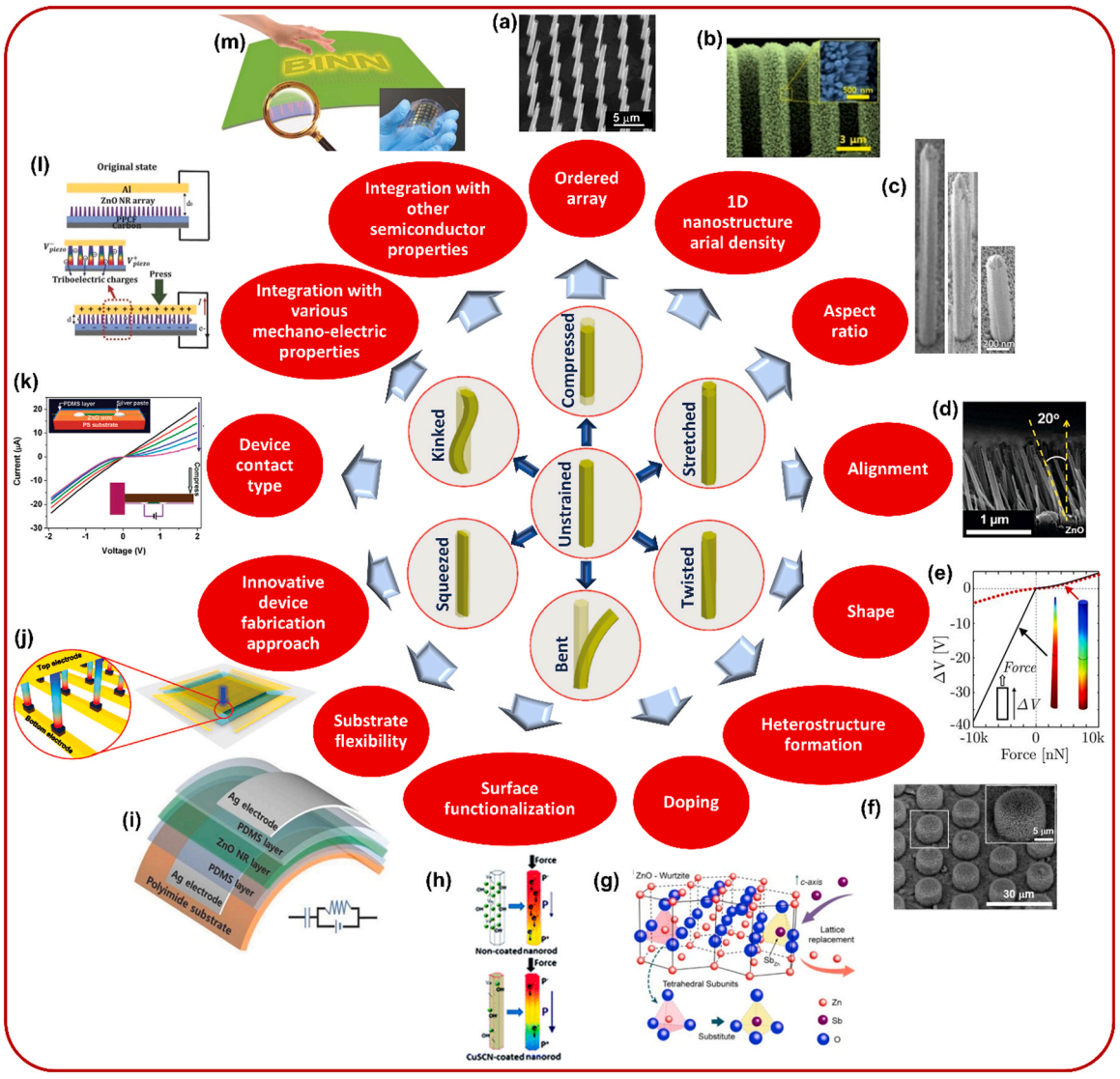

Fig. 2. Various kinds of deformations of 1D ZnO nanostructure (schematics in the inner circle). Different aspects of ZnO in 1D form (outer circle), which make this material as a superior active component of piezotronic devices. (a) Reproduced with permission [148]. Copyright 2022, Springer Nature. (b) Reproduced with permission [211]. Copyright 2015, American Chemical Society. (c) Reproduced with permission [131]. Copyright 2021, Springer Nature. (d) Reproduced with permission [238]. Copyright 2011, American Chemical Society. (e) Reproduced with permission [152]. Copyright 2012, Wiley-VCH GmbH. (f) Reproduced with permission [191]. Copyright 2015, Wiley-VCH GmbH. (g) Reproduced with permission [247]. Copyright 2020, Elsevier. (h) Reproduced with permission [212]. Copyright 2014, Royal Society of Chemistry. (i) Reproduced with permission [408]. Copyright 2017, Wiley-VCH GmbH. (j) Reproduced with permission [118]. Copyright 2013, American Association for the Advancement of Science. (k) Reproduced with permission [264]. Copyright 2008, American Chemical Society. (l) Reproduced with permission [91]. Copyright 2016, Wiley-VCH GmbH. (m) Reproduced with permission [135]. Copyright 2015, Wiley-VCH GmbH.

devices. However, high aspect-ratio 1D nanomaterials have some drawbacks that prevent them from being widely used in piezotronics. For instance, it is extremely difficult to prevent a severe buckling effect in 1D nanostructures with large aspect ratios [64,69,172,187]. The output characteristics of the piezotronic devices may also be severely compromised by this effect, as it significantly decreases the piezoelectric properties by adding extra axial strain.

1.4. Why ordered array of 1D nanostructures?

Ordered arrays of vertically aligned 1D semiconductor nanostructures are considered as viable candidates for the realization of all-dielectric metamaterials, artificial electromagnetic materials, and piezoelectric materials whose properties can be tailored to enable new functions and improved performances in associated devices compared to naturally existing materials. By utilizing the advancements in nanofabrication and growth techniques, nanostructure assemblies can nowadays be precisely designed in order to fully control and adjust their material properties. A variety of approaches have been developed to synthesize selective-area, well-ordered 1D ZnO nanostructure arrays [57,116,117,131,147,188–192]. Various types of 1D ZnO nanostructure arrays with control over their orientation, shape, dimension, and spacing are shown in Fig. 3 [193–196]. Ordered nanostructure arrays demonstrate a superior ability in regulating the piezoelectric properties to a certain direction and range, which is beneficial for optimizing the efficiencies and achieving a reproducible performance. When compared to their randomly distributed counterparts, ZnO nanostructures in regularly organized arrays are far more favorable. Here are some important aspects of 1D nanostructures organized in an ordered array.

- Regular arrays of uniform-sized nanomaterials offer a better understanding of the piezotronic properties, improving the associated

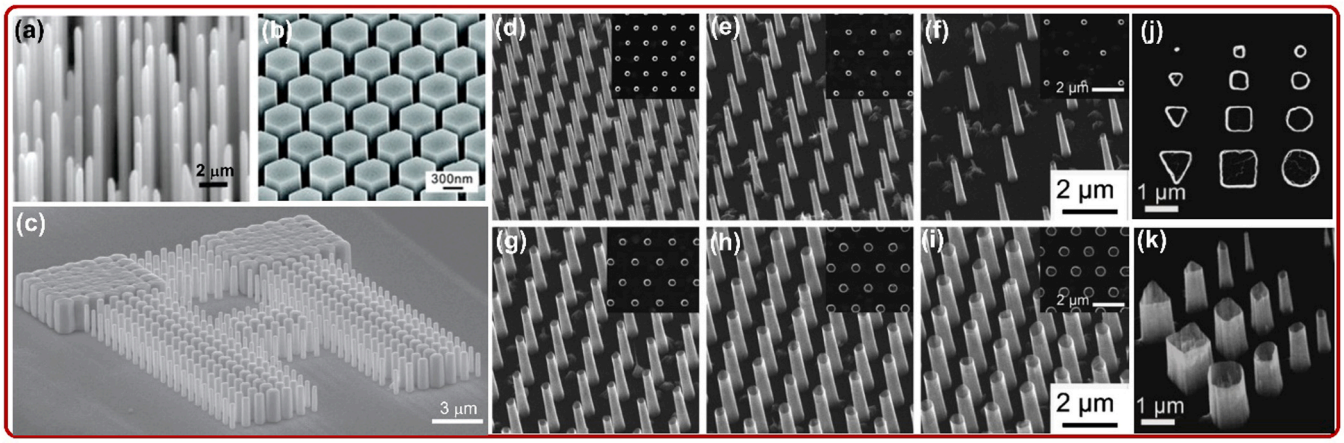

Fig. 3. Different forms of vertically aligned 1D ZnO nanostructures. (a) ZnO NWs with a random distribution. Reproduced with permission [193]. Copyright 2007, American Chemical Society. (b) Site-specific ZnO NR arrays. Reproduced with permission [194]. Copyright 2013, Royal Society of Chemistry. (c) Castle-like 3D architecture of ZnO NR arrays with variable diameter and interspacing. Reproduced with permission [195]. Copyright 2015, Springer Nature. (d–i) Bird's eye SEM images of position- and diameter-controlled ZnO NT arrays. (d–f) Hexagonal ZnO NT array, with spacings of 1.2, 1.6, and 2.4 μm, respectively, having a fixed diameter. (g-i) ZnO NT arrays of diameters 400, 600, and 800 nm, respectively, with a fixed interspacing. The scale bar is identical for (d–f) and (g–i), respectively. The insets in (d–i) are the corresponding top-view SEM images. (j–k) The top-view and tilted-view SEM images of shape-controlled ZnO NTs grown on SiO_2 growth masks with different shapes, respectively. Reproduced with permission [196]. Copyright 2009, Wiley-VCH GmbH.

device performances in terms of sensitivity, detection range, reliability, longevity, and reproducibility. The dimension- and position-controlled ZnO NTs in an ordered array offered a proper understanding of the effect of NT diameter, height, and tube-wall thickness on the sensing performances of piezoelectric pressure sensor [131]. Individually addressable piezotronic sensor arrays were realized from a selective-area, well-ordered arrays of vertical ZnO NWs having control in dimension and array interspacing [192].

- The flexible device fabricated by the ordered array of ZnO nanomaterials has better device performance and flexural modulus. As can be seen in Fig. 4(a), G. Tian et al. demonstrated that the flexural modulus of the ZnO NRs in the regularly ordered array was 35.74% lower than that of the unpatterned ZnO NRs [120]. The output voltage of the developed PNG device was increased approximately 1.62 times higher than that of the original continuous structure as a result of the suppression of the screening effect [120]. After introducing patterned growth of ZnO NRs by replacing random growth on indium tin oxide (ITO)-Polyethylene terephthalate (PET) substrate, D. Yang et al. demonstrated a 6-fold improvement in output current from a ZnO NR-based PNG [119].
- Depending upon the dimension and spacing of the nanostructure arrays, a controlled pixel array can be constructed in the case of a pressure/strain-based tactile image sensor. The number of nanostructures included in a pixel, its size, its array periodicity, and the resolution of the mapped image may all be further controlled in this way. By utilizing an ordered array of ZnO NTs on graphene (Gr), Y. Tchoe et al. fabricated an individually addressable device matrix as shown in Fig. 4(b) [134]. Later, addressable pixel arrays were fabricated from the ordered array of ZnO NTs on Gr by J. B. Park et al. for pressure mapping, where the number of ZnO NTs in each pixel was regulated [148]. An ultra-high resolution tactile image sensor was demonstrated by using the ZnO NWs controlled in dimension and array interspacing [132].
- Site-specific and aligned 1D nanostructures are geometrically advantageous in production of complex devices and their close-packed integration for real-world applications. For example, the vertically well-aligned NWs/NRs/NTs enable them to locally metalize the selective parts of the nanostructures along their own axis. As a result, 3-terminal devices can be constructed on vertical 1D ZnO nanostructure-based heterojunction arrays, as shown in Fig. 4(c) [125,129,197]. Fig. 4(c(i–iv)) displays the 3-terminal vertical field effect transistor (VFET) arrays fabricated by dimension- and position-controlled ZnO NTs on Gr [125]. A 3-terminal vertical surround-gate FET (VSG-FET) was realized by using patterned ZnO NW arrays in a group on SiC epilayer substrates, as shown in Fig. 4(c (v–vi)) [197].
- The real-world application of piezotronics requires close-packed integration of devices in a tiny space with controlled integration density. It is crucial to align 1D nanostructures in a parallel, scalable, and highly reproducible way regardless of the particular materials in order to incorporate them into close-packed device applications [198]. Additionally, the well-organized 1D nanostructure arrays can effectively reduce the parasitic impact and non-unity ideal factor brought on by the creation of undesirable cross-connections between close-packed devices [129].
- The efficiency of energy converting/storing devices with typical planar architectures has, up to this point, been increased to be close to the matching theoretical values, which are difficult to improve further without reforming the device structures. As an alternative, organized 1D nanostructure arrays have recently been demonstrated their potential to function as a strong building block for the construction of devices that can convert or store energy more efficiently.
- Individual 1D nanostructure-based devices can become fragile under excessive pressure or strain, which can have a significant impact on how well they work. Integrating 1D ZnO nanostructure assemblies in the form of bundles in a patterned order is an alternative approach that provides stiffness without substantially lowering the device performance index [199]. By integrating high density 1D nanostructures into bundles, device performance can also be enhanced considerably as compared to the device made of its individual counterpart. In reality, defects like cross-aligned nanostructures, voids in large patterning are found which hinder the performance of fabricated devices. Therefore, well-organized bundles can be used more effectively in flexible piezotronics as compared to individual 1D nanostructures because of their mechanical stability, structural quality, improved device performances, and reproducibility.
- Piezotronics is driving the rapid development of multifunctional devices, sensors, human-machine interface chips, displays, and self-powered systems. These regularly ordered, morphology-controlled arrays of 1D ZnO nanostructures are going to be the backbone for this rapid development of piezotronics [57,68,116,118,131,132,191, 192,200,201]. Researchers are anticipating more compact and tiny

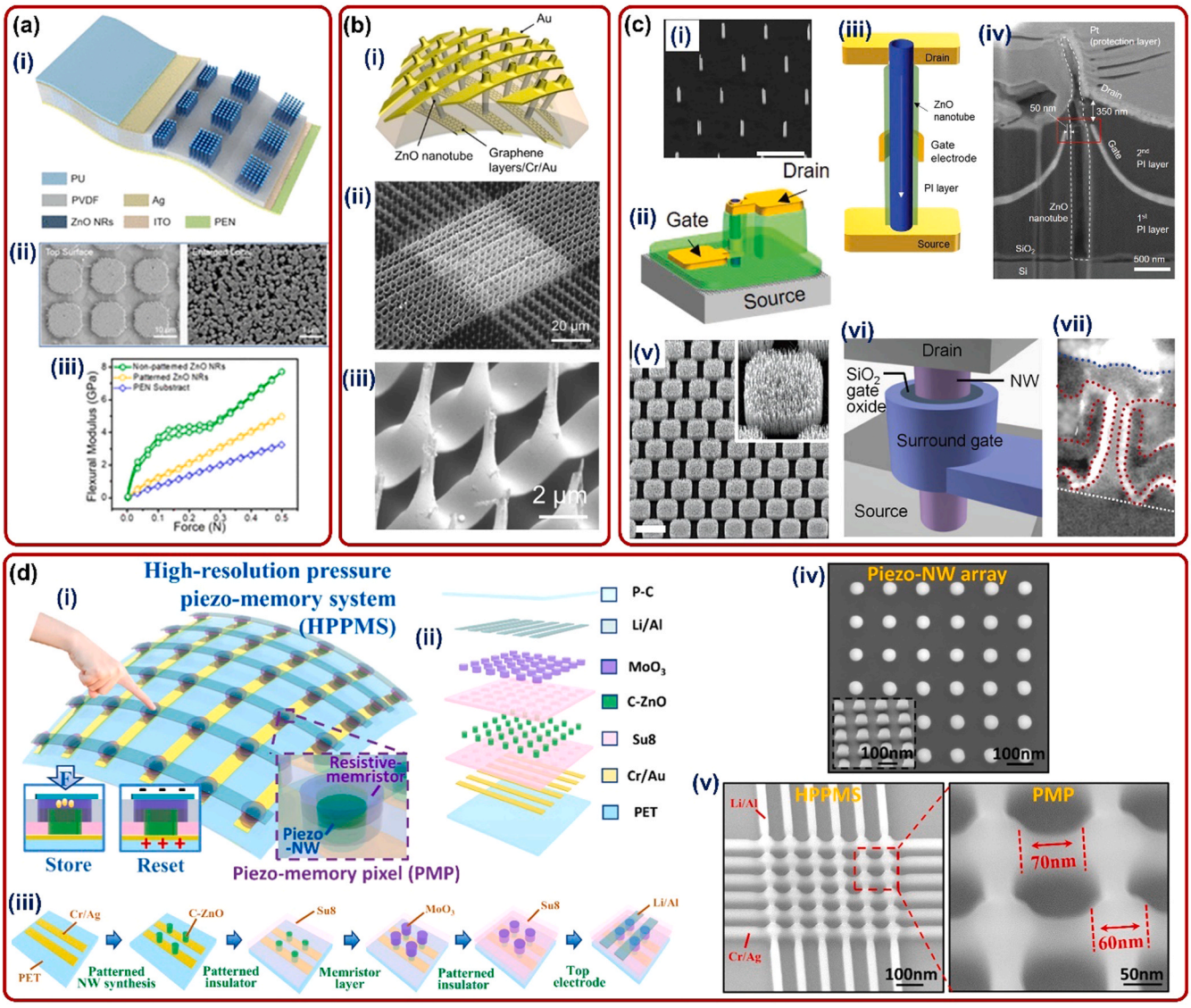

Fig. 4. Regularly ordered arrays of ZnO nanostructures: advantages in complex device fabrication and performances. (a) 3D structure of a patterned ZnO NRs device with PVDF acting as a barrier layer: (i) Schematic illustration indicating different layers used for building the device. (ii) The topographies of the patterned ZnO NRs. (iii) The flexural modulus of the substrate and different samples based on a 3-point bending test through dynamic mechanical analysis. Reproduced with permission [120]. Copyright 2020, American Chemical Society. (b) Two-terminal ZnO NT-based vertical device array: (i) Schematic illustration of an individually addressable device with Au and Gr/Cr/Au electrode lines contacting individual ZnO NTs. (ii) Tilted SEM images of the fabricated device. (iii) Enlarged view clearly demonstrating precise alignment of the top electrodes with the ZnO NT device array. Reproduced with permission [134]. Copyright 2020, Elsevier. (c) Three-terminal ZnO NT-based vertical device array: (i) SEM images of the ZnO NT arrays. (ii) Schematic illustration of a fabricated three-terminal VFET arrays. (iii) Schematic of a single VFET indicating each layer within it. (iv) Corresponding cross-sectional SEM image [125]. (v) Vertical ZnO NW arrays on SiC epilayer substrates used for vertical surround-gate (VSG) FET. (vi) Schematic illustration of the critical components of VSG-FET. (vii) A SEM cross-sectional image of a VSG-FET. Reproduced with permission [197]. Copyright 2004, American Chemical Society. (d) Resistance-memristor and morphology-controlled ZnO NW-based bionic pressure piezo-memory system: (i) The design of a high-resolution pressure piezo-memory system (HPPMS), which consists of resistive- and piezoelectric-switching NWs (right-lower). The electrical bias resets and stimulations of the piezo-potential-NWs can be used to realize the force recording and refreshing procedures using resistance-memristor (left-lower). (ii) The HPPMS's multi-layer structure gives rise to useful elements like piezo-NWs and resistive memristors. (iii) The fabrication process of the HPPMS device. (iv) The SEM images of the fabricated ZnO piezo-NW array which has a high degree of uniformity in both height and diameter. The ZnO piezo-NW array is depicted in the inset image in a 45° tilted-view SEM image. (v) The SEM image of the piezo-memory pixel array in HPPMS (left) and corresponding enlarged view indicating the 60 nm pixel-size and 70 nm interspacing (right). Reproduced with permission [132]. Copyright 2021, Elsevier.

devices as directed by Moore's law. For instance, a complex neuromorphic tactile sensor with pixel size of only 60 nm is demonstrated by C. Jiang et al. by utilizing site- and morphology-controlled ZnO NW arrays (Fig. 4(d)) [132]. The high-resolution pressure piezo-memory system (HPPMS) was utilized as a competent neuromorphic tactile sensor, that offered non-volatile force-resistive conversion and force-tunable synaptic functions [132].

The limitations associated with individual 1D nanostructures, irregular 1D ZnO arrays and their random alignment, and thin film structures have been overcome by incorporating well-ordered 1D ZnO nanostructures into piezotronics sensors. These devices now have better performance, additional functionalities, reproducibility, and higher stability. However, the large-area device fabrication is the main drawback for the implementation of regularly ordered 1D ZnO nanostructure arrays as a building block for real-world piezotronic devices. It should be

mentioned that it is challenging to select a specific type of materials to satisfy all needs. For particular applications to replace large area thin-films and NW-films, ordered arrays of 1D ZnO nanostructures still have limitations.

1.5. HS approach

A well-known technique called the HS approach may make it possible for nanoscale piezotronic devices to work better and more effectively. In the HS strategy, researchers are able to modify/improve the piezoelectric properties of the 1D wurtzite materials in accordance with the needs by integrating novel materials with extra functionalities and complexities. Heteroepitaxy is advantageous with 1D ZnO nanostructures because they provide effective strain relaxation from the lateral surfaces [181]. Different classes of HSs are introduced for 1D ZnO-based piezotronics including (a) axial HS, (b) core-shell HSs, (c) nanoparticles (NPs) decorated HSs, (d) branched/hierarchical HSs, and (e) functionalized HSs [109,113–115,128,191,202–206]. Various types of 1D ZnO nanostructure-based HSs are depicted in Fig. 5. These HSs were utilized further for a variety of cutting-edge nanoscale devices. Three are several advantages of these various types of HSs and depending on the requirements, this approach can offer the following benefits over the bare ZnO nanostructures.

- Interface band alignment at the heterointerface can result in strong built-in electric fields and hence can provide self-power [207].
- HS approach can offer opportunities for fabricating suitable Schottky and p-n heterojunctions [208,209]. S. Lu et al. demonstrated a 10-fold increase in the performance of PNG composed of Au NP-coated ZnO nanoarrays as compared to the device composed of pristine ZnO [209]. The drastic suspension of the piezopotential screening effect which resulted from the formation of Schottky junctions on the ZnO surface was attributed to this improvement [209].
- HS approach can provide more capability for large-scale processing and integration with Si-based electronics [25,66,210].
- The HS technique can provide possibilities for device integration in a series, which results in the enhancement of device performance. By

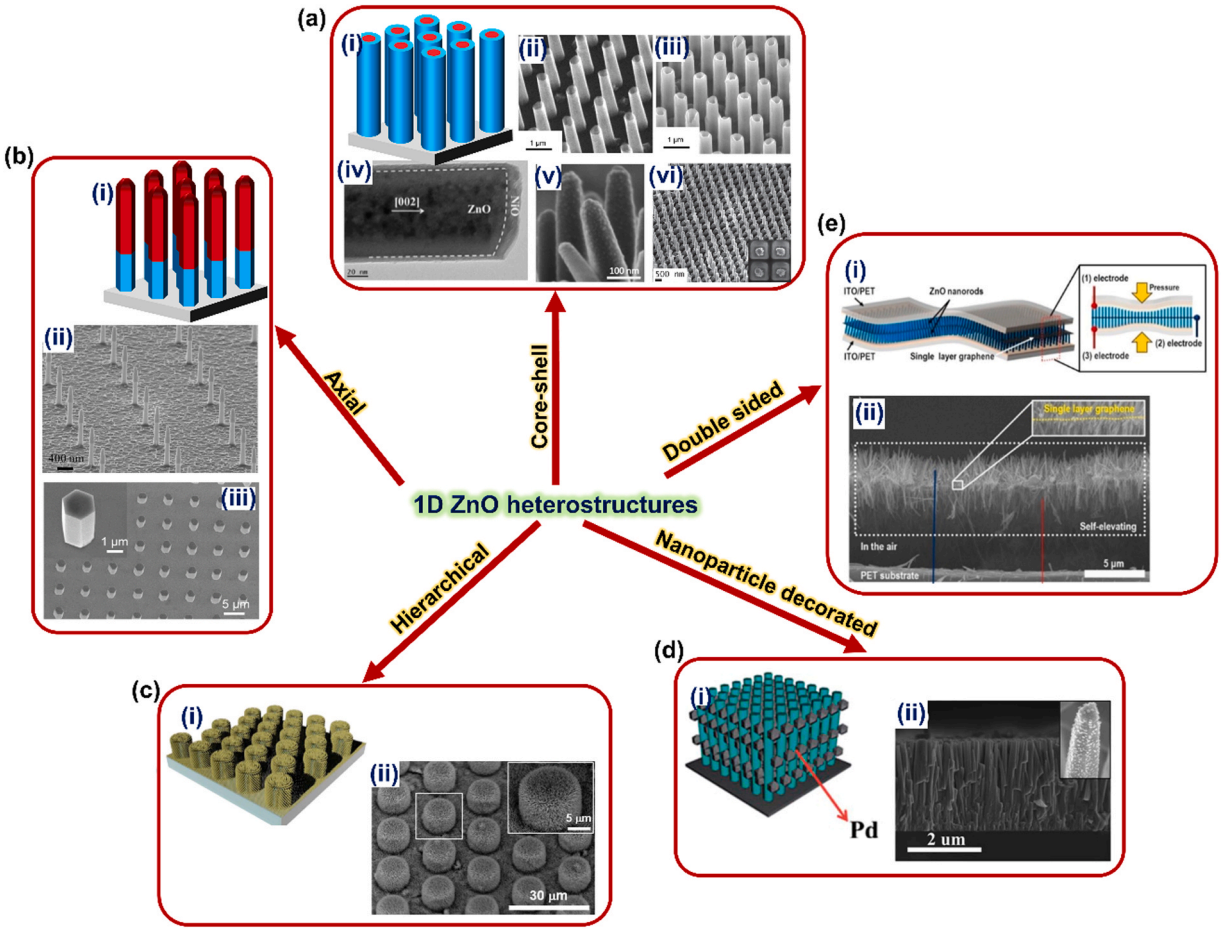

Fig. 5. Different kinds of 1D ZnO nanostructure-based HSs. (a) Core-shell HS: (i) Schematic illustration. (ii) Bare ZnO NT arrays. (iii) ZnMgO-coated ZnO NT arrays. Reproduced with permission [202]. Copyright 2009, Wiley-VCH GmbH. (iv) ZnO-NiO NWs core-shell. Reproduced with permission [72]. Copyright 2016, Elsevier. (v) ZnO NW-Co_3O_4 core-shell. Reproduced with permission [109]. Copyright 2019, American Chemical Society. (vi) ZnO-coated Si nanopillar arrays. Reproduced with permission [203]. Copyright 2014, Wiley-VCH GmbH. (b) Axial HS: (i) The schematic illustration. (ii) p-Si/ZnO axial NW HS. Reproduced with permission [479]. Copyright 2022, Springer Nature. (iii) As-grown ZnO NW arrays on the flexible p-GaN film. Reproduced with permission [128]. Copyright 2019, Elsevier. (c) Hierarchical HS: (i) Schematic illustration. (ii) Tilted SEM image of ZnO NWs (diameter: ≈50 nm and aspect ratio: 20) on the PDMS MPs (diameter: ≈10; height: ≈10; and pitch: ≈20 μm). Reproduced with permission [191]. Copyright 2015, Wiley-VCH GmbH. (d) NP-decorated HS: (i) Schematic illustration of the Pd NP-decorated ZnO NW HS utilized as self-powered active ethanol sensor. (ii) SEM image of the Pd/ZnO NW arrays in a side view (the inset is an enlarged view of one single Pd/ZnO NW). Reproduced with permission [204]. Copyright 2014, Royal Society of Chemistry. (e) Double-sided HS: (i) Schematic illustration of the ZnO NRs/Gr/ZnO NRs double-sided HSs and the respective piezotronic device in which epitaxial double HS are installed. (ii) SEM image of the ZnO NRs/single-layer Gr epitaxial double HS that are uniformly grown and distributed over the entire Gr area (yellow colors correspond to single-layer Gr in the inset image). Reproduced with permission [113]. Copyright 2015, Elsevier.

creating a heterojunction with a Si micropillar (MP) array, M. R. Hasan et al. showed that a ZnO NR-based PNG's output power could be increased by 5.6 times [211].

- Incorporating additional material as a lamination can potentially prolong the lifetime of a device. This provides support for the weak 1D ZnO nanostructures from damage during transferring from rigid substrates to foreign substrates for flexible and wearable applications [131,134,148].
- The HS method aids in preventing the electron screening effect in 1D ZnO [105,108,209].
- Additional ligands by surface functionalization can be useful for attaching molecules in case of piezoelectric bio-chemical as well as gas sensors [28].
- HS formed by surface passivation can also improve the crystalline quality of the ZnO nanomaterials. After surface passivation with the copper thiocyanate (CuSCN), N. Jalai et al. found that the density of defects on the ZnO surface was reduced, and consequently the carrier concentration in the ZnO [212].
- Opportunities are opened to create organic/inorganic heterojunctions [141,213]. For instance, the limited biocompatibility of the active components in a few piezotronic sensors restricts their use in wearable medical devices. The gap can be filled by developing HS from organic materials that are naturally biocompatible and capable of amplifying received vital signals from the body [214]. A wide variety of biophysical, biochemical, and environmental signals can be measured by bio-integrated wearable piezotronic systems, which can offer vital information about general health condition and quantify human performance [11].
- The HS approach proposes to combine piezoelectricity with other mechano-electric properties for synergistic management [90–94].
- 1D ZnO nanostructure-based HSs offer a wide variety of applications because of their additional functionality. After functionalizing a Li-doped ZnO NW array with oleic acid, J. I. Sohn et al. showed 30 times increase in piezoelectric output voltage from the device [215].

1.6. 1D/2D combination

A particular type of HS that offers unique features is vertically aligned and well-ordered 1D nanostructures on 2D materials. This type of HS is beneficial for the implementation of high-density integration of 1D nanostructure-based devices and mechanical deformability as suitable for bendable and stretchable electronics and optoelectronics. The material properties of the 2D material can be integrated with the piezoelectric 1D ZnO nanostructures and thus new functionalities to enable the 1D/2D heterojunction for versatile nanotechnology applications. Some of the key advantages of 1D/2D HSs are:

- By utilizing 2D nanomaterials as substrate (Gr, hexagonal boron nitride (h-BN), and transition metal dichalcogenides (TMDs)) selective, catalyst-free growth of 1D ZnO nanostructure can be achieved [125,131,134,148,216–218]. By employing catalyst-free, direct growth of ordered 1D ZnO nanostructures on 2D layered nanomaterials, 1D/2D HSs can be straight applicable for piezoelectric sensors as well as different other piezotronic devices. 2D layers offer advantages because of their mechanical flexibility and excellent electrical and thermal properties [90,125,131,134,148,219]. According to M. Panth et al., the strain detection performance of ZnO NWs grown on Gr was 7–8 times better than that of ZnO NWs grown on polycrystalline ZnO seeds [220].
- The weak van der Waals (vdW) forces between the 2D nanomaterial with the substrate can be utilized for the efficient 1D/2D nanomaterial transfer to any foreign substrates. Thus, it provides the opportunity for the materials to be implemented as flexible and wearable device application [107,131,134,148,221].
- Gr-based substrates provide mechanical stability to the 1D ZnO nanostructure. Additionally, 1D ZnO on 2D Gr exhibits behavior consistent with appropriate semiconductor/metal junctions or contacts, which are crucial parts of semiconductor devices [131,134,148,221]. Conducting Gr can act as a flexible, stretchable, and transparent electrode for different piezotronic as well as optoelectronic applications [131,134,148,221–227].
- Depending on the difference in the electronic affinities and/or carrier concentrations of the materials in contact, 1D semiconductors on 2D semiconductors (such as TMDs) generate heterointerfaces in which the p-n junction may also be accessible [129,174,228].
- 1D ZnO on 2D flexoelectric substrate can trigger the synergy in applications [111].
- The hybrid or composite 1D/2D materials offer a wide range of material platforms, providing a window into novel approaches to intriguing structures and potential uses for such assembled architectures in the future. These architectural frameworks enable the integration of 1D nanostructures into the micro- and macro-scales and serve as the foundation for the construction of 1D materials into higher hierarchical domains [229].

1.7. Flexibility of 1D ZnO-based piezotronic devices

Smart sensing technologies are currently receiving a lot of interest for health monitoring [10,67,153,230–234]. Flexible piezoelectric sensors are important components of sensing technology for portable and wearable human health monitoring devices. In addition to being crucial for personalized signatures, conformability with a curve or rough surface for the sensors is also important for touchpad technology, bioimaging, and human-machine interfaces. Flexible piezotronic sensors should have a wide detection range, high resolution, high sensitivity, fast reaction, and long-term stability in order to keep their sensing ability unaltered with arbitrary substrate deformation. The development of composite polymers with conductive fillers (i.e., the active phase), such as carbon nanotubes (CNTs), metallic nanofibers, and NPs, has thus received a significant amount of attention in the study on piezoelectric/piezoresistive sensors [235–237]. However, when considered from the point of view of a healthcare application, such as vital sign monitoring, the sensing performance of these composite elastomer-based sensors is very poor. Furthermore, their performance easily degrades in the ambient atmosphere. When using flexible sensors made of inorganic materials, it is necessary to assemble electronic circuits and active piezoelectric components onto flexible substrates that enable the sensors to be stretched, compressed, bent, and twisted into irregular shapes without compromising the piezoelectric functionalities. Therefore, the development of piezotronic sensors based on piezoelectric nanomaterials, particularly 1D ZnO nanomaterials on a flexible substrate, has received considerable scientific attention.

1.8. Other important aspects of 1D ZnO arrays and associated piezotronic devices

1.8.1. Alignment of the 1D ZnO arrays

The 1D ZnO-based piezotronics have drawn the greatest attention for the NW arrays with vertical alignment. Aligning them obliquely is one of the suggested methods for maximizing the deformation in 1D nanostructures [28,238]. Theoretical simulations on InN NWs found that the tilt angle of an obliquely aligned NW with respect to the substrate directly correlated with the strain-induced piezopotential, whereas the experimental results suggest that the tilt angle of the NW around 60° may be the best geometry for the highest piezopotential to be applied in DC/AC PNGs [239]. However, there are some drawbacks of these tilted nanostructure arrays. There is a high chance of unwanted cross junctions while fabricating closed-packed device arrays by using these tilted nanostructures. Additionally, it is challenging for this type of structure to establish selective contact in the vertical direction. In reality, piezotronic device functionality completely determines the need for 1D nanomaterial alignment. In this regard, horizontally aligned 1D ZnO

nanostructures were also used in piezotronics [57,156,240–243], which performed better than vertically aligned nanostructures in terms of device performance [240]. However, fabricating or integrating horizontal arrays of 1D ZnO nanostructures with precise dimensions and spacings has never been easy.

1.8.2. Shape of 1D nanostructures

Recently, researchers have discovered that incorporating unique geometrical structures might further enhance the physical and chemical properties of nanomaterials [244]. FEM analysis on ZnO NWs predicted that the truncated conical-shaped NW would be more advantageous than uniform diameter cylindrical-shaped NWs [28,152]. It also demonstrated that the conical devices have enhanced piezopotential and stronger depletion at the tip of the conical NW. Through experiment, K. Y. Shin et al. suggested that the ZnO NN has a better piezoelectric performance in comparison with the NR [153]. AFM nanoindentation was used to evaluate the elastic modulus, which quantifies the resistance to elastic deformation for the ZnO NR/polyvinylidene fluoride (PVDF) and ZnO NN/PVDF hybrid films. The values were calculated to be approximately 25 and 3 GPa, respectively [153]. A. Araneo et al. demonstrated how altering the piezopotential-force relation in the case of conical NWs can result in better NGs, piezotronic, and piezophototronic devices [152]. J. B. Park et al. demonstrated highly sensitive pressure sensor arrays based on the tapered ZnO NT arrays on Gr and utilized them for breath and pulse detection [131]. However, conical shaped-1D nanostructures, which often act like ineffective functionally-graded piezo--materials, should be avoided in piezoelectric and piezotronic devices in favor of uniform cylindrical cross-sections because they have piezo-performance that is more resistant to mechanical size effects [154].

1.8.3. Doping of ZnO nanostructures

In comparison to other common piezoelectric ceramics, pristine ZnO has a comparatively low piezoelectric coefficient [28,245]. Doping is considered as one of the well-known strategies to enhance the piezoelectric coefficients of 1D ZnO [30,58,246]. There are two main categories for improving the piezoelectric characteristics of ZnO through selective doping. The first one is the change of the original crystal lattice's atoms, which includes the alternation of chemical bonds, polarizations, and bond lengths caused by the atomic replacement. The second effect is the change in the carrier concentration, which plays a critical role in reducing the internal resistance and the piezoelectric screening effect. Substitutional doping can increase the asymmetry in structure of the host material by replacing its atoms with dopants, which can also contribute to the enhancement of piezoelectric properties, or even introduce piezoelectricity into a non-polar material [245]. P-type doping, in particular, can lower the carrier concentration and, as a consequence, lower the piezopotential screening. In the case of n-type doping, the dopant can lower crystal lattice strain along the ZnO crystal's polar c-axis, raise the piezoelectric coefficient, and enhance piezoelectric output performance [30]. Sb [30,58,208,247], Li [173, 215,248–250], Tb [30,251], halogen ions [30,252], Al [253–255], and Fe [256] are demonstrated to be suitable dopants for doping 1D ZnO nanostructures, and the piezoelectric sensing capabilities of the corresponding devices improved after doping in comparison to the undoped one. Recently, Y. Sun et al. described a method for increasing the piezoelectricity of ZnO by doping it with rare earth ions to suppress its atomic-scale piezoelectric screening effect [257]. In comparison to undoped ZnO, Y^{3+} doping showed a 91.8% drop in carrier concentration and an increase of 53.8% in surface piezoelectric response. The extent of doping also has a considerable impact on the piezoelectric performance of 1D ZnO. According to K. C. Pradel et al., high doping concentration in Sb-doped ZnO NW samples led to an increased screen effect, which dramatically decreased the piezoelectric output [58]. Piezopotential measurements of a ZnO NWs incorporated with a Li dopant source varying from 0 (undoped) to 100 mM were performed by J. I. Sohn et al [215]. It was observed that the output voltage was increased with Li concentrations up to 25 mM due to a continuous decline in donor concentrations, whereas the output voltage was gradually reduced with further increasing Li concentrations due to the compensation effect, such as the formation of acceptor complexes, deep levels, and interstitials, resulting from higher Li concentrations [215].

1.8.4. 1D nanostructure aspect ratio

ZnO nanostructures in 1D forms are favorable for bending upon applying tiny pressure and the bending ability is greater for the longer ZnO nanostructures with fixed lateral dimensions. Different groups have demonstrated that the piezopotential is proportional to the aspect ratio of the 1D ZnO nanostructures and consequently the device performances through both experimental and theoretical modelling [28,101,131,152, 169,258–260]. By using FEM, M. Riaz et al. reported that the calculated output electric potential of ZnO NW-based PNG increases with the aspect ratio of the ZnO NWs and finds maxima when the aspect ratio is 80 [260]. The excessive deflection in the NW might cause charge-carrier screening on the outer surfaces of the NWs and hence there was a drop in output electric potential beyond the NW aspect ratio of 80. According to R. Agrawal et al., as the diameter of [0001]-oriented ZnO NWs decreases from 80 to 20 nm, their elastic modulus rises from 140 to 160 GPa [101]. In the case of vertically aligned ZnO NTs, J. B. Park et al. reported that the pressure response decreases with the increase in the tube-wall thickness when the length and the diameter of the tube were fixed [131]. For a ZnO NW diameter of 100 nm, when the aspect ratio was changed from 12 to 50, the density of electrical energy generated in a PNG and the efficiency increased up to a maximum of 241 nJ cm^{-3} and 1.8%, respectively [259].

1.8.5. Device contact type

The Schottky contact between the metal contact and ZnO NW is a crucial component for the current modulation as well as generation process. Therefore, the modulation of SBH through Schottky contacts are one of the key factor in context of piezoelectric sensors, PNGs and other piezotronic devices [95,261–264]. PNGs were initially constructed to establish a Schottky contact at one end and an ohmic contact at the other end by selecting metals with appropriate work functions [144]. In case of piezoelectric sensors, piezopotential can effectively tune/control the charge carrier's transport process by modulating the SBH at local contact through strain-induced piezoelectric polarization charges that are presented at the site of the metal-semiconductor interface. Hence, the performances of Schottky-contact sensors are ultimately enhanced [95]. When compared to ohmic contact devices, Schottky contact led to an increase in the sensitivity of NW sensors by up to 4 orders of magnitude. The sensitivity of a sensor was increased by more than 300% by utilizing the piezotronic effect to tune the piezo-polarization charge-induced SBH [95]. Comparing the performance of the Schottky-contacted NW sensor to that of the Ohmic-contacted NW sensor, the former offers a high performance in terms of sensitivity, reaction time, etc [263,265,266]. An optimized SBH is necessary for the sensor to operate at its highest level of sensitivity because an unfavorable SBH can prevent current from flowing through and resemble an Ohmic-contacted device [267]. 10-fold enhancement in PNG was obtained with Au NPs/ZnO nanoarrays Schottky junction as compared to pristine ZnO [209].

1.8.6. Hybridization of mechano-electrical properties

Utilizing the synergy in performance of sensors for physiological monitoring and health care applications, hybrid piezotronic devices can be integrated with other mechano-electrical features [111,112,250, 268–271]. Hybrid NGs can meet the energy and power requirements of wearable and portable electronic gadgets by enhancing the efficiency of energy harvesting [91,93,94,96,270–275]. Y. P. Lim et al. combined high triboelectric output voltage and piezoelectric output current in a hybrid piezo/triboelectric NGs (H-P/TENGs) made of ZnO NR/PVA and

obtained 17-fold improvement in electrical outputs when compared to the pristine one [93]. Y. S. Chen et al. integrated piezoelectricity with a capacitive pressure composed of ZnO NW/PMMA and obtained an increase of capacitance change by as much as a factor of 23 over pristine polymer devices [112]. B. C. Kang et al. obtained 6-fold enhancement in pressure sensitivity by developing wearable pressure/touch sensors based on hybrid ZnO NW/PDMS dielectric composites [269]. An eco-friendly and stretchable flexoelectricity-enhanced piezoelectric NG based on zinc-aluminum layered double hydroxide (ZnAl:LDH) nanosheets-ZnO HS on stretchable PDMS substrates was demonstrated by C. Yoon et al [270]. The multi-property coupling effects between magnetic field, piezoelectricity, and photoexcitation were investigated in ZnO NW arrays by S. Yan et al [276]. An improvement in the current responses up to 9 times and 3 times under piezo-magnetotronic and piezo-photomagnetotronic engagements, respectively, were obtained from ZnO/Co_3O_4 core/shell heterojunction NW arrays. The improved performances were attributed to the improved charge carrier separation and transportation at the core/shell interface [276]. Coupling of pyroelectric and piezoelectric effects was investigated by J. Liu et al. for the photoresponse enhancement from a self-powered heterojunction photodetector composed of glass/Mo/Cu(In,Ga)Se_2/CdS/ZnO NW/ITO [277]. By combining the ferroelectric p-type La-doped bismuth ferrite film and n-type ZnO NW arrays in a photovoltaic system, Y. Zhang et al. were able to take advantage of the piezo-phototronic effect and ferroelectric polarization [278]. By simultaneously applying 2.3% compressive strain and upward polarization, the short-circuit current and open-circuit voltage improved by 54.7% and 8.4%, respectively, in comparison to the photovoltaic performance of the heterojunction without strain and poling.

1.8.7. Compatibility of the piezotronic devices with Si electronics

Practical application involves the interfacing of the piezotronic devices with a commercial integrated circuit (IC) chip. For instance, highly sensitive and conformable health monitoring piezoelectric sensors can be mounted to the human body to realize signal conversion, but the signal transmission needs multiple wires which are connected to the laborious workstation to analyze the signal. This inconvenience may limit the application of these piezoelectric sensors in human health monitoring. In order to drive the mechanical action-based signals produced by a human to operate the Si-based CMOS chip, piezotronics was developed [20]. Earlier reports demonstrated the commercial viability of the ZnO-based sensors [25,66,210]. For instance, successful integration was made from ZnO-based piezoelectric sensors to an existing and shipping touchscreen driver IC [210].

2. The synthesis of high-quality, 1D ZnO nanostructure arrays

Various strategies have been developed so far for synthesizing 1D ZnO nanostructures, and it mostly depends on the vapor-liquid-solid (VLS) growth method, vapor-solid-solid (VSS) growth method, chemical vapor deposition (CVD) method, and solution-based hydrothermal method. However, piezoelectric properties of these ZnO nanostructures are greatly affected by their high crystalline quality, well-alignment, control over morphologies, and tunability in majority charge carriers. Therefore, the piezoelectric and piezotronic device performances are greatly influenced by the method used to create the 1D ZnO nanostructure [65,279]. It was discovered that CVD, solution process, and electrochemical deposition were the most commonly employed synthesis techniques to grow vertically aligned, highly crystalline, 1D ZnO nanostructures for piezotronic application [37]. Table 1 summarize the synthesis methods of different kinds of 1D ZnO nanostructures to be utilized for a variety of piezotronic applications.

2.1. CVD

CVD is the most extensively explored approach to the formation of 1D semiconductor nanostructures such as whiskers, NRs, and NWs [116,123,188,197,280–286]. Typically, metal nanoclusters are used as catalysts in CVD to synthesize 1D nanomaterials via the VSS and VLS growth processes. Often, pure Zn powder or a combination of ZnO is employed as the Zn vapor source to create ZnO nanostructures in a horizontal tube furnace where ZnO NRs/NWs are commonly grown. Noble metal catalysts are considered to be the nucleation site for the growth of nanostructures. ZnO NWs have been successfully grown on sapphire, GaN, AlGaN, and ALN substrates through the VLS process [281]. By controlling the size, dimension, and position of the catalyst, patterned growth approaches have developed to obtain well-organized, morphology--controlled 1D nanostructures as shown schematically in Fig. 6(a(i–iv)) [123,188,282,283,287]. X. X. Zhang et al. successfully fabricated site-specific ultrafine (as thin as 10 nm) ZnO NW arrays with varying diameters by using multi-stage CVD growth (Fig. 6(a(v–viii))) [283]. By precisely controlling the thickness of the Au catalyst, B. Kumar et al. demonstrated a PNG that was made from vertically aligned NW-nanowall ZnO on Gr using CVD at 900 °C [288]. The drawbacks of the CVD approach include high operational costs and synthesis temperatures (over 450 °C) that are undesirable for polymeric substrates, which prevent the direct growth of 1D ZnO nanostructures on flexible plastic-based substrates. In general, 1D ZnO nanostructures constructed using high-temperature vapor phase deposition techniques have fewer defects and enormous control in morphology for selective are growth, making them the best prospects for piezotronics study [139].

Metal-organic chemical vapor deposition (MOCVD) is a special type of CVD that was widely used for the 1D growth of semiconductors. A high-purity metal-organic source is used to synthesize different ZnO nanostructures in a 1D form including, NW, NR, NT, NN, and nanowall [117,125,129,131,148,196,202,289–298]. G. C. Yi and coworkers developed a catalyst-free MOCVD for growing 1D ZnO nanomaterials [196,291,293–295]. Recently, J. B. Park et al. grew morphology-controlled ZnO NT arrays on Gr by using MOCVD [131,148]. The methodology is schematically shown in Fig. 6(b)) along with the scanning electron microscopy (SEM) images of the synthesized ZnO NTs [148]. Note that, no catalyst was employed for ZnO NT formation, which leads to the preparation of high purity ZnO nanomaterials by excluding the possible incorporation of catalytic impurities, which is highly beneficial of a diverse range of device applications. MOCVD enables the growth of 1D ZnO nanostructures along the c-axis orientation as single crystals [196,293,295,298], which makes it advantageous for piezotronic applications [65,139]. Additionally, ZnO nanostructures could be grown using catalyst-free MOCVD at temperatures as low as 400–500 °C, which is substantially lower than the normal growth temperature of 900 °C needed for catalyst-assisted NW formation [292]. The ability to grow high-purity ZnO NRs at a low temperature is expected to greatly increase the versatility and power of these building blocks for nanoscale photonic and electronic device applications.

2.2. Solution-based hydrothermal process

Utilizing a standard flexible substrate with a low melting temperature is challenging in CVD due to the high growth temperatures. Techniques for solution route synthesis make it possible to create 1D ZnO nanostructures on flexible substrates. Due to its relatively low synthesis temperature (<100 °C), the majority of existing research concentrated on a solution-based hydrothermal approach to produce ZnO NRs on flexible (polymeric) substrates [37]. Preparing a ZnO seed layer and hydrothermal growth of nanostructures are the two primary steps in a conventional hydrothermal process. The schematic representation of the construction of 1D ZnO nanostructure arrays by this process is shown in Fig. 7(a). Dimension- and position-controlled growth was included in a subsequent stage involving electron beam lithography. Large-scale arrays of highly ordered ZnO NRs grown by hydrothermal method on various pre-patterned ZnO seed layers were demonstrated by S. B. Kim et al [299]. Moreover, researchers have demonstrated the epitaxial

Table 1
Summary of 1D ZnO nanostructures including its different shapes, structure of active materials used in the associated piezotronic devices, 1D ZnO synthesis methods, fundamental function of the device, and relevant applications.

Active materials for piezotronic devices	1D ZnO synthesis method	Fundamental function of the device	Sensitivity	Applications	Ref.
ZnO NW	VLS	Force, strain		PNG	[373]
ZnO NW/MW	Thermal evaporation	Strain	Gauge factor 1250	Piezoelectric modulation	[170]
ZnO NW	Thermal evaporation	Strain		PNG	[453]
ZnO NW/Gr	CVD	Force, strain		PNG	[288]
ZnO NW	Hydrothermal	Strain, piezopotential-gated FET	2.1 uS	Tactile image sensor	[118]
ZnO NW	CVD/PVD	Strain		Sound-driven PNG	[379]
ZnO NT/Gr	MOCVD	Pressure	4.4 kPa^{-1}	Breath and pulse monitor	[131]
ZnO NT/Gr	MOCVD	Pressure	1.95×10^{-3} kPa^{-1}	Pressure-based image sensor	[148]
ZnO NW (oblique)	Hydrothermal	Strain		PNG	[238]
ZnO NW/Gr/ZnO NW	Hydrothermal	Pressure		PNG	[113]
CuSCN-passivated ZnO NR	Solution	Strain		PNG	[212]
ZnO NW	Solution	Strain		PNG	[241]
ZnO NW/Gr	Solution	Strain		PNG	[221]
ZnO NW	Solution	Force, strain		PNG, wireless data transmission	[437]
ZnO NR	Solution	Force, strain		PNG	[454]
ZnO NR	Solution	Strain		PNG	[455]
ZnO NW/Gr	Solution	Pressure	1.7 nA kPa^{-1}	Photosensor	[224]
ZnO NW/GaN	Solution	Strain		Self-powered photodetector	[456]
Au NP/ZnO MW	CVD	Strain		Light-induced piezopotential-gated FET, logic computation	[368]
ZnO NW/MW	CVD	Strain		Photonic synapse	[171]
ZNO NR/textile	Hydrothermal	Strain		PNG, human energy harvester	[457]
ZnO NW	Solution	Strain		PNG, detection of human face wrinkling	[406]
ZnO NW	Solution	Strain		PNG, active skin sensor, eye-ball motion detector	[407]
ZnO NN/PVDF	Solution	Strain		Heart rate monitoring	[153]
ZnO NW homojunction	Solution	Strain		Gesture recognition	[208]
ZnO NR	Hydrothermal	Strain		Wound healing	[408]
ZnO NT	Hydrothermal	Strain		PNG	[149]
ZnO NT	Solution	Strain		PNG	[151]
Pt/ZnO NN	Thermal evaporation	Force		PNG	[155]
ZnO NR	Solution	Pressure	0.62 V kPa^{-1}	Human motion sensor	[59]
Hierarchical PVDF/ZnO NW core-shell nanofibers	Solution	Strain		Gait recognition, pulse, and muscle movement monitor	[428]
ZnO NW/MW	Solution	Strain		Detection of protein kinases	[429]
Sb-doped ZnO NW	Solution	Strain		Gesture recognition	[247]
Li-doped ZnO NW	Hydrothermal	Strain		PNG	[248]
ZnO NR, AZO NR	Solution	Pressure	ZnO: -0.768 kPa^{-1}, AZO: -0.223 kPa^{-1}	e-skin, pulse monitor	[254]
MoO_3/ZnO NW	Hydrothermal	Force, pressure		Neuromorphic tactile sensor	[132]
ZnO NR	Hydrothermal	Pressure	403 mV MPa^{-1}	Self-powered e-skin	[400]
MoO_3/CBP/TAZ/ZnO NW	Hydrothermal	Pressure, Piezo-OLED-gated transistor	61.2 μS	Image sensor	[130]
ZnO NW	Solution	Pressure		Self-powered e-skin	[336]
WO_3/ZnO NW	Solution	Pressure		Pressure visualization and recording system	[200]
ZnO NW	Solution	Pressure		Enhanced UV detection, image sensor	[127]
ZnO NW/GaN	Hydrothermal	Pressure	12.88×10^{-6} kPa^{-1}	Electroluminescent imaging of pressure distribution	[136]
ZnO NW/Si MW	Hydrothermal	Pressure		Light emission enhancement, image sensor	[201]
ZnO NW/PDMS MP	Hydrothermal	Pressure	-6.8 kPa^{-1}	e-skin	[191]
ZnO NW/Organic	Hydrothermal	Pressure		Light emission enhancement, image sensor	[334]
ZnO NW	Hydrothermal	Pressure		PNG, vehicle sensor	[439]
ZnO NR	Solution	Pressure	0.25% kPa^{-1}	FET	[458]
ZnO NW/GaN	Solution	Pressure		Pressure image sensor	[128]
ZnO NW/PEDOT: PSS	Hydrothermal	Pressure		Light emission enhancement, image sensor	[135]
ZnO NR	CVD	Pressure		PNG	[459]
ZnO NW	CVD	Strain		Sound-driven PNG	[460]
ZnO NW/Gr	CVD	Strain		High-performance photosensor	[77]
ZnO NW/Gr	Sputtering	Strain		High-performance photosensor	[461]
ZnO NW	CVD	Strain		Lateral piezopotential-gated FET	[26]
Vertical and lateral array of ZnO NW	Physical vapor deposition	strain		Self-powered LED	[240]
ZnO NW/MW	CVD	Strain		Flammable/toxic (H_2, H_2S) gas sensor	[176]
ZnO NW	Electrodeposition on templet	Strain		Vibration-induced PNG	[323]
ZnO NR	Electrodeposition	Pressure		PNG	[320]
Core-shell ZnO/NiO NR	Electrodeposition	Strain		Piezoelectric modulation	[324]

(*continued on next page*)

Table 1 (*continued*)

Active materials for piezotronic devices	1D ZnO synthesis method	Fundamental function of the device	Sensitivity	Applications	Ref.
ZnO NW	Electrodeposition on templet	Strain		Piezoelectric modulation	[325]
ZnO NR	Electrodeposition	Strain		Piezoelectric modulation	[462]
ZnO NW/PMMA	VSS	Pressure, force	9.95×10^{-3} cm^2 gf^{-1}	Hybrid piezo/capacitive pressure sensor	[112]
ZnO NW/PDMS	VSS	Pressure	8.77×10^{-4} Pa^{-1}	Hybrid piezo/capacitive touch sensor	[269]
ZnO NW/PVA, ZnO NR/PVA, ZnO NR/PVA hierarchical	Hydrothermal	Pressure		Hybrid piezo/triboelectric NGs	[93]
ZnO NR	Hydrothermal	Pressure		Hybrid piezo/triboelectric NGs	[91]
ZnO NR	Hydrothermal	Force, pressure		Hybrid piezo/MOS capacitor NGs	[272]

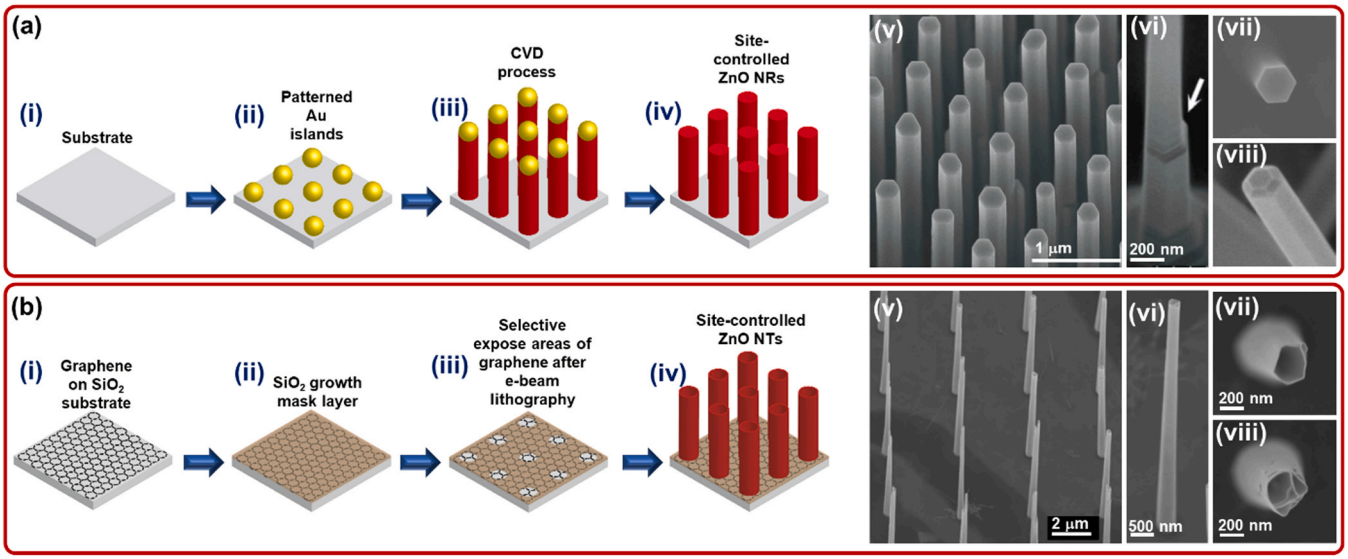

Fig. 6. 1D ZnO nanostructure arrays by CVD method. (a) Multi-stage CVD for site-specific growth of ZnO NRs: (i-iv) Schematic illustration of steps. (v) Tilted-view SEM images of ZnO NR arrays after the two-stage CVD. (vi) The details of the junction produced by the two-stage growth procedure. (vii, viii) Two different types of NR tips confirming ultra-flat top and truncated-pyramidal top structure, respectively (the scale bar is same as in (vi)). Reproduced with permission [283]. Copyright 2011, Institute of Physics. (b) Dimension- and position-controlled growth of ZnO NTs on Gr by MOCVD process: (i–iv) Schematic illustration of steps. (v) 30° tilted-view SEM images of ZnO NT arrays on Gr. (vi) 30° tilted-view SEM image of a single ZnO NT. (vii, viii) Top-view SEM images confirming two different cross-sections of ZnO NTs. Reproduced with permission [148]. Copyright 2022, Springer Nature.

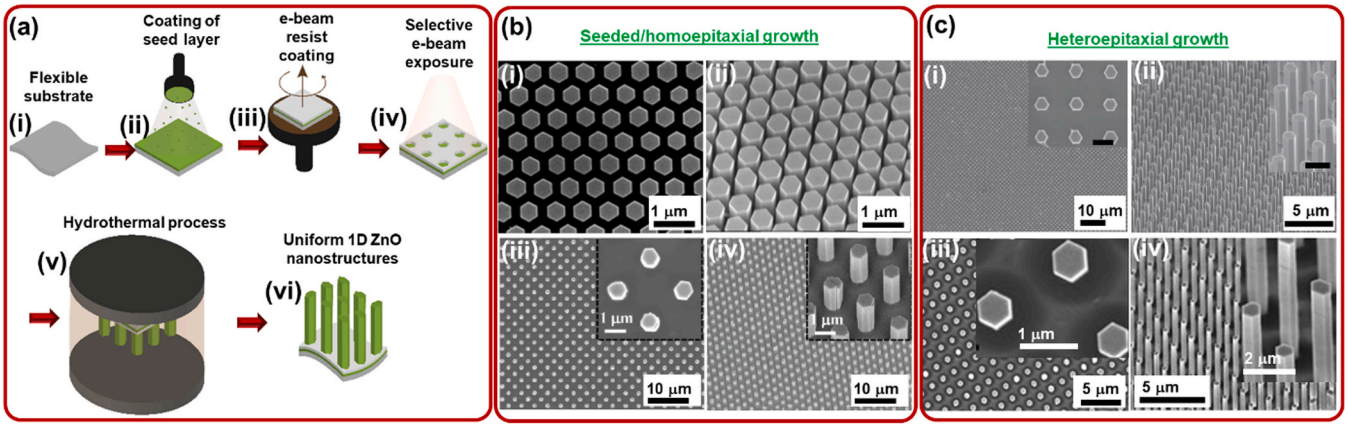

Fig. 7. 1D ZnO nanostructure arrays by hydrothermal method. (a) Schematic diagrams: (i-vi) Steps involved in a typical hydrothermal process for the fabrication of site-controlled ZnO NR arrays. (b) Seeded growth: (i) Top-view and (ii) tilted-view SEM images of ZnO NR arrays grown by hydrothermal process on patterned ZnO seed layer. Reproduced with permission [299]. Copyright 2012, American Chemical Society. (iii–iv) The top- and 45°tilted-view SEM images of vertically aligned homoepitaxially grown ZnO NW arrays on a Si substrate with a textured ZnO seed layer. Reproduced with permission [301]. Copyright 2010, American Chemical Society. (c) Heteroepitaxial growth of vertically aligned ZnO NW arrays: (i) Top and (ii) 45° tiled views of aligned ZnO NW arrays with uniform diameter, height, and 2 μm period spanning centimeter-scale area (insets are the enlarged images with scale bar size 1 μm). Reproduced with permission [190]. Copyright 2010, Wiley-VCH GmbH. (iii) Top-view and (iv) 45°-tilted-view SEM images of vertically aligned ZnO NW arrays on GaN substrate in large-scale uniform pattern (insets show the corresponding enlarged views). Reproduced with permission [301]. Copyright 2010, American Chemical Society.

patterned growth of vertically aligned and site-specific periodically distributed ZnO nanostructures by hydrothermal method and explored their piezotronic as well as piezo-phototronic properties [128,136,190,300]. Z. L. Wang and his co-workers explored the hydrothermal process for the wafer-level production of high-quality ZnO NWs [301]. S. Xu et al. demonstrated both epitaxial as well as non-epitaxial approaches for the e-beam lithography-patterned aligned growth of ZnO NWs at a low temperature (<100 °C) on general inorganic substrates such as GaN and Si, without using catalyst [300]. Y. Wei et al. utilized the homoepitaxy as well as the heteroepitaxy for the site-controlled, well-aligned growth of ZnO NWs as shown in Fig. 7(b(iii, iv)) and Fig. 7(c(iii, iv)), respectively [301]. In case of a seeded growth of ordered arrays on 1D ZnO in different substrates, the seed window and the growth conditions were found to define the geometry of the 1D ZnO and their relative alignment in the array, whereas the crystalline characteristics of the ZnO seed layer determined their alignment and crystal properties [302]. M. Parmar et al. fabricated a selective-area, well-ordered arrays of vertical ZnO NWs which were individually contacted at their base [192]. They revealed that each NW in the array could produce an electrical response to strain without the need for external biassing to take advantage of the piezotronic effect. The geometry of the solution-processed 1D ZnO nanostructures can be tuned to exhibit a wide range of morphologies, well-defined edges, and improved surface profiles. H. Liu et al. demonstrated a "windmill" pattern of size 300 μm × 500 μm containing more than 300 000 ZnO nanostructure units with various diameters and pitch lengths [303]. Hydrothermal method is utilized for large-scale production of patterned ID ZnO nanostructures in both vertically [118,140,190,300,301,304–307] as well horizontally [308,309] alignment. Additionally, for certain purposes, this approach allows the fabrication of 1D ZnO nanostructures on any substrate [309] and for any length [118,304,310] (even exceptionally long). A solution-based chemical bath deposition (CBD) approach was also employed to create selective-area, well-ordered ZnO NW arrays with adjustable polarity [311–314]. Through a polarity transfer from the nucleation surface [311], the CBD method provides the option of choosing the O- or Zn-polarity of 1D ZnO nanostructures [315,316], which has significant implications for piezotronic and piezoelectric devices. The solution process, however, also has a few drawbacks. For instance, because of the low growth temperature, crystal defects in the created nanostructures are unavoidable. Despite having high concentrations of different kinds of defects, 1D ZnO nanostructures made using a low-temperature wet chemical method are widely utilized in PNGs [139].

2.3. Electrodeposition process

Electrochemical deposition is another well-established method for growing 1D ZnO nanostructures for its utilization in piezotronics [37,317–326]. Similar to hydrothermal, it is also a two-step process in which ZnO seed layers are typically used for growing well-aligned 1D ZnO nanostructures on flexible as well as conducting substrates [37,320,321]. Growing time, precursor concentration, and externally applied voltage were the parameters in an electrochemical deposition that influenced ZnO nanostructures alignment, length, and diameter. Low setup costs, ease of use, a limitless selection of substrate possibilities, and a rapid synthesis process are all benefits of this approach. The primary issues, however, which restrict its use in piezotronics are the fabrication of good crystal quality 1D ZnO nanostructures, inadequate control in the site-specific controlled growth of 1D ZnO array, non-uniform distribution of nanostructures, etc.

Precisely designed and controlled arrays of 1D ZnO nanostructures are currently receiving significant scientific attention because of the advancement of nanofabrication and synthesis techniques. Numerous nano/microfabrication approaches have been developed for the realization of ordered arrays of 1D ZnO nanostructures. This nano/microfabrication involves a sophisticated patterning technology which includes mostly the porous templet methods [116,285,327] and various types of lithographic techniques such as colloidal/nanosphere lithography [282,299,328–331], e-beam lithography [57,130,192,196,202,295,300,311–314,332,333], photolithography [117–120,126–128,132,136,188,191,200,201,334–342], laser interference lithography [189,190,194,301,343–345], nano-imprinting [346–350], and focused ion beam lithography [351,352]. Porous template-directed approaches provide a type of powerful and universal way for generating 1D nanostructure arrays on a large scale at a relatively low cost, in contrast to cleanroom-based conventional lithography procedures. Pattern defects, lacking close-packed integration of nanostructures, reproducibility, improper shape and directionality during the nanostructure growth, and undesirable functionality issues are the main drawbacks of this process [149,319,323,353–355]. Similar to the porous templet, the colloidal/nanosphere lithography is also a simple, low-cost and time-effective method for the fabrication of well-controlled 1D ZnO nanostructure arrays [282,299,328–331]. However, there are a few limitations to colloidal lithography, such as the surface impurity, presence of voids in the pattern, limited control in the array interspacing, undesired irregularity of the array, etc [356,357]. However, a particular approach may stand out due to concerns linked to the device shape, functionality, and the type of the desired end-product or the application. In this regard, cleanroom-based sophisticated lithography techniques come out as the most appropriate technique for the fabrication of dimension- and position-controlled regular array of 1D ZnO nanostructures [57,117,118,120,311,343–345,351,352]. Excellent precision, high-resolution, flexibility in pattern size, enormous control in design parameters, highly reliable and reproducible patterns are the main advantages of these techniques. It can be noted that these pattering techniques can only be utilized to produce small-scale, well-ordered, close-packed nanostructures with excellent resolution. A summary of regularly ordered arrays of 1D ZnO nanostructures as well as nanostructure assemblies, smallest features of the patterned ZnO along with the associated patterning method, and relevant piezotronic utilizations are provided in Table 2. However, the majority of real-world applications for piezotronic technology require very homogeneous and reproducible active material manufacturing in large quantities. There may be a wide variety of other inventive approaches in addition to the ones that have been previously published. With excellent material and substrate compatibility, there is a considerable chance that more complex and desired patterns can be created on a large surface. It is possible to achieve both structural and functional complexity with smart patterning process design. Therefore, to accomplish on-demand large-area synthesis of well-ordered 1D ZnO nanostructures, the collaboration of scholars from various domains would be quite significant.

3. Design and fabrication of piezotronic devices and their arrays

The application of piezotronic sensors depends on the thoughtful novel design and fabrication of devices for sensing various mechanical forces. Typically, piezotronic sensors are fabricated by forming electrodes on either side of the active piezoelectric materials. In the case of 1D ZnO nanostructure-based devices, the fabrication process entails three crucial steps: synthesis of active materials, formation of the top (free ends of the 1D nanostructures), and the bottom (substrate side of the active materials) contacts. Usually, top contacts are formed by directly deposition of conducting materials (metals, conducting polymers, etc.). Two distinct methods are employed to create the bottom contacts. The first one deals with active material growing directly on a predefined conducting substrate. The other involves transferring the active component from the parent substrate, which is followed by the formation of the bottom contact. The procedures used to construct a device using the first technique outlined by Y. Peng et al. are schematically shown in Fig. 8(a(i–iv)) [128]. The scanning electron microscopy (SEM) images of the fabricated device are shown in Fig. 8(a(v, vi)) [128]. This kind of fabrication method is well-researched, approved by scientists, and used for a variety of piezotronic applications [118,135,

Table 2
Summary of regularly ordered arrays of 1D ZnO nanostructures as well as nanostructure assemblies, smallest features of the patterned ZnO along with the associated patterning method, and relevant piezotronic utilizations.

Material	Individual nanostructures/ nanostructure assemblies	Features of the smallest structure	Patterning method	Piezotronic utilization	Ref.
ZnO NT/Gr	Individual nanostructure	NT diameter: 200 nm pitch: 4 μm NT wall thickness: 30 nm	e-beam lithography	Breath and pulse monitor	[131]
ZnO NT/Gr	Individual nanostructure	NT diameter: 200 nm pitch: 4 μm NT wall thickness: 12 nm	e-beam lithography	Pressure-based image sensor	[148]
ZnO NWs	Individual nanostructure	NW diameter: 150 nm pitch: 2 μm	Combination of photo- and e-beam lithography	2D mapping of force	[192]
MoO_3/ZnO NW	Individual nanostructure	NW diameter: 60 nm pitch: 70 nm	Photolithography	Neuromorphic tactile sensor	[132]
ZnO MR/GaN	Individual nanostructure	MR diameter: 2 μm pitch: 3 μm	e-beam lithography	Piezo-phototronic LED	[57]
ZnO-nanofilm/ PDMS/Si MW	Individual nanostructure	MW diameter: 2 μm pitch: 5.2 μm	Photolithography	Piezo-phototronic LED, image sensor	[126]
ZnO NW/GaN	Individual nanostructure	NW diameter: 2 μm pitch: 5 μm	Photolithography	Piezo-phototronic LED	[128]
ZnO NW/GaN	Individual nanostructure	NW diameter: 1.5 μm pitch: 4 μm	Photolithography	Piezo-phototronic image sensor	[136]
ZnO NR	Individual nanostructure	NW diameter: 750 nm pitch: 1 μm	Laser interference lithography	Fine transport tuning with coupled piezotronic effect and photoexcitation	[344]
ZnO-nanofilm/Si MP	Individual nanostructure	MP diameter: top 1.7 μm, bottom 4.1 μm pitch: 5 μm	Photolithography	Piezo-phototronic LED, image sensor	[335]
ZnO NP	Individual nanostructure	NP diameter: 300 nm pitch: 500 nm	Metal nanotube membrane-based templet	Piezoelectric modulation	[116]
ZnO NR	Individual nanostructure	NR diameter: 200 nm pitch: 500 nm	Nanoimprint lithography	Robotic skin	[346]
ZnO NW	Individual nanostructure	NW diameter: 500 nm pitch: 5 μm	e-beam lithography	Piezoelectric modulation	[463]
Single-layer MoS_2/ZnO NR	Individual nanostructure	NW diameter: variable diameter pitch: 4 μm	e-beam lithography	Strain-engineering	[464]
ZnO NR	Individual nanostructure	NR diameter: 90 – 170 nm pitch: variable	e-beam lithography	Piezoelectric modulation	[465]
ZnO NW	Individual nanostructure	NW diameter: 500 nm pitch: 8 μm	nanolithography	Fingerprint sensor	[466]
ZnO NW	Nanostructure assembly	Pattern size: 20 μm pitch: 100 μm	Photolithography	Piezopotential-gated transistor, tactile image sensor	[118]
ZnO NR	Nanostructure assembly	Pattern size: 10×10 μm^2	Photolithography	Piezoelectric modulation	[120]
ZnO NW	Nanostructure assembly	Pattern size: 8×8 μm^2 NW diameter: 300 – 500 nm	Photolithography	Piezoelectric modulation	[467]
ZnO NW	Nanostructure assembly	Pattern size: 500 nm pitch: 2 μm	e-beam lithography	Piezoelectric modulation	[302]
ZnO NW	Nanostructure assembly	Pattern size: ~500 nm pitch: 10 μm	e-beam lithography	Piezoelectric modulation	[468]
ZnO NW	Nanostructure assembly	Pattern size: 1×1 mm^2	Photolithography	Piezoelectric modulation	[119]
MoO_3/CBP/TAZ/ ZnO NW	Nanostructure assembly	Pattern size: 2 μm pitch: 3 μm	e-beam lithography	Piezo-OLED-gated transistor, image sensor	[130]
ZnO NW	Nanostructure assembly	Pattern size: 20 μm pitch: 100 μm	Photolithography	Piezophototronic UV sensor	[127]
ZnO NW/ PEDOT: PSS	Nanostructure assembly	Pattern size: 5.8 μm pitch: 1.2 μm	Photolithography	Piezo-phototronic image sensor	[135]
WO_3/ZnO NW	Nanostructure assembly	Pattern size: 20×20 μm^2 pitch: 480 μm	Photolithography	Pressure visualization and recording system	[200]
ZnO NW/Si MW	Nanostructure assembly	Pattern size: 2.5 μm pitch: 2.5 μm	Photolithography	Light emission enhancement, piezo-phototronic image sensor	[201]
ZnO NW/PDMS MP	Nanostructure assembly	Pattern size: 10 μm pitch: 10 μm	Photolithography	Static and dynamic pressure-sensitive e-skins	[191]
Organic/ZnO NW	Nanostructure assembly	Pattern size: 3 μm pitch: 8 μm	Photolithography	Piezo-phototronic LED, image sensor	[334]
ZnO NW	Nanostructure assembly	Pattern size: 20 μm	Photolithography	Self-powered flexible vision e-skin	[336]
ZnO NW	Nanostructure assembly	Pattern size: 8×8 μm^2 NW diameter 150 nm	Photolithography	Energy harvester	[199]
ZnO NR, AZO NR	Nanostructure assembly	Pattern size: 2×2 mm^2	Photolithography	e-skin	[254]
ZnO NR	Nanostructure assembly	Pattern size: 1×1 cm^2	Photolithography	e-skin	[400]
ZnO NW/Si MP	Nanostructure assembly	Pattern size: 1.02 μm pitch: ~2 μm	Photolithography	Piezoelectric modulation of PNG	[211]
ZnO NW	Nanostructure assembly	Pattern size: 50 μm pitch: 100 μm	Photolithography	Piezo-phototronic solar cell	[138]
ZnO NW/Al_2O_3/ CdS	Nanostructure assembly	Pattern size: 20 μm pitch: 300 μm	Photolithography	Piezopotential-gated transistor as optoelectronic synapses	[342]

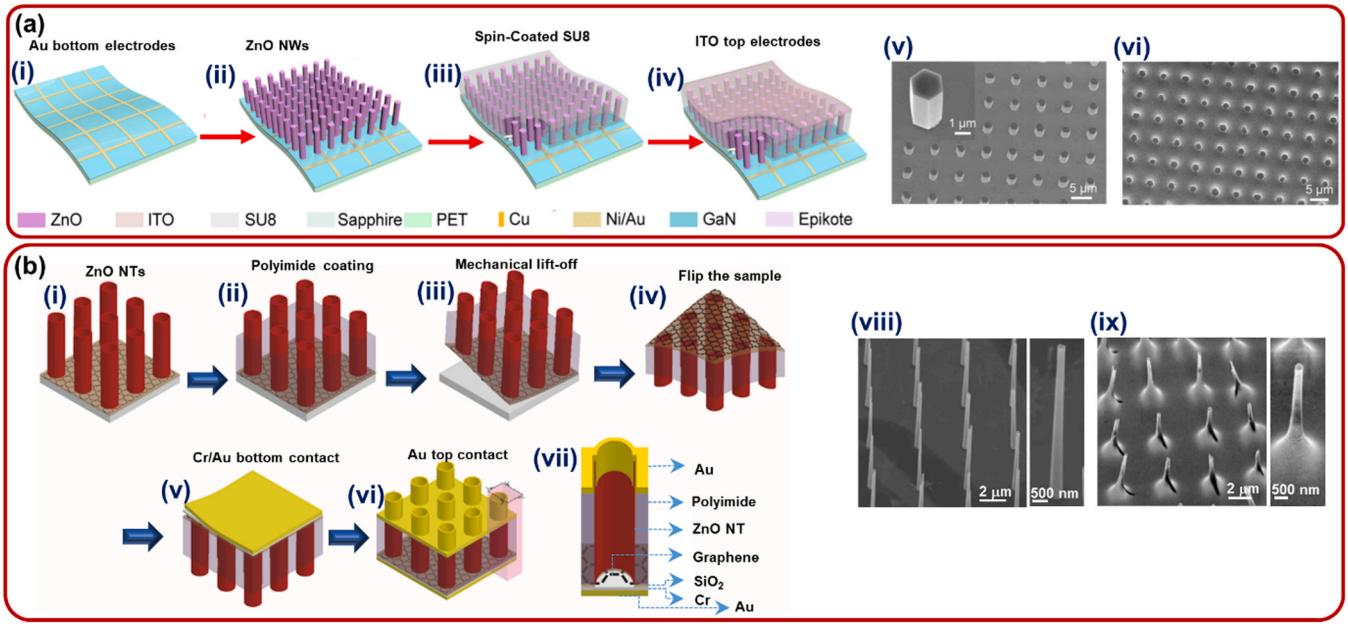

Fig. 8. Different methods of flexible device fabrication. (a) Fabrication of devices by direct growth of active material on a predefined electrode arrays on a flexible substrate: (i–iv) Schematic fabrication process of the flexible ZnO NW-based device array. (v) SEM image of the as-grown ZnO NW arrays on the flexible p-GaN film, with an average diameter of 2 μm, and length of 4 μm. (vi) SEM images corresponding to ITO layer deposited onto the wrapped and etched ZnO NWs as a top common electrode. Reproduced with permission [128]. Copyright 2019, Elsevier. (b) Fabrication of devices by the transfer of active material to a flexible substrate: (i–vii) Schematic illustration of steps for the fabrication of the ZnO NT-based pressure sensors. (vii) The schematic cross-section of a device indicating each layer within it. (viii) 30° tilted-view SEM images of (left) ZnO NT arrays on Gr along with a (right) single ZnO NT. (ix) 30° tilted-view SEM images of (left) ZnO NT-based pressure sensor arrays on Gr along with a (right) single ZnO NT-based pressure sensor. Reproduced with permission [148]. Copyright 2022, Springer Nature.

136,192,200,358]. The steps in the second approach of device fabrication, as reported by J. B. Park et al., are schematically shown in 8(b (i-vii)) [148]. Fig. 8(b(viii, ix)) depicts the SEM images of the fabricated device [148]. They used the ZnO NTs on Gr as an active material to construct pressure sensors. Utilizing the weak vdW force between the bottom Gr and the SiO_2 substrate, an efficient lift-off technique was used for the ZnO NT/Gr. For effective material transfer, the free-standing ZnO NTs were supported by a polyimide layer. Following the lift-off procedure, Schottky junctions were made on the exposed tips of the ZnO NTs by depositing a 100 nm Au layer. To produce ohmic connections between ZnO, Gr, Cr, and Au, the freestanding NT arrays were then turned over, and a 10/90 nm Cr/Au layer was created on the bottom side. In order to investigate their pressure response characteristics, the freestanding pressure sensing devices were finally transferred to the necessary foreign substrates.

Vertical 1D nanostructures have demonstrated to be very difficult to construct high-density independently operated two- or three-terminal device array architectures from them [134]. A two-terminal crossbar electrode array was developed for fabrication high-density, individually addressable device arrays to avoid extreme device complexity [118, 134]. By addressing the crossbar array electrode nanodevices, J. B. Park et al. demonstrated two-terminal piezoelectric tactile sensor arrays with a very high resolution [148]. Dimension- and position-controlled, vertically aligned ZnO NTs on Gr were used as an active piezoelectric material for the tactile sensor matrix. The electrode arrays on the top and bottom ends of the ZnO NTs were defined via e-beam lithography. The step-by-step process of the 8 × 8 matrices for the device is schematically shown in Fig. 9(a(i–v)) along with a single pixel in Fig. 9(a(vi)) containing 5 × 5 ZnO NTs. SEM images at different stages of the fabrication process were also shown in Fig. 9(a(vii–xi)). A magnified view of the completed device as a SEM image is shown in Fig. 9(a(xii)) [148]. Y. Tchoe et al. fabricated cross-bar arrays of electrodes in a similar way where each ZnO NTs can be addressed individually by ultra-violet (UV) light illumination [134]. Piezo-phototronic devices were created using vertically aligned ZnO NWs by X. Han et al [127]. They demonstrated a UV sensor array of 32 × 40 pixels, each of which had a Schottky-contacted UV photodetector made of ZnO NWs and Au nanopatterns. Fig. 9(b(i–v)) and 9(b(vi–x)) provide the schematic representation and associated optical pictures of the fabrication processes, respectively. The schematic representation of the entire ZnO NW-based UV sensor array is shown in Fig. 9(b(xi)), and the corresponding SEM image is shown in Fig. 9(b(xii)). The spatial resolution of 100 μm (254 dpi) was achieved by designing the ZnO NWs pattern with 20 μm × 20 μm in dimension and 80 μm in spacing [127].

In order to create an active taxel-addressable pressure/force sensor matrix for tactile imaging, W. Wu et al. proposed large-array three-dimensional (3D) circuitry integration of piezotronic transistors based on vertical ZnO NWs [118]. The schematic drawing, optical and SEM images, and topological profile image of the assembled 3D SGVPT array are all displayed in Fig. 9(c). The fundamental building block of the nanoarray device was a cluster of vertically grown ZnO NWs with a height of 30 μm (Fig. 9(c(iv))), which were synthesized by a low-temperature hydrothermal method. Crossbar electrodes joined the two ends of each element, enabling each unit addressable individually. The actual nanoarray device featured a pixel density of 92 × 92 per square centimeter and a spatial resolution of 234 dpi [118].

X. Han et al. successfully integrated WO_3 electrochromic devices by the integration of a ZnO-NW-matrix pressure sensor which was efficient enough to realize simultaneously the spatial pressure visualization and recording [200]. Fig. 9(d) illustrates the structure and fabrication process of the pressure visualization and recording system along with the associated SEM images [200]. Through an Au electrode layer, each pixel was connected to a particular group of ZnO NWs on top of the NWs. The ZnO NW sensors used the piezotronic effect to record the distribution of external pressures, and the electrochromic device directly expressed this information by changing the color. Furthermore, this device was efficient for independently recording the external pressure distribution through the color memory effect of the WO_3 material. Such systems have promise for use in smart robots, military applications, and human-electronic interfaces [200].

4. Integration of 1D ZnO nanostructures on a substrate/supported matrix for flexible and wearable application

Flexible piezotronic sensors have recently drawn a great deal of research attention due to their numerous applications in robotics, prosthetics, human-machine interfaces, and the monitoring of human activity and health [10,67,147,153,230–234,359,360]. For instance, piezotronic pressure sensors that can detect pressures produced by internal or external bodily processes are crucial for assessing physiological health and preventing injuries. The successful integration of 1D ZnO

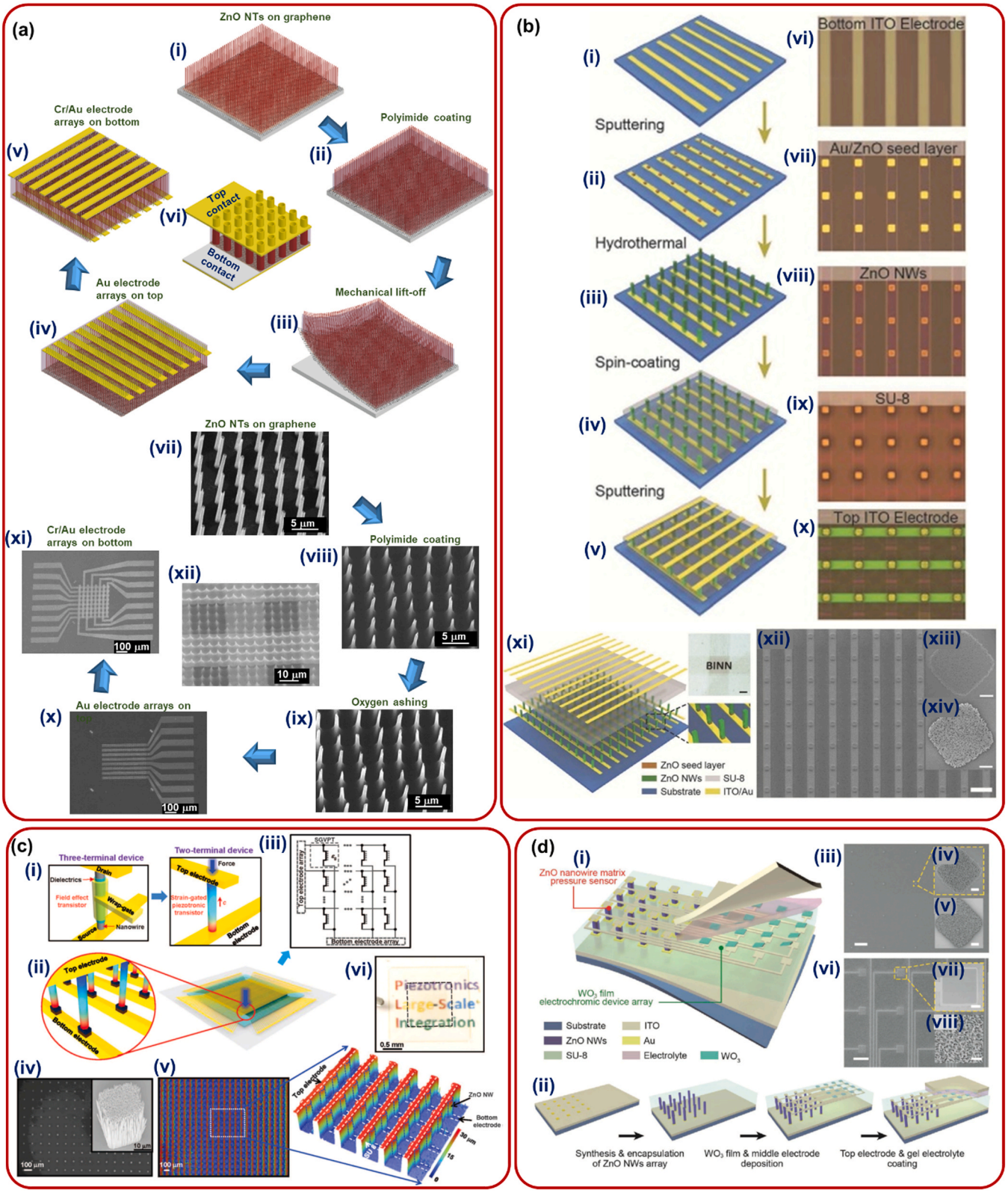

(caption on next page)

Fig. 9. Different types of ordered arrays of 1D ZnO nanostructure-based devices. (a) Addressable pressure sensors by using ZnO NTs on Gr: (i–v) Schematic illustration of the steps for the fabrication of cross-bar array electrodes, and (vi) enlarged view of an addressable device containing 5 × 5 ZnO NTs. (vii–xi) SEM images at different stages of the fabrication of individually addressable device arrays. (xii) SEM image of a complete device. SEM images in (vii–xii) are 30° tilted. Reproduced with permission [148]. Copyright 2022, Springer Nature. (b) ZnO NW-based piezo-phototronic device array for UV sensing: (i–v) Schematic illustration and (vi–x) the corresponding optical images of the device fabrication process. (xi) schematic illustration of the complete structures of the ZnO NW-based UV sensor array (inset is an optical image of the as-fabricated device with a scale bar of 1 mm). (xii) SEM image of the as-fabricated device before spin-coating a layer of SU-8, the scale bar is 100 μm. ZnO NW (xiii) before and (xiv) after spin-coating a layer of SU-8, the scale bar is 5 μm. Reproduced with permission [127]. Copyright 2015, Wiley-VCH GmbH. (c) Taxel-Addressable matrix of piezopotential-gated vertical-NW piezotronic transistors (SGVPT): (i) Comparison between three-terminal voltage-gated NW FET (left) and two-terminal piezopotential-gated vertical piezotronic transistor (right). The color gradient in the strained SGVPT represents the strain-induced piezopotential field. Red and blue colors indicate positive and negative piezopotential, respectively. ZnO NWs in SGVPT were grown along the *c*-axis (red arrow). (ii) Schematic illustration of a 3D SGVPT array with taxel density of 92 × 92 and scheme for spatial profile imaging of the local stress (indicated by the downward blue arrow). The zoom-in schematic shows the corresponding enlarged view. (iii) Equivalent circuit diagram of the 3D SGVPT array. (iv) SEM of SGVPT array taken after etching back the SU-8 layer and exposing top portions (~20 μm) of the ZnO NWs. The inset shows a 30° tilted-view of the exposed ZnO NWs for a single taxel. (v) Topological profile image of the SGVPT array (top-view). At right, a 3D perspective view of the topological profile image reveals the vertical hierarchy of the SGVPT assembly; the color gradient represents different heights, as indicated. (vi) Optical image of the transparent 3D SGVPT array on a flexible substrate. The peripherals are the pads of the device, and the central region highlighted by black dashed lines is the active array of 3D SGVPTs. Reproduced with permission [118]. Copyright 2013, American Association for the Advancement of Science. (d) Pressure visualization and recording (PVR) system from ZnO NW arrays: (i) Schematic illustration of the structure of the PVR system. (ii) Schematic of the fabrication steps. (iii) SEM image of the as-fabricated ZnO NW matrix before spin-coating a layer of SU-8 photoresist. The scale bar is 200 μm. Enlarged images of the ZnO NWs (iv) before and (v) after spin-coating the SU-8 layer. The scale bars are 5 μm. (vi) SEM image of the as-fabricated middle Au electrode and WO_3 film array. The scale bar is 200 μm. (vii) The WO_3 film deposited on the ITO electrode and (viii) its magnified view. The scale bars are 20 μm and 200 nm, respectively. Reproduced with permission [200]. Copyright 2017, Wiley-VCH GmbH.

nanostructure into a flexible platform depends on a few key factors. These are, the properties of the flexible substrate, the selection of the insulating material, the flexibility of the host matrix, and the method of integration or embedding.

One of the essential components of flexible piezotronic devices is a flexible substrate. High stretchability, superior mechanical strength, light-weight, transparency, and low cost are all desirable qualities for flexible substrates. Additionally, it must be also thermally and electrically insulated in normal and stretched conditions. PET [128,200,334], Polydimethylsiloxane (PDMS) [191], SU-8 [118,128,200], polyimide [131,134,148], polymethyl methacrylate (PMMA) [136,334], and PVDF [120] are well-accepted by the researchers as a flexible and stretchable substrate for the flexible piezotronic devices. In general, the flexibility of 1D ZnO nanostructure-based piezotronic devices is achieved by generating a flexible/bendable active material that can be bonded to a flexible substrate. The flexible active material is typically prepared to occupy the 1D ZnO's intermediate space, which acts as a filler. With characteristics resembling those of the flexible substrate, the filler would need to serve as a host material. Additionally, it also needs to be chemically stable and unable of influencing the piezoelectric characteristics of 1D ZnO nanomaterials. It might also serve as a channel of insulation between the counter electrodes. Sometimes the filler is selected in a way that results in HSs with the ZnO structures for additional functionality.

The integration of the 1D ZnO nanostructures into the flexible substrates comes next, and this has been considered to be a very challenging task from a fabrication point of view. By directly manufacturing ZnO nanostructures on a flexible substrate, a group of researchers has created 1D ZnO-based flexible piezotronic sensors [128,200,305]. These are some drawbacks of adopting this technique. For example, high-quality ZnO requires high growth temperature which can affect the substrate enormously. High temperature growth can also induce additional impurities to the ZnO nanostructures. Post-annealing, surface modification, and HSs formation with ZnO nanostructures are also a challenge. Furthermore, the creation of patterns is difficult to generate dimension- and position-controlled ZnO nanostructures.

Transferring the sensor or active material from a rigid substrate to a flexible foreign substrate is an alternative strategy. Polyimide [131,134,148] PDMS [240] and PMMA [361] are widely used to transfer the active materials. Wide range of substrate selection and ability to fabricate high-quality/close-packed sensors are the major advantages for this case. The transfer process has also the potential to control the alignment, for example vertically aligned array to its horizontal array [240]. Additionally, the flexible polymers employed in the transfer process can support the packaging of the respective devices, which can improve their mechanical robustness and shield them from harmful invasive chemicals [131,240]. A common issue in the transfer process is polymer contamination, damage, or folding of layered materials, which may significantly reduce their electrical properties and hinder the quality of the interface along with the associated devices.

5. Performance of piezotronic devices

In the past two decades, researchers have devoted a great deal of attention to the implementation of piezoelectric 1D ZnO nanostructure and its arrays into piezotronic devices. Pressure/force sensing, strain sensing/modulation, and the piezopotential-gated transistors are the three main principles upon which piezotronic devices, particularly sensors, operate. To sustain the significant performance of the 1D ZnO-based piezotronic devices, major focus is therefore needed for exploring these fundamental functions. This section will discuss about the performances of the above-mentioned functions on various types of piezotronic devices, emphasizing the device performances, its controlling and improvement strategies, the role of various 1D architectures in device performances, multifunctional natures, flexible and portable characteristics, and commercial viability. Table 1 summarize the different 1D ZnO nanostructured-based piezotronic devices and their dependence on the above-mentioned fundamental functionalities.

5.1. Pressure sensors

ZnO has excellent piezoelectric properties, which make it extremely responsive to impulses caused by pressure. Thus, numerous pressure sensors based on various ZnO nano-architectures, particularly 1D nanostructures, have been studied in recent years. High-stability ZnO film was initially introduced as a piezoelectric pressure sensor because of the large area and easy fabrication process [362]. The advantages of 1D ZnO nanostructures over bulk or thin film forms make them more appealing to researchers. In 2006, Z. L. Wang group unveiled a single ZnO NW-based pressure sensor [165]. Since then pressure sensors based on ZnO nanomaterials have undergone rapid development from single NW to bundle of NWs, NW/NR/NT arrays and their different forms of HSs. K. C. Pradel et al. fabricated a pressure sensor based on an ultra-long Sb-doped p-type single ZnO NW, which was up to 60 μm in length [58]. Piezoelectric pressure sensors were fabricated by using vertically aligned and position- and dimension-controlled ZnO NT arrays grown on Gr layers [131,148]. The device fabrication steps are shown previously in Fig. 8(b(i–vii)). Schematic representations of the devices are shown in Fig. 10(a(i–iii) along with a cross-section of such a typical device revealing the layers that are present and the measurement system that was utilized to assess the performance of the ZnO NT-based pressure

sensors [131]. Fig. 10(a(iv)) displays the real-time current response of a prototype from one of these devices at a fixed bias of 0.4 V and various applied pressures. These sensors demonstrated great sensitivity (−4.4 kPa^{-1}) due to the ultrathin walls and high aspect ratios of the ZnO NTs, as illustrated in Fig. 10(a(v)). In addition, they demonstrated a fast response time, a stable response with enormous durability, and mechanical flexibility [131]. The effect of NT wall thickness and the aspect ratio on the pressure sensing performances were investigated and revealed that the relatively low wall thickness and large length of the ZnO NTs suggest a relatively high sensitivity to external pressures [131]. Furthermore, J. B. Park et al. demonstrated how pressure sensing capabilities may be controlled by altering the quantity of ZnO NTs used in a tiny sensor [148]. Schematic representation in Fig. 10(b(i)) shows the measurement system for applying ultra-low pressures, while Fig. 10(b (ii) compares the pressure sensing performances from sensors containing different no. of ZnO NTs. The investigation revealed that the sensitivity was unaltered by reducing the no. of ZnO NTs while the detection range was reduced [148]. M. Ha et al. developed a highly-sensitive pressure sensor for static and dynamic pressure sensing based on ZnO NWs arrays on the PDMS MP arrays [191]. The hierarchical and interlocked structures of the sensor showed a high sensitivity of − 6.8 kPa^{-1}, an ultrafast response time of < 5 ms, a low pressure detection limit of 0.6 Pa, as well as a high vibration frequency of 250 Hz for sound detection [191]. A long-range textile piezoelectric pressure sensor (T-PEPS) based on ZnO NR arrays was developed by Y. Tan et al. for wearable applications [59]. Such sensors displayed remarkable performance, including a low detection limit of 8.71 Pa, high output voltage of 11.47 V, and good mechanical stability. The schematic design of the prototype T-PEPS illustrating the various layers is shown in Fig. 10(c(i)), and the piezoelectric sensing mechanism of the T-PEPS is shown in Fig. 9(c(ii-iii)).

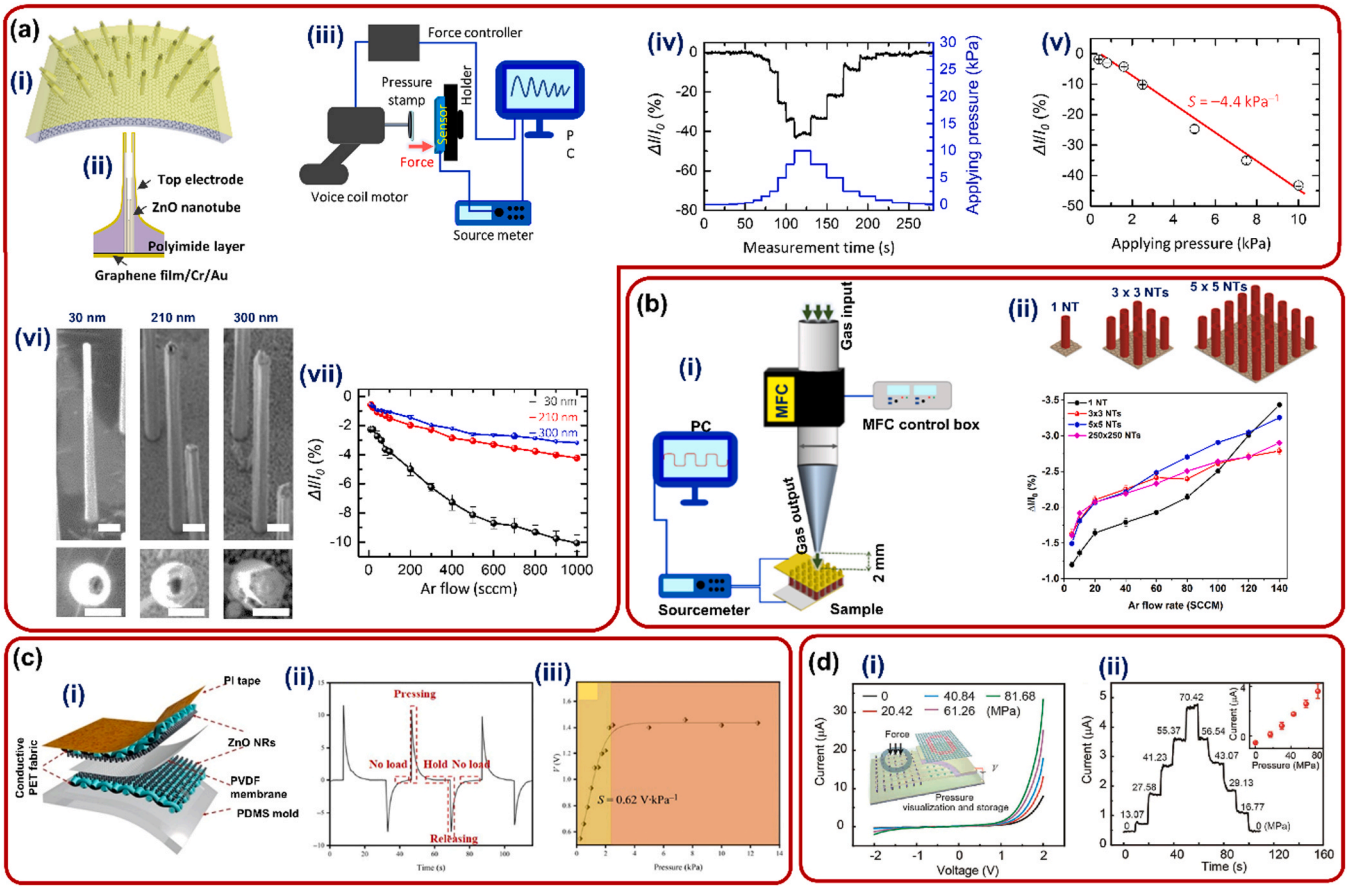

Fig. 10. Piezoelectric pressure sensors. (a) A pressure sensor fabricated by using ZnO NT arrays heteroepitaxially grown on Gr: (i) Schematic representation of a complete pressure sensor. (ii) A schematic cross-section of a prototype indicating each layer within it. (iii) Schematic diagram of the measurement system used to characterize the performance of the ZnO NT pressure sensors. The pressure was applied by a voice coil motor (VCM). (iv) Real-time current response of ZnO NT pressure sensors under a fixed bias of 0.4 V with different applied pressures. (v) Current varying ratio ($\Delta I/I_0 = (I\text{-}I_0)/I_0$) of ZnO NT pressure sensors under different applied pressures. The linear fit indicates a sensitivity of − 4.4 kPa^{-1}. (vi) SEM images of ZnO NTs with different wall thicknesses, which are 30, 210, and 300 nm having the same length of 18 μm. The top and bottom panels show tilted and cross-sectional views, respectively. The scale bars in the top and bottom panels are of 1 μm and 500 nm, respectively. (vii) Comparison of the pressure responses of the corresponding devices as a function of the applied gas flow rate. Reproduced with permission [131]. Copyright 2021, Springer Nature. (b) Comparison of pressure responses by the variation of sensor size: (i) Schematic representation of the experimental setup when the pressure was imparted by a constant flow of inert gas. (ii) Characteristics of pressure sensors containing single, 3 × 3, 5 × 5, and 250 × 250 ZnO NTs, respectively which compares the real-time pressure responses with different argon gas flow rates ranging from 5 to 140 SCCM. The upper panel shows the schematics of single, 3 × 3, and 5 × 5 ZnO NTs, respectively, involved in those tiny pressure sensors. The bottom panel shows the responses as a function of argon flow rate from pressure sensors containing different number of ZnO NTs. Reproduced with permission [148]. Copyright 2022, Springer Nature. (c) A high-performance textile piezoelectric pressure sensor (T-PEPS) based on ZnO NR arrays: (i) Schematic design of the sensor explaining different layers. (ii–iii) The piezoelectric sensing mechanism of the T-PEPS. (ii) Output voltage of T-PEPS under different states. (iii) Output voltage response under different pressures. The sensitivity of T-PEPS was 0.62 V·kPa^{-1} in the pressure range of 0 − 2.25 kPa. Reproduced with permission [59]. Copyright 2021, Springer. (d) Piezotronic effect on pressure sensing by a PVR: (i) I–V characteristics of a single ZnO NW pixel under various applied pressures. The inset shows the schematic of a PVR upon applying a pressure on a single pixel. (ii) I–t characteristics of the ZnO NW pixel under various pressures to illustrate the stability and sensitivity at + 1 V. The inset displays the current changes under external pressures at + 1 V. Reproduced with permission [200]. Copyright 2017, Wiley-VCH GmbH.

The sensitivity of the sensor was 0.62 $VkPa^{-1}$ in the pressure range of 0–2.25 kPa [59]. X. Han et al. introduced a WO_3-film electrochromic device array (10 × 10 pixels) and a ZnO-NW-matrix pressure sensor for dynamic pressure visualization and recording (PVR) system with a spatial resolution of 500 μm [200]. The I-V and I-t characteristics of a PVR device are shown in Fig. 10(d(i)) and (d(ii)), respectively. Each PVR pixel was used as a pressure sensor to accurately and satisfactorily measure dynamic pressure in the range of 0–70.42 MPa. By adopting a ZnO NN/PVDF hybrid structure, K. U. Shin et al. demonstrated a highly sensitive, wearable, and wireless pressure sensor based on the organic-inorganic heterojunction [153]. Notably, the hybrid nanomaterials had a minimum detectable pressure of only 4 Pa. Heart rate monitoring was another application of the gadget. Through the use of ZnO and Al-doped ZnO (AZO) NRs on a flexible PDMS substrate, M. S. Suen et al. demonstrated a flexible, and highly sensitive pressure sensor [254]. Under static and dynamic pressure, the high-aspect-ratio interlocked ZnO NR structures demonstrated good sensitivity (ZnO: −0.768 kPa^{-1}, AZO: −0.223 kPa^{-1}). The devices were also used for various strain sensing applications [254].

According to recent research on multifunctional pressure sensors, the overall performance of 1D ZnO nanostructure-based pressure sensors can be enhanced by the effective coupling of piezoelectric, semiconducting, and optical properties. A high-performance pressure sensor was developed by J. Sun and co-workers by exploiting the piezo-phototronic effect of the n-ZnO NW array/p-Cu_2O film structure [73]. The switch ratio and sensitivity were improved by applying pressure (from 0 to 8 P_0, where P_0 was the initial pressure) and light illumination (0–11.7 mW cm^{-2}), reaching values of 376% and 918%, respectively [73]. Based on piezotronic and piezo-phototronic phenomena, B. Yin et al. demonstrated a high-performance pressure sensor from a ZnO/NiO core/shell NR array [72]. The switch ratio and sensitivity of the pressure sensor were improved by around 353% and 445%, respectively, under UV (365 nm) illumination [72]. The enhancement of the performance of pressure sensors based on 1D ZnO nanostructures was explained by modulating the generation, separation, and recombination of photo-generated electron-hole pairs during optoelectronic processes in piezoelectric-semiconductor materials [72,121]. B. C. Kang et al. developed wearable pressure/touch sensors based on hybrid ZnO NW/PDMS dielectric composites. Investigation into the impact of ZnO NW incorporation on the performance of pressure sensors led to an improvement in sensitivity of 8.77×10^{-4} Pa^{-1} in low-pressure regions compared to pristine PDMS (1.32×10^{-4} Pa^{-1}). The combination of the hybrid dielectric composites' piezoelectric characteristics and increased effective dielectric constant was attributed to this improvement [269].

5.2. Strain sensors

In the case of 1D ZnO nanostructures, a strain sensor can provide the quantitative deformations of the active material under various types of strains caused by its stretching, compressing, sheering and twisting, etc. A strain sensor based on a single ZnO piezoelectric fine wire (PFW) (Fig. 11(a)) was first introduced by J. Zhou et al. in 2008 [170]. Thermal evaporation was used to create ZnO MWs with lengths ranging from hundreds of microns to millimeters and diameters between 2 and 6 μm. A single ZnO MW was transferred to a flexible polystyrene substrate at first. As schematically depicted in Fig. 11(a(i)), each end of the MW was

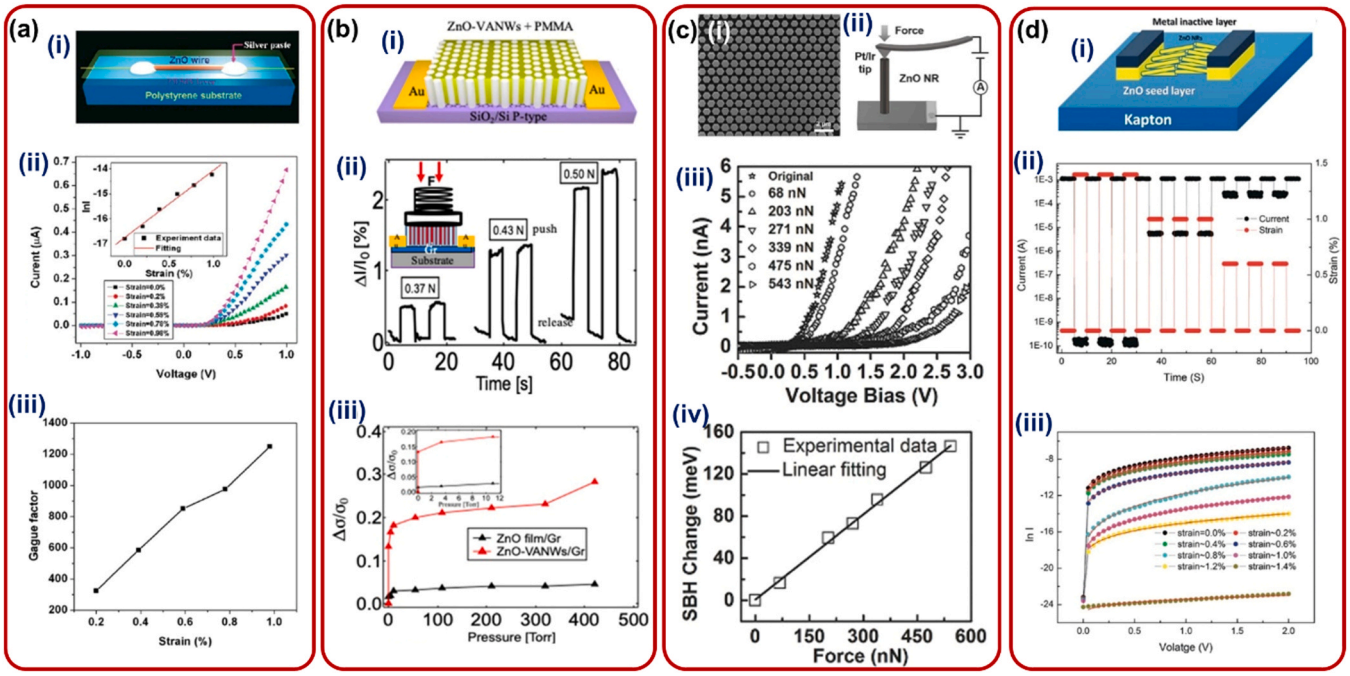

Fig. 11. Piezoelectric strain sensors. (a) A single ZnO PFW-based strain sensing device: (i) Schematic of the strain sensor. (ii) I−V characteristics of a prototype device under different strains. Inset is ln I (in a unit of ampere) as a function of the applied strain. (iii) GFs derived from (ii) as a function of strain. Reproduced with permission [170]. Copyright 2008, American Chemical Society. (b) A ZnO NWs/Gr nanohybrid strain sensor: (i) Schematic description of the sensor passivated with PMMA layer. (ii) Dynamic strain response at different forces of 0.37, 0.43, and 0.50 N. The inset shows a schematic of the spring apparatus for applying force. (iii) Strain response ($\Delta\sigma/\sigma_0$) as a function of gas pressure measured from ZnO NWs/Gr (red) and ZnO film/Gr (black) devices. Reproduced with permission [220]. Copyright 2020, American Chemical Society. (c) A strain sensor from dimension- and site-controlled ZnO NR arrays on a photoresist templet: (i) SEM images on the ZnO NR arrays. (ii) Schematic of conductive-AFM setup for transport measurement. (i) Measured I–V curves of Zn-terminated ZnO NR under compressive force. (j) Calculated SBH change as a function of force. Reproduced with permission [344]. Copyright 2017, Wiley-VCH GmbH. (d) A ZnO bridging NR strain sensor: (i) Schematic diagram of the fabricated ZnO device. (ii) Current response of the strain sensing device grown with nutrient solution concentration of 25 mM to different stretch strains. (iii) I−V characteristics of a strain sensing device with ultrahigh "on" – "off" ratio at different stretch strain and their corresponding fitting using the thermionic emission-diffusion theory. The red lines are the theoretical fit of ln I−$V^{1/4}$. Reproduced with permission [365]. Copyright 2011, American Chemical Society.

then connected to the substrate using Ag paste. For protection, the device was encapsulated with a PDMS layer. The strain sensor displayed a great sensitivity, high stability, and a fast response with a gauge factor (GF) of up to 1250. The ZnO PFW strain sensor on a flexible substrate was triggering its fascinating prospective applications in biomedical sciences and cell biology [170]. A flexible strain sensor with vertically aligned ZnO NWs arrays was reported by W. Zhang et al [363]. This strain sensor outperformed the strain sensing device based on a single ZnO NW, yielding GF of up to 1813 [363]. M. Panth et al. demonstrated a ZnO NW/Gr/PET-based high sensitive strain sensors (Fig. 11(b(i–iii)) with a high sensitivity of up to 3.15×10^{-2} kPa^{-1}, at lower pressures of 1.1×10^{-6} −11 Torr, together with a fast response time of ~0.10 s [220]. As compared to strain sensors with a similar structure but a polycrystalline ZnO seed layer on Gr during the growth of vertically aligned ZnO NWs, they demonstrated 7 times enhanced sensitivity for the seedless growth of ZnO NWs on Gr [220]. ZnO NR's transport property variation with strain and light was described by P. Lin et al [344]. Large-scale patterned and polarity-controlled ZnO NR arrays with uniform morphology (Fig. 11(c(i))) were utilized for manipulating the surface polarity-dependent electrical transport at Pt/Ir–ZnO heterointerface under various amount of strain. By altering the deflection voltage with the atomic force microscopy (AFM) tip as illustrated in Fig. 11 (c(ii)), when different vertical compressive forces were applied. By increasing the applied force gradually, they revealed that the turn-on voltage of Pt/Ir–ZnO Schottky contact was increased from 68 to 543 nN (Fig. 11(c(iii))). Furthermore, they estimated the change in SBH with the variation in compressive force as shown in Fig. 11(c(iv)) [344]. Recently, Q. Yu et al. introduced a strain sensor based on piezotronic tunneling junction with structure of Ag/HfO_2/n-ZnO NW/MW at device scale [364]. The piezotronic tunnelling strain sensor outperformed conventional Schottky-barrier-based ZnO NW strain sensors, having a high on/off ratio of 478.4 and a high GF of 4.8×10^5 at the strain of 0.10% [364]. N. Liu et al. have demonstrated a novel, fully packaged strain sensor based on ZnO bridging NRs [365]. The sensors were constructed using a single hydrothermal reaction to grow ZnO NRs on a flexible Kapton substrate. A PDMS layer was then used to completely package the sensors. Fig. 10(d(i)), 10(d(ii)), and 10(d(iii)) show the schematic diagram of the fabricated ZnO device, the strain sensor's current responses at various strains, and their I-V characteristics, respectively. The ZnO bridging NR strain sensors feature large GFs (up to 6.7×10^8), ultrahigh scale (10^7) scale "on"/"off" ratios, good stability, and a fast response time [365].

With the rapid development of fabrication technologies, various kinds of high-quality 1D ZnO materials, newly introduced heterointerfaces, development of piezotronics properties and their improvement strategies, and the advancements of flexible platform have helped the 1D ZnO-based strain sensors to undergo significant progress in flexible and stretchable electronics for their wide range of applications ranging from e-skins, human-machine interfaces, novel wearable/implantable human-health monitoring devices to disease diagnosis. The potential applications of 1D ZnO-based strain/pressure sensors are summarized in Table 1 and further discussed in Section 6. Signal interference from atmospheric disturbances such as sound, light, temperature, weather, humidity, wind, and other factors, as well as external sources like capacitive, resistive, and photon-induced responses, is one of the primary drawbacks for strain/pressure sensors. Plenty of approaches, including material engineering, HS/functionalization, encapsulation of the devices, decoupling of outputs, etc., have been implemented by researchers to address this issue, and in the years to come, research on these topics will continue to be one of the frontier topics.

5.3. Piezopotential-gated transistors

In 2006, X. Wang et al. introduced a ZnO NW-based piezoelectric FET (PE-FET), in which the source to drain current was controlled by the strain-induced piezopotential [165]. A ZnO NW (or NB) that bridged across two ohmic contacts was the basic building block of a PE-FET. SEM images of the ZnO NW under various bending conditions are presented in Fig. 12(a(i)), and the corresponding I-V characteristics are displayed in Fig. 12(a(ii)). The schematic diagrams representing the mechanisms responsible for the current modulation, which were computed from FEM analysis, are shown in Fig. 12(a(iii–v)). The carrier trapping effect and the generation of a charge depletion zone during elastic deformation were considered as the possible mechanisms for the PE-FET. Thereafter, 1D ZnO-based piezopotential-gated FETs have been the subject of extensive research over the past years [105,150,163,167,366]. Piezo-gated transistors based on vertical ZnO NWs were integrated into a substantial number of 3D circuits by W. Z. Wu et al. as an active taxel-addressable pressure/force sensor matrix for tactile imaging [118]. Using the vertically aligned ZnO NWs topped with Au droplets fabricated on GaN/sapphire substrates using a VLS method, piezopotential-gated piezotronic transistors had also been realized [175]. When Ag paste placed over the as-formed ZnO conductive layer served as the source and Au droplets at the tips of the NWs as the drains, each NW functioned as a single transistor. Through the use of a conductive AFM probe, the drain-source voltage was applied. The gate voltage was the inner crystal piezoelectric potential generated along the NWs by the stress applied using the AFM probe (Fig. 12(b(i)). Strain-dependent I-V characteristics were observed in the ZnO NW transistors which showed typical rectifying behavior under different applied forces (Fig. 12(b(ii))) [175]. The transistor operated in both forward and reverse bias states to satisfy a variety of applications, including forward biased transistors as LEDs and reverse biased transistors for photodetectors [175].

Based on an ultralong Sb-doped p-type ZnO NW, K. C. Pradel et al. constructed piezopotential-gated piezotronic transistors [58]. The piezoelectric outputs of various concentrations of Sb-doped ZnO NWs were realized using conductive AFM measurements (Fig. 12(c(i–iii))). Undoped n-type ZnO NW samples displayed a negative output voltage, whereas Sb-doped NW samples exhibited a positive one. A schematic representation is shown in Fig. 12(c(iv)) demonstrating the difference in the screening of piezo-polarization charges, and the opposite polarity of piezoelectric outputs between transversely bent n- and p-type NWs. Because of the larger screening effect of the free charge carriers, a significantly reduced piezoelectric output was also noted for the sample that was more heavily doped. For positive drain bias, the current through the device increased under tensile strain and decreased with compressive strain (Fig. 12(c(v))). On the other hand, the reverse pattern was observed when the drain bias was negative, with the current rising under compressive strain and falling with increasing tension. Suitable band diagrams (Fig. 12(c(vi–viii)) were used to demonstrate the mechanism of the piezotronic effect [58].

Recently, X. Han et al. demonstrated a two-terminal ZnO NW/Al_2O_3/CdS heterojunction-based optoelectronic synapses (ZAC-OS) array with strain-modulated synaptic weight (Fig. 12(d(i–vi)) [342]. The ZAC-OS device could react to light stimuli in a neuromorphic way because of the strong UV and green light absorption, as well as the persistent photoconductivity (PPC) effect of ZnO NWs and CdS film. Through the piezo-phototronic effect, the device's synaptic weight was flexibly manipulated by external strain-induced piezopotential, demonstrating a controllable change of the excitatory postsynaptic current (EPSC) in multilevel, strengthened memorization of the EPSC, and improvement in the rate and efficiency of image recognition. The ZAC-OSs device's features indicate that it could find use in robotic vision, neuromorphic computing, adaptive visual-perception systems, etc [342].

Piezopotential-gated FET was also realized for a MoS_2/ZnO 2D/1D hybrid structure, where a few-layer MoS_2 flake acted as a conductive channel and piezoelectric ZnO NWs acted as a gate triggered by local pressure [174]. The source-drain current can be tuned for 25% at a 6.25 MPa applied stimulus on a packaged device, which is equivalent to the effects of adding an additional 5 V to the back gate voltage. This

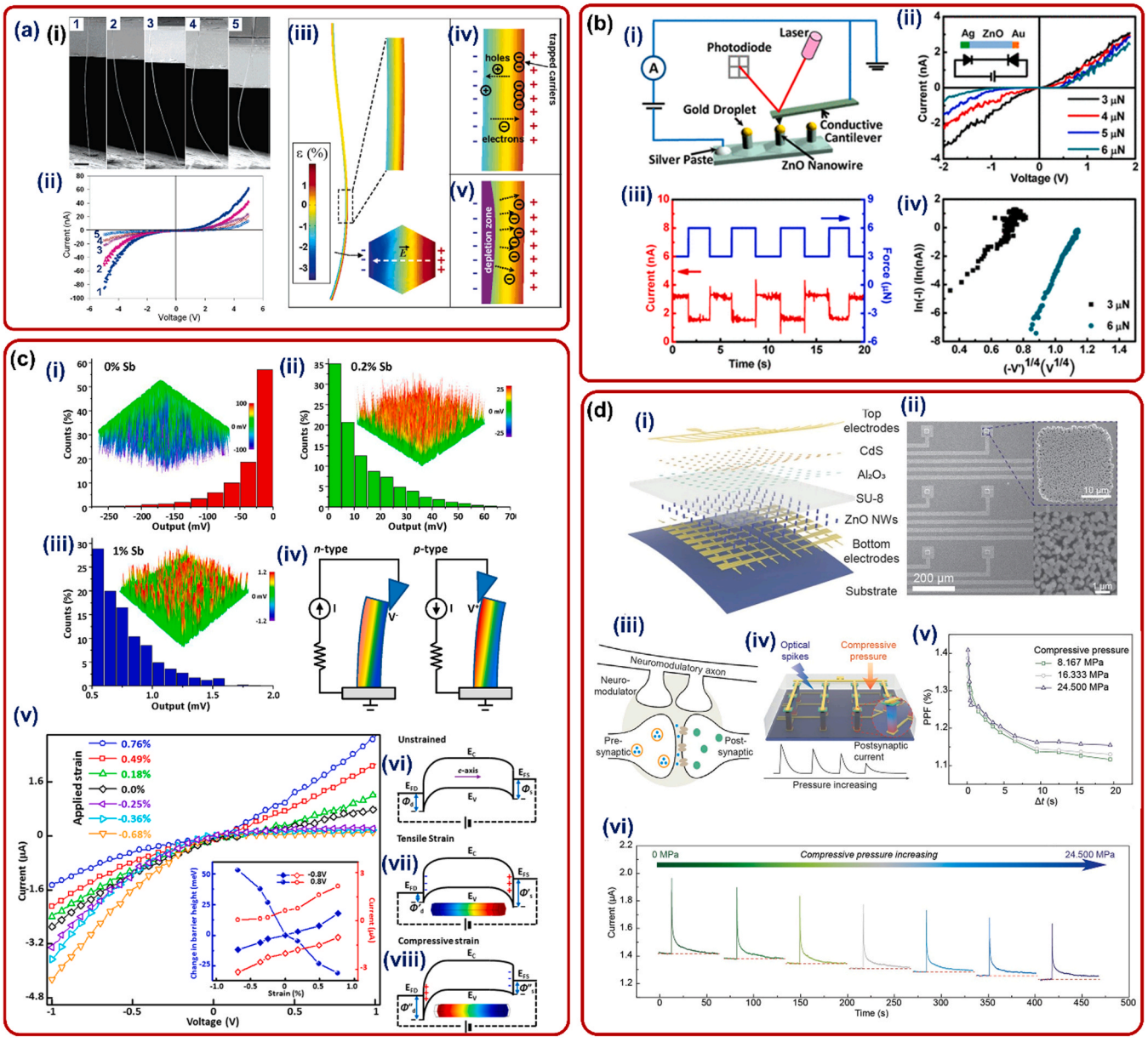

Fig. 12. Piezopotential-gated transistors. (a) Piezopotential-gated transistor realized by bending of single ZnO NW: (i) SEM images with the same magnification showing the five typical bending cases (1−5) of the ZnO NW; the scale bar represents 10 μm. (ii) Corresponding I-V characteristics of the ZnO NW for each of the five different bending conditions. (iii–v) Schematics showing the mechanisms responsible for the current modulation. (iii) A FEM of the strain distribution along the ZnO NW when it was bent. (iv) The carrier trapping effect. (v) The creation of a charge depletion zone. Reproduced with permission [165]. Copyright 2007, Wiley-VCH GmbH. (b) Piezopotential-gated piezotronic transistors using the vertically aligned ZnO NWs capped with Au droplets grown on GaN/sapphire substrates: (i) Schematic of the conductive AFM system used for nanoscale positioning and electrical measurement. (ii) Typical I–V characteristics of a sample with double-Schottky junctions under various compressive forces. (iii) Current response to a force pulse from 3 to 6 μN. The blue line represents the applied force, while the red is the resulting current. (iv) Plots of ln(−I) as a function of $(-V)^{1/4}$, by using the data from the negatively biased region in part (ii). Reproduced with permission [175]. Copyright 2012, American Chemical Society. (c) Piezopotential-gated piezotronic transistors based on an ultra-long Sb-doped p-type ZnO NW: Conductive AFM measurements of the piezoelectric outputs of (i) 0, (ii) 0.2, and (iii) 1% Sb-doped ZnO NWs. The percentage of observed peaks for each output range is represented in a histogram. (iv) Schematic demonstrating the difference in the screening of piezo-polarization charges, and the opposite polarity of piezoelectric outputs between transversely bent n- and p-type NWs. Piezopotential distribution is shown by a color gradient, with positive piezopotential denoted by red and negative piezopotential indicated by blue. Observation of the piezotronic effect was made in 0.2% Sb-doped NWs. (v) I−V curves of the NW under different levels of strain. Inset displays the measured current and calculated change in SBH as a function of strain at two fixed drain biases. (vi−viii) The suitable band diagrams at the Schottky junction explaining the piezotronic effect. Reproduced with permission [58]. Copyright 2013, American Chemical Society. (d) Piezopotential-gated ZnO NW/A-l_2O_3/CdS heterojunction-based optoelectronic synapses (ZAC-OS) array: (i) Schematic illustration of the device structure. (ii) SEM image of the ZnO NWs array aligned with bottom ITO electrodes. Inset: SEM image of a ZnO NWs pixel (upper) along with its enlarged view (lower). (iii) Illustration in schematic form of an organic neuromodulator. (iv) Schematic representation of the ZAC-OSs device demonstrating the modulation of the excitatory postsynaptic current while subjected to compressive pressure. (v) Paired-pulse facilitation index under various compressive pressure circumstances as a function of the time interval of paired UV light. (vi) Under different strain conditions, the photoresponse behavior with a single UV light stimulation. Reproduced with permission [342]. Copyright 2023, Wiley-VCH GmbH.

research laid the groundwork for the use of 2D TMD material-based hybrid piezopotential-gated FETs in the artificial intelligence industry. The piezoelectric potential produced by ZnO under external force can also substitute the gate voltage regulation sensing properties of transistors, which was realized in a 1D/2D hybrid piezopotential-gated FET composed of ZnO NR array and 2D indium selenide (InSe) [367].

To convert mechanical input from the devices into electrical controlling signals, a logic circuit using piezopotential-gated transistors has also been developed [368–371]. Initially, a single ZnO NW-based piezopotential-gated transistor was employed to demonstrate the universal logic operations such as NAND, NOR and XOR gates [369]. Later, flexible ZnO bridging NR array-based piezotronic devices were utilized to demonstrate several logic operations including inverter, NAND, and NOR with good rectifying behaviors [371]. Highly enhanced piezotronic and piezo-phototronic effect-based logic computations were achieved by H. Li et al. by coupling localized Schottky barriers in Au NP-decorated ZnO MW with piezopotential produced upon straining [368]. They have fabricated two series logic devices such as inverter, NAND, AND, NOR, OR, XOR and 2:1 multiplexer gates with good rectifying behaviors and obtained a high I_{max}/I_{min} current ratio of 9.3×10^4. Piezotronic logic circuits may process the encoded data and generate electronic output signals that can be implemented to drive embedded electronics and sensors in micro/nanoelectromechanical systems, human-machine interfaces, adaptive computing, and communications.

Flexible and stretchable human-integrated electronics with superior spatial and temporal resolution are now partly owing to the benefits of piezopotential-gated FETs in achieving micro/nanofabrication and integration of sensor arrays with excellent electric signal amplification function [372]. Working with a commercial chip based on two-electrode piezotronic FET configurations results in a significant reduction in the chip's functional size due to the absence of because of the absence of the third electrode, which covers up a significant portion of the overall chip surface. Introducing these piezopotential-gated FETs into piezotronic sensors can directly modulate the output reading upon applying external stimuli and reduce the power consumption of the FET by supplying the piezoelectric power directly to the gate electrode. Over the conventional 3-terminal VFETS, the piezopotential-gated VFETs have a significant advantage as they can retain effective control over individual devices while greatly simplifying the device structure and circuitry fabrication. In the case of close-packed device arrays, piezopotential-gated VFETs also eliminate the possibility of unintended cross-talks between the adjacent devices. In addition to serving as strain-induced current modulator, piezotronic transistors also function as signal comparators and amplifiers [372]. These features may enable the development of new piezotronic analogue-to-digital translators (ADCs). However, there are a few limitations on using piezopotential-gated FET in every area of the semiconductor industry. For example, carrier injection in piezopotential-gated FET is closely related to the interface contact mode between the electrodes as well as to the work function of the electrodes and the band gap of the active materials. Furthermore, the selection of materials in piezopotential-gated FET is constrained by the piezoelectric properties, whereas a broad range of semiconductor materials can be used in conventional FETs.

6. Application of piezotronic devices

With the advancement of suitable nanostructured materials in an appropriate form and alignment, flexible substrates, facile and controllable fabrication methods, and multifunctionality of flexible piezotronic devices have demonstrated their potential applications in advanced nanotechnology, including PNGs/self-powered sensors, strain/pressure mapping-based image sensor, and human activity and health monitoring.

6.1. PNGs/self-powered sensors

Small-scale energy harvesting technologies, particularly piezoelectric energy harvesting, have gained popularity during the past 20 years. The fundamental principle of PNG is the generation of deformation-induced piezopotential in a piezoelectric semiconducting crystal upon applying dynamic stress, which serve as a driving force for the transient flow of charge carries in the external load. The generated output voltage across the external load can supply of energy of a small-powered piezotronic devices. Furthermore, the tuning of it can be a crucial component for piezoelectric sensors. The need for self-powered sensor nodes was driven by the rapid development of the piezotronic sensor networks. PNGs based on 1D ZnO nanostructure arrays have been found to be the best candidate for replacing the requirement for external power sources in small-powered devices [37]. A summary of self-powered sensors composed of 1D ZnO nanostructure-based PNGs are presented in Table 3. Initially, vertical ZnO NW-based PNG was proposed in 2006 by Z. L. Wang and coworkers [373]. The current flow and subsequent power generation through an external circuit were expected to be driven by the piezopotential generated inside ZnO upon deformation. The efficiency of the NW-based piezoelectric power generator was estimated to be 17–30%. The output power density was ~10 pW mm^{-2} when the density of NWs per unit area on the substrate was 20 μm^{-2}. They assumed that the generated power might be sufficient to operate a single 1D nanostructure-based device. By selecting a NW array with dimensions of 10 μm × 10 μm, they predicted that the generated power might be enough to drive a single NW/NB/NT-based device [373]. Later, PNGs using ZnO NT arrays were also demonstrated. By forming a Schottky contact between the metal tip and the NT, the piezoelectric potential was estimated, and the PNG produced an output voltage of up to 35 mV [151].

In the area of PNG, increasing device flexibility and voltage/current output is the primary future objective [374]. The performance of 1D ZnO-based PNGs can be enhanced using a variety of conventional techniques. Examples include using HSs of various piezoelectric materials, appropriate doping, manipulation of morphologies, choosing the right surfaces, and integrating various mechano-electrical properties. S. Lu introduced a novel strategy to weaken the piezopotential screening effect by forming Schottky junctions on the ZnO surface through the introduction of Au NPs onto the surface [209]. With this approach, the piezoelectric-energy conversion performance was greatly enhanced. The output voltage and current density of the Au/ZnO nanoarray-based PNG reached 2 V and 1 μA cm^{-2}, respectively, 10 times higher than the output of pristine ZnO nanoarray-based PNGs [209].

G. Tian et al. introduced a discretely structured design for understanding the potential screening behavior of ZnO NRs into NG performances [120]. Piezoresponse force microscopy (as shown schematically in Fig. 13(a(i))) and FEM were employed to carefully reveal the electron's dynamic characteristic and the mechanism of potential screening effect. As can be seen from the PNG performances in Fig. 13(a(ii–iv)), the developed PNG device output voltage was enhanced about 1.62 times higher than that of the original continuous structure [120]. D. Yang et al. further compared the performance of PNGs fabricated from patterned and unpatterned ZnO NWs on ITO-PET substrate (Fig. 13(b)) [119]. When compared to the device made from unpatterned ZnO NWs, the patterned ZnO-based PNGs demonstrated a 6-fold increase in output current. About 150 nA of maximum output current was observed, which was sufficient to power up a few micro- and nanoelectronic devices. The improved output performance in PNGs was mainly attributed to the patterned growth mode, which might significantly reduce the piezoelectric potential screening effect caused by free electrons in ZnO [119]. In a ZnO-PVDF-based PNG, A. Anand et al. investigated the impact of random and vertically oriented ZnO NR [375]. They reported that PNG performance was improved 7 times with such a vertically aligned ZnO-PVDF device. Because of the direction of the molecular dipoles, the alignment of ZnO NRs enhances remanent polarization, resulting in a

Table 3
Summary of 1D ZnO-based PNGs for self-powered sensors.

Active materials for self-powered sensors	1D ZnO alignment	PNG performances		Applications	Ref.
		V_{OC}	I_{SC}		
ZnO NW	Vertical array	50 mV	200 nA	Deformation sensor, detection of human face wrinkling	[406]
ZnO NW	Single NW	0.23 V	6.9 μA	pH, glucose, and photon sensors	[378]
ZnO NW	Vertical array	0.11 V	0.6 μA	Active skin sensor, eye-ball motion detector	[407]
ZnO NW	Vertical array	58 V	138 μA	Induce innervation of the nerve of a frog	[469]
ZnO NW	Lateral NWs	0.49 V		Blood glucose level monitor	[413]
ZnO NW	Vertical array	0.16 V		Detection and rapidly control of blood glucose concentration	[412]
ZnO NW	Vertical array	~50 mV	500 pA	Breath and heartbeat	[384]
ZnO NW	Vertical array	~1 V	1.12 nA	Photosensor	[470]
ZnO NW	Vertical array, lateral array	1.26 V for LING, 0.243 V for VING	26 nA for LING, 18 nA for VING	UV and pH sensor	[241]
ZnO NW	Vertical array	58 mV		Sound-driven humidity sensor	[471]
parylene C/ZnO NW	Vertical array	10 V	0.11 μA	Body movement sensor	[213]
ZnO NW homojunction	Vertical array	284 mV	10.6 nA	Gesture recognition	[208]
ZnO NW	Vertical array	10 V	0.6 μA	Photon detection	[437]
ZnO NR	Bidirectional	1.8 V	85 nA	Wound healing	[408]
Fe-doped ZnO NW	Vertical array	0.85 V	0.6 μA	Humidity sensor	[256]
ZnO NW, SnO_2/ZnO NW, CeO_2/ZnO NW	Vertical array	0.58 V ZnO, 0.55 V for SnO_2/ZnO, 1.17 V for CeO_2/ZnO		Humidity sensor	[426]
ZnO NW	Vertical array	0.45 V	4 nA	Gas sensor	[435]
ZnO NW	Bi-axial NWs	0.63 V	33 nA	Smart skin	[472]
ZnO NW	Vertical array	2.1 V	105 nA	Hg^{2+} detection	[377]
Hierarchical PVDF/ZnO NW core-shell nanofibers	Vertical NWs	2.23 V	~12 nA	Gait recognition, pulse, and muscle movement monitor	[428]
Sb-doped ZnO NW	Vertical NWs	140 mV	100 pA	Gesture recognition	[247]
SnO_2/ZnO NW core/shell	Vertical array	0.8 V	172.5 nA	H_2 sensor	[386]
Pd/ZnO NW	Vertical array	0.52 V		Ethanol sensor	[204]
ZnO NR	Vertical array	12.5 V	0.04 μA	Artificial skin	[382]
Enzyme/ZnO NW	Vertical array	0.3 V		Lactate, glucose, uric acid, and urea sensor	[410]
ZnO NW	Vertical array	0.54 V		Kidney-disease diagnosis	[419]
ZnO NW	Vertical array	148 mV		Glucose sensing in the body fluid (tear, saliva, urine, and blood)	[411]
ZnO NW/PVDF	Vertical array	1 V	1 μA	Footstep sensor	[431]
ZnO NW	Vertical array	8 V	0.6 μA	Vehicle sensor	[432]
$ZnSnO_3$/ZnO NW	Vertical array	0.533 V		Liquefied petroleum gas (LPG) sensor	[433]
ZnO NR	Vertical array	3 V		Human motion sensor	[59]
PVDF/ZnO NW/reduced graphene oxide	Composite NW	6.06 V	3.46 μA	Cardiac pacemaker	[473]
ZnO NR	Vertical array	0.35 V	1.2 nA	Self-powered e-skin	[400]
ZnO NW	Vertical array	0.079 V		Self-powered e-skin, image sensor	[336]
ZnO NW	Vertical array	1.5 V	30 nA	Vehicle sensor	[439]
Cu/ZnO NW	Vertical array	0.552 V		H_2S sensor	[474]
In_2O_3/ZnO NW	Vertical array	0.902 V		H_2S sensor	[475]
α-Fe_2O_3/ZnO NW	Vertical array	0.589 V		Ethanol sensor	[476]
ZnO NW	Helix-shaped substrate with NW pointing outward	0.23 V	5 nA	Spring balance	[477]

stronger electric field. A PNG based on a hierarchical HS composed of ZnO NWs on a highly ordered Si MP array was demonstrated by M. R. Hasan et al. (Fig. 13(c(i–iv)) [211]. When compared to the device for ZnO NWs on a flat substrate, they noticed that the peak output voltage from the hierarchical HS array-based PNGs was significantly higher by about 5.7 times, from 0.7 to 4.0 V. The explanation for the enhanced mechanism was based on the heterojunction formed on the Si MP arrays by connecting the ZnO NRs in series, which are thought of as a single source of piezoelectric potential [211].

Not only the vertical array of ZnO nanostructures but its horizontal array was also used for fabricating high-output PNG [156,240–242]. G. Zhu used a two-step method named scalable sweeping-printing-method, for fabricating flexible, high-output NG (HONG) from ZnO NWs in horizontally aligned arrays [240]. The ZnO NWs were transferred to a receiving substrate in the first phase to create horizontally aligned arrays. After that, electrodes of the parallel stripe type were deposited to connect all the NWs. Fig. 13(d(i–iv)) displayed the schematic illustration, the SEM image, as well as the HONG's performances. An open-circuit voltage of up to 2.03 V and a peak output power density of about 11 mW cm^{-3} were obtained using a single layer of the HONG structure. A significant step toward the development of self-powered devices that harvest energy from the environment was made when the generated electric energy was successfully stored using capacitors and then utilized to light up a commercial LED [240]. S. Xu et al. demonstrated both vertical NW array integrated PNG (VING) as well as a multiple lateral-NW-array integrated PNG (LING) by combining a rational chemical growth of ZnO NWs with novel nanofabrication process [241]. When 700 rows of lateral ZnO NW arrays were integrated into LING, a maximum voltage output of 1.26 V was produced, compared to 0.243 V for VING. A unique "self-powered" nanosystem made entirely of ZnO NWs had been used to demonstrate the integration of a PNG with a pH or UV nanosensor [241].

In contrast to those of a single HS composed of ZnO NR/Gr, D. M. Shin et al. developed epitaxial double-HS of ZnO NRs in NR/Gr/NR

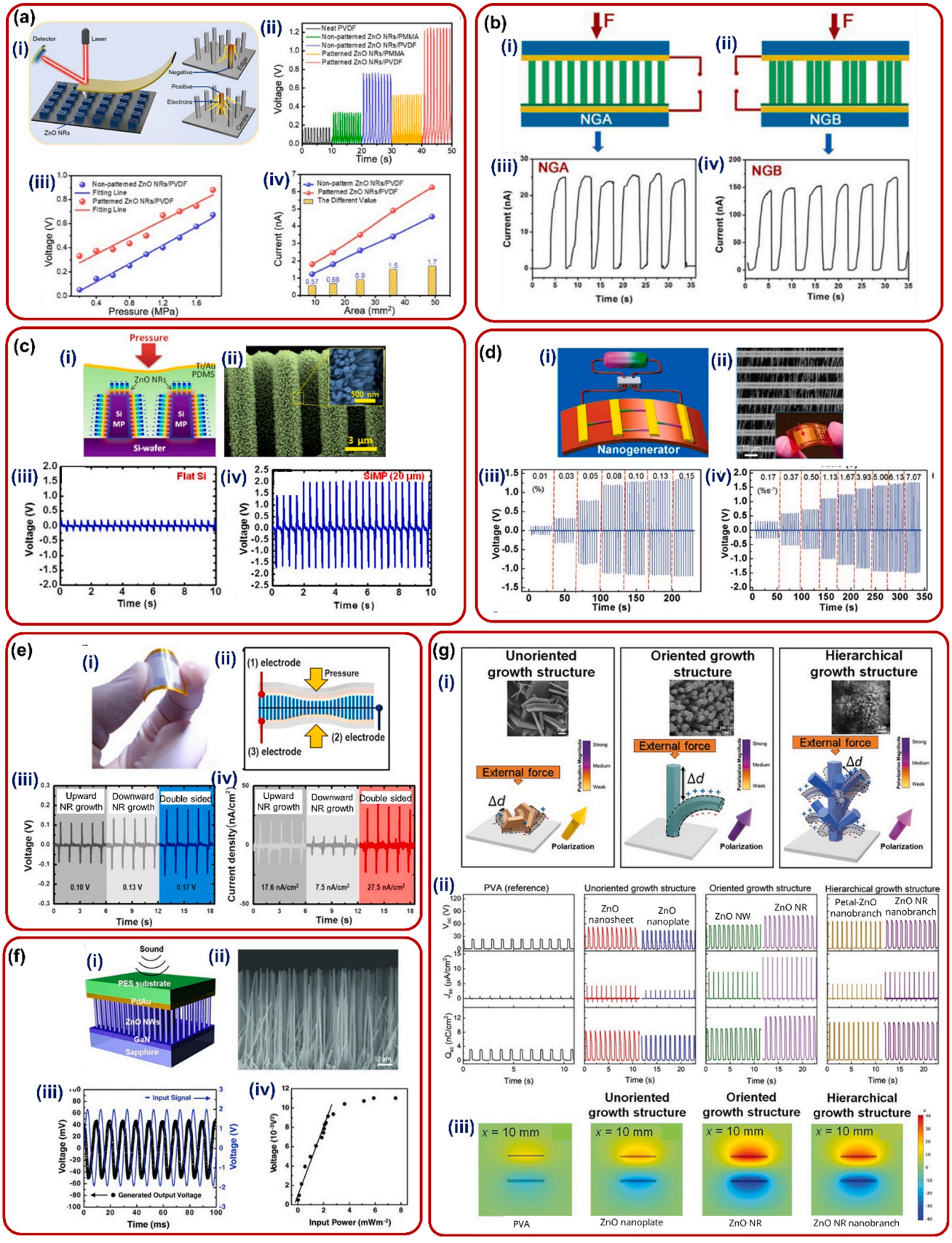

(caption on next page)

Fig. 13. PNGs. (a) PNG from discretely patterned ZnO NRs: (i) Schematic illustration of the PNG from discretely patterned ZnO NRs along with the piezoresponse force microscopy and the adoptive testing approach. (ii) The piezoelectric voltage response of the different samples under 2 MPa pressure. The output voltage (iii) and current (iv) of patterned and unpatterned ZnO NRs at various pressures and active regions. Reproduced with permission [120]. Copyright 2020, American Chemical Society. (b) Flexible PNGs from patterned ZnO NWs on flexible substrates: Schematic illustration of the PNGs fabricated by using (i) without patterned (NGA), and (ii) patterned (NGB) ZnO NWs. Current outputs generated from NGA (iii) and NGB (iv). Reproduced with permission [119]. Copyright 2017, Royal Society of Chemistry. (c) Hierarchical ZnO NRs on Si MP arrays for performance enhancement of PNGs: (i) Schematic of device structure. (ii) Cross-sectional SEM image of ZnO NRs grown on Si MP arrays with a length of length 10 μm. Output voltage measured from ZnO NRs on (iii) a flat Si-substrate, and (iv) Si MP arrays of length 20 μm and a strain frequency of 2.2 Hz. Reproduced with permission [211]. Copyright 2015, American Chemical Society. (d) Flexible high-output NGs based on lateral ZnO NW array: (i) Schematic of NG structure, in which Au was used to form Schottky contacts with the ZnO NW arrays. (ii) SEM image of ZnO NW arrays bonded by Au electrodes. Inset is the demonstration of an as-fabricated NG. The arrowhead denotes the NG's actual working region. (iii, iv) Open circuit voltages of the HONG at a fixed deformation frequency of 0.33 Hz when the increasing strain rates were 5% s^{-1} and 0.1% s^{-1}, respectively. Reproduced with permission [240]. Copyright 2010, American Chemical Society. (e) Freestanding ZnO NR/Gr/ZnO NR epitaxial double HS for PNGs: (i) Photograph of the fabricated NG. (ii) Schematic of the device with epitaxial double HSs. (iii) Piezoelectric output voltages and (iv) current densities from the just upwardly, downwardly and the double-sided grown NRs. Reproduced with permission [113]. Copyright 2015, Elsevier. (f) Sound-driven PNG with piezoelectric ZnO NWs: (i) Schematic of an integrated PNG in which the flexible PdAu-coated PES substrate was acting as both a top electrode and a vibration plate was installed above the ZnO NW arrays. (ii) SEM image of an ZnO NW array on a GaN/sapphire substrate. (iii) The input signal for the generation of a sound wave and the output voltage from the piezoelectric ZnO NW arrays as a result of the sound wave. (iv) Output voltage vs. the input power of the applied sound wave at a fixed frequency of 100 Hz. Reproduced with permission [379]. Copyright 2010, Wiley-VCH GmbH. (g) The effect of ZnO growth structures on the performance of a hybrid piezo/triboelectric NG: (i) A schematic diagram illustrates how ZnO with various orientations including unoriented, oriented, and hierarchical structures experiencing a different degree of deformations in response to vertical compression forces. The deformed nanostructures are shown by the dashed line. The polarization generated by ZnO nanostructures in response to external pressures is represented by the arrow. The SEM images of the unoriented, oriented, and hierarchical ZnO structures are also shown. (ii) The comparison of open-circuit voltage (V_{oc}), short-circuit current density (J_{sc}) and short-circuit charge density (Q_{sc}) of the fabricated NGs for the reference (PVA only), unoriented, oriented, and hierarchical growth structures at constant applied force of 50 N. (iii) Corresponding electric potential distributions versus silicon rubber simulated by using COMSOL Multiphysics. Reproduced with permission [93]. Copyright 2022, Wiley-VCH GmbH.

configuration and demonstrated a 2-fold improvement in total output voltage and current density [113]. The digital photograph, schematic of double-HS and the PNG performances are shown in Fig. 13(e(i–iv)). The coupling of the piezoelectric effects from both upward- and downward-grown NRs was thought to be the cause of the improved device performance in double-HS [113]. Y. Sun et al. demonstrated a two-layer ZnO NR arrays with equal c-axis orientation for PNG [376]. The output voltage and current of the Au/ZnO-Polyacrylonitrile/ZnO-Cu PNG (1.6 V, 16.4 A) were more than 5 and 2.3 times, respectively, that of the Au/ZnO/Cu device. It is obvious that the hybrid PNG's from two-layer ZnO NR arrays with equal c-axis orientation were crucial in controlling electrical impulses and enhancing electrical output performance. A layer-by-layer stacking was introduced by S. Xu et al. in a multilayer PNG, where pyramid-shaped metal-coated ZnO nanotip (NTP) arrays and hexagonal-prism-shaped ZnO NW arrays were integrated [60]. A high output power density of 0.11 μW/cm^{-2} at 62 mV is achieved for a four-layer integrated PNG. A. Mahmud et al. demonstrated a PNG based on the hybrid nanostructures of 1D/2D ZnO to combine the advantages of PNGs based on ZnO NWs/NRs with high electromechanical coupling and PNGs based on 2D ZnO nanosheets having good mechanical stability [111]. The average peak-to-peak output open circuit voltage and short circuit current at a force of 5 N and a frequency of 5 Hz were up to 10.18 V and 15.9 μA, respectively. This supports the idea that the gadget could be used to self-power an array of sensors in an aircraft structural health monitoring system. A completely stand-alone, self-powered environmental sensor composed of a single-wall carbon nanotube-based FET and a ZnO NW PNG was implemented by M. Lee et al. for the detection of Hg^{2+} ions and evaluation of their concentration in water [377]. Additionally, PNG could use glucose oxidase and laccase as catalysts to transform chemical energy from biofluids like blood and glucose into electrical energy. After being integrated with a number of NW-based sensors, a prototype biofuel cell made of a single ZnO NW was able to produce an output power of up to 0.5–3μW and function as a self-powered pH, glucose, and photon sensor [378].

The vibration of 1D ZnO nanostructures can also produce sufficient strain to generate power [379,380]. S. N. Cha et al. demonstrated a sound-driven PNG based on ZnO NWs (Fig. 13(f)) [379]. In the direct compression mode, as illustrated schematically in Fig. 13(f(i)), the sound wave was employed to vibrate the top contact electrode, which generated electric potential through the vertically well-aligned ZnO NWs. An AC output voltage of roughly 50 mV was obtained from the PNG when sound with an intensity of 100 dB was delivered to it [379]. Tuning fork-shaped NG was developed by W. Deng et al. to enhance energy conversion performance at a lower frequency [380]. The designed PNG showed that the peak values of the open-circuit voltage and the short-circuit current as 160 mV and 11 nA, respectively at 13 Hz. Additionally, a maximum instantaneous peak power of 0.92 μW cm^{-3} across a matched load of 9 MΩ was obtained [380].

A. S. Dahiya et al. demonstrated a flexible, high-performance mechanically robust NG on PDMS substrate based on inorganic/organic HSs by using ZnO NWs (inorganic) and parylene C (organic) matrix [213]. The NG devices exhibited excellent performances with a high open-circuit voltage ≈ 10 V, short-circuit current density ≈ 0.11 μA cm^{-2}, and peak power ≈ 3 μW under a vertical compressive force applied by a mechanical shaker [213]. A flexible PNG based on ZnO NTs hosted in a polycarbonate (PC) membrane with variable pore diameter was designed by S. Stassi et al [149]. A maximum output voltage of 1.15 V, a maximum current of 100 μA, and a maximum output power density of 287.5 mW cm^{-3} were achieved using the PC membrane of pore size 100 nm. These outstanding outcomes demonstrated the nanostructured ZnO-PC composite's potential as a material for energy-harvesting applications [149].

N. Cui et al. exploited ZnO NW/Fe_3O_4 to demonstrate magnetic force-driven contactless NGs and utilized them as a noncontact energy harvester and sensor [381]. The output voltage and current of the PNG were measured to be as high as 3.2 V and 50 nA, respectively, which was sufficient to power up a liquid crystal display. To harvest the electrical energy from biomechanical motion, a biocompatible, biodegradable, and stretchable silk hydrogel was designed as an artificial piezoelectric energy-generating skin (EG-skin). In this skin, the addition of ZnO NR increased the piezoelectricity eight times over that of the original silk hydrogel, improved the electrical responsiveness by two times, and produced 1 mW cm^{-2} of power [382].

In order to overcome the limitations of a single component-based NG, hybrid piezo/triboelectric NGs (H-P/TENGs) made of ZnO NR/PVA were designed by Y. P. Lim et al [93]. These devices combined high triboelectric output voltage and piezoelectric output current during continuous contact-separation cycles. H-P/TENG's performances were investigated by altering the various 1D ZnO nanostructures, including unoriented, oriented, and hierarchical structures and an improvement in NG output was obtained by 6–17 times. The effect of ZnO growth structure on the performance of a hybrid piezo/triboelectric NG composed of ZnO/PVA are shown in Fig. 13(g). Particularly, ZnO NR

with well-aligned structures along the c-axis exhibited the highest improvement in electrical outputs when compared to the pristine one, and its power density reached up to 15.9 W m^{-2} (almost a 17-fold increment) [93].

PNGs from 1D ZnO nanostructures are not only limited to produce power from external strain/pressure, but researchers also have demonstrated small-scale power PNGs by using a variety of biological stimuli, including biomotions, muscle stretching, and many more [19,30,34–36,43–48,54,55,60,70,71,78,79,96,144,205,208,242,247,273,382–391]. This demonstrates the enormous potential of PNGs for effective sensing of a variety of environmental stimuli, such as intensive healthcare and human activity monitoring.

6.2. Strain/pressure mapping-based image sensor

Tactile sensing has gained significant attention as a result of the rapid development of flexible electronics, artificial intelligence (AI), robotics, and e-skin as it serves as a key component in human-machine interactions. A functional tactile sensing device for next-generation robotics and human-machine interfaces requires large-scale integration of pressure sensor arrays with high spatial resolution, high sensitivity, wide detection range, fast response, and good substrate flexibility [10,148,172,173,191,232,236,372,392–394]. A variety of flexible and stretchable tactile sensors with different pressure sensing mechanisms have been studied, including resistive, capacitive, triboelectric, and piezoelectric types [10,148,172,173,191,232,233,236,392,393,395–399]. Due to its promising performance, which includes high sensitivity, quick response times, and the capacity to detect dynamic pressures, piezoelectric tactile sensors are extensively explored [10,118,133,148,173,232]. In an effort to address the issues still present in the field of tactile image sensors, 1D ZnO nanostructures on flexible substrates have received a significant amount of attention among the various piezoelectric materials and nanostructure types [10,133,135,148,232]. Table 4 shows a summary of 1D ZnO-based piezotronic image sensors and their performance parameters. W. Wu et al. demonstrated vertical ZnO NW-based large-area, integrated piezotronic transistor arrays as an active taxel-addressable matrix for tactile imaging with a device density of 92 × 92 (Fig. 14(a(i–v))) [118]. A high special resolution of 233 dpi was achieved for mapping pressure including enormous device flexibility, good reliability, and stability over 1000 cycles. In the electrical design of image sensors, this type of piezotronic matrix could potentially replace conventional FETs and function as an active, self-powered touch sensor [118]. J. B. Park et al. demonstrated individually addressable, high-density, dimension- and position-controlled, vertical, and freestanding piezoelectric sensor arrays by using ZnO NT arrays on CVD-grown Gr layers (Fig. 14(b(i–v))) [148]. Fig. 14(b) shows, (i) schematic illustration of a complete device array along with the process for pressure mapping, (ii) digital image of the device array, (iii) SEM image of a device, (iv) SEM of a substance used to be mapped, and (v) the contour plot demonstrating the capability of 8 × 8 addressable device arrays for imaging the spatial profile of the applied stress [148]. A spatial resolution as high as 1058 dpi was demonstrated for a Schottky diode-based tactile sensor composed of ZnO NTs on a flexible substrate. Additionally, they demonstrated the outstanding flexibility and electrical stability of the free-standing sensor arrays for high-resolution tactile imaging [148]. M. S. Suen et al. demonstrated a flexible, highly sensitive, tactile sensor and simultaneously designed a 3 × 3 sensor array on flexible PDMS substrate for multi-touch applications [254]. An artificial e-skin was developed by constructing high-aspect-ratio interlocked ZnO as well as Al-doped ZnO NRs, which can induce a change in the contact area to improve the sensor sensitivity under static and dynamic pressure [254]. For the high-sensitivity detection and mapping of finger touch, W. Deng et al. demonstrated a self-powered tactile sensor array based on the field-limited ordered ZnO NRs [400]. During pressing (sensitivity ~ 403 mV MPa^{-1}, external pressure ~ 0.7 MPa) and bending experiments, the fabricated device exhibited good linearity and flexibility in response to various external forces [400]. The pressure/strain mapping devices based on purely piezoelectric properties of 1D ZnO nanostructures confront challenges to achieve high spatial resolution and high integration, because of complex fabrication techniques, poor pressure response and large signal-to-noise ratio.

By introducing the piezo-phototronic effect, mechanical energy can be converted into electrical and optical energy. As a consequence, the spatial resolution of the pressure mapping can be enormously enhanced by controlling charge-carrier generation, separation, recombination, and/or transport at the metal-semiconductor or semiconductor-semiconductor heterojunction/interface [67,68,127,128,130,135–137,143,200,401]. C. Jiang et al. demonstrated a dynamin range pressure mapping interactions (DPTPMI) device with wide dynamic range and high pressure sensitivity using a dual piezo-phototronic transistor (DPT) pixel for location-aware detection [130]. A typical device involved a piezo-NW (ZnO) channel and a piezo-OLED gate as one module with dual enhancements of the piezo-phototronic effect. The fabricated DPT demonstrated pressure sensitivity of 61.2 μS kPa^{-1} in the effective working zone with a spatial resolution of 5 μm (5080 dpi) [130]. C. Pan

Table 4
Summary of 1D ZnO-based piezotronic image sensors and their performance parameters.

Material system	Sensing method	Sensitivity	Device type	Spatial resolution (dpi)	Ref.
ZnO NW	Piezotronic	2.1 uS	Piezopotential-gated transistor	234	[118]
ZnO NR, AZO NR	Piezotronic	ZnO: − 0.768 kPa^{-1}, AZO: − 0.223 kPa^{-1}	Schottky diode	127	[254]
ZnO NR	Piezotronic	403 mV MPa^{-1}	Ohmic	2.5	[400]
ZnO NT	Piezotronic	1.95 × 10^{-3} kPa^{-1}	Schottky diode	1058	[148]
ZnO thin film	Piezotronic	0.225 kPa^{-1}	Thin film transistor (TFT)	254	[393]
ZnO thin film			TFT	8.5	[478]
Li-doped ZnO thin film	Piezotronic		TFT	85	[173]
2D ZnO nanoplatelets	Piezotronic	7.82 × 10^{-2} meV	Transistor	12,700	[172]
MoO_3/CBP/TAZ/ZnO NW	Piezotronic	61.2 μS	Piezo-OLED-gated transistor	5080	[130]
ZnO NW/Al_2O_3/CdS	Piezo-phototronic		Piezopotential-gated transistor	80	[342]
ZnO NW	Piezo-phototronic		Schottky diode	254	[127]
WO_3/ZnO NW	Piezo-phototronic		LED	50.8	[200]
ZnO NW	Piezo-phototronic		Ohmic	280	[336]
ZnO NW/GaN	Piezo-phototronic	12.88 × 10^{-6} kPa^{-1}	LED	6350	[136]
ZnO-nanofilm/Si MP	Piezo-phototronic		LED	4885	[335]
ZnO-nanofilm/PDMS/Si MW	Piezo-phototronic		LED	4300	[126]
ZnO NW/PEDOT:PSS	Piezo-phototronic		LED	3628	[135]
ZnO NW/GaN	Piezo-phototronic		LED	9769	[128]
Organic/ZnO NW	Piezo-phototronic		LED	3167	[334]
ZnO NW/Si MW	Piezo-phototronic		LED	5080	[201]
ZnO NW/MoO_3	Piezotronic		Schottky diode	19,500	[132]
Human Skin				508	[128,135]

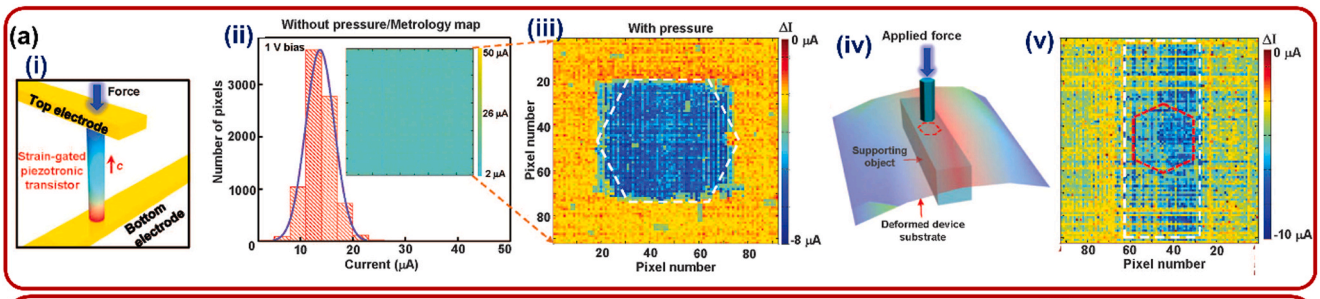

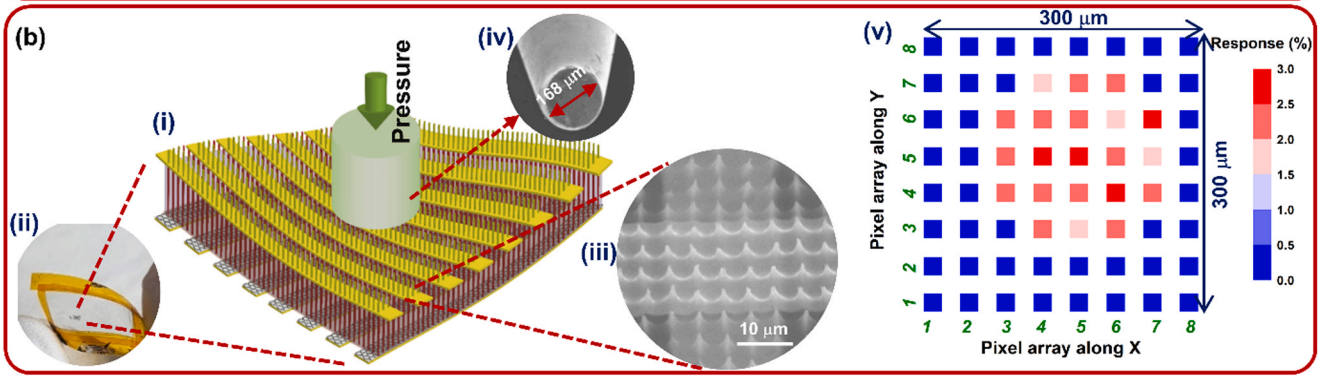

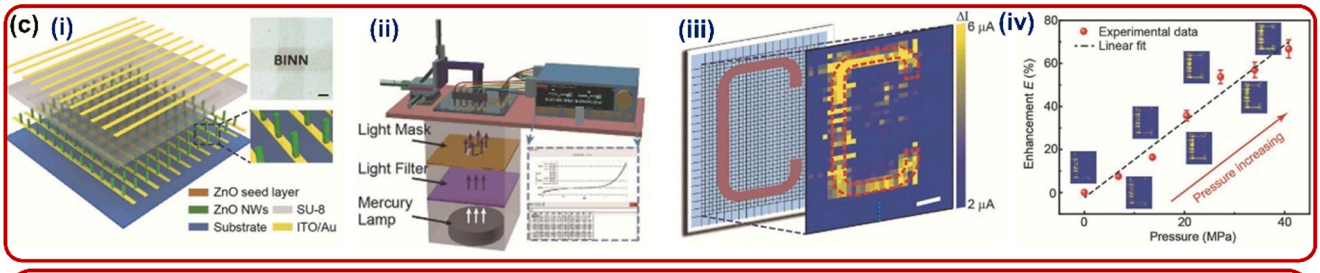

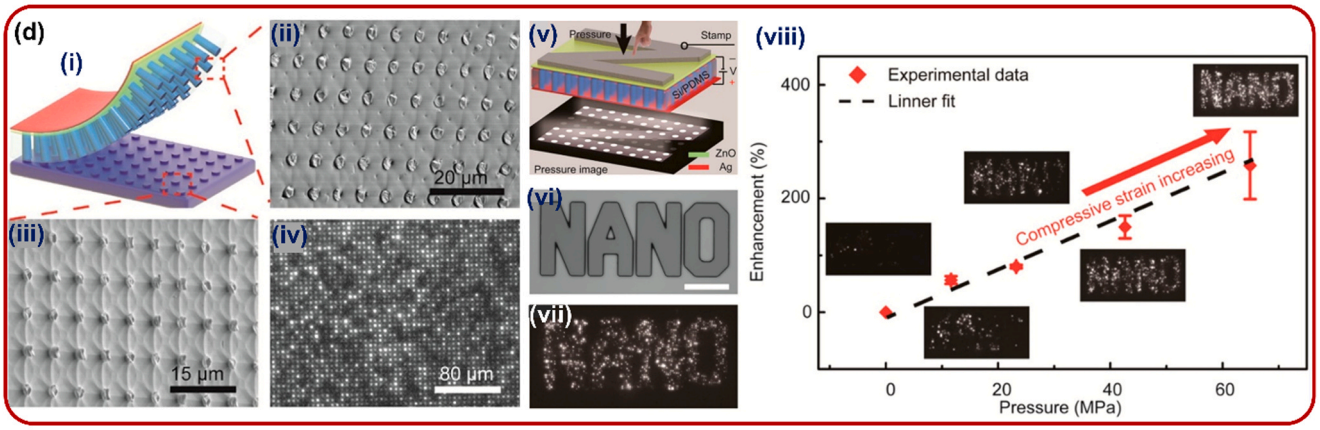

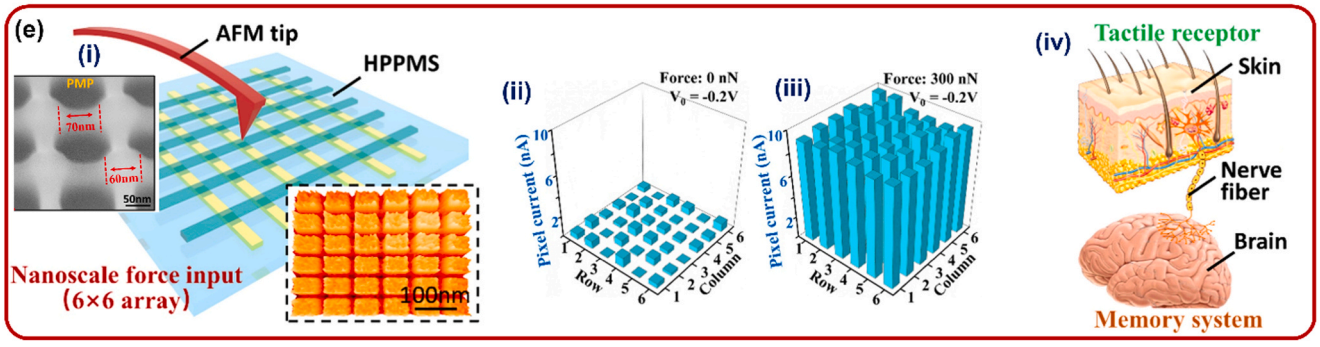

(caption on next page)

Fig. 14. Image sensor. (a) Taxel-addressable matrix of vertical ZnO NW piezopotential-gated transistors for active and adaptive tactile imaging: (i) Schematic illustration of two-terminal SGVPT. (ii) Metrology mapping (inset) and statistical investigation of the fully integrated 92 × 92 SGVPT arrays without applying stress. (iii) Current response contour plot demonstrating the SGVPT array's ability to image the spatial profile of applied stress. Prior to and following the application of a normal stress, a color scale indicates the current differences for each taxel. The white dashed lines highlight the physical shape of the applied stress. (iv) The 3D schematic illustrating how the SGVPT array was used for shape-adaptive sensing. (v) The variations in taxel current values between the bent SGVPT array under additional stress and the unstrained SGVPT array. The location of the additional stress is delineated by the red dashed lines. Reproduced with permission [118]. Copyright 2013, American Association for the Advancement of Science. (b) Individually addressable flexible pressure sensor matrices with ZnO NT arrays on Gr for pressure mapping: (i) Schematic illustration of the procedure for pressure mapping. (ii) Digital photograph of a flexible, individually addressable device. (iii) A part of an individually addressable device as shown in a SEM image. (iv) SEM image for the tip of a probe used for pressure-resolved imaging. (v) Contour plot illustrating how an 8 × 8 addressable device arrays can image the spatial profile of applied stress. Reproduced with permission [148]. Copyright 2022, Springer Nature. (c) UV sensing and illumination distribution imaging by the piezo-phototronic effect in ZnO NW arrays: (i) Schematic illustration of the structures of the ZnO NW-based image sensor array. Inset is an optical image of the as-fabricated device. The scale bar is 1 mm. (ii) Experiment setup to measure the enhancements by the piezo-phototronic effect. (iii) Current difference between strain-free and 40.38 MPa pressure conditions, with illumination intensity of 1.38 mW cm^{-2} and forward biased voltage of 1 V on top electrode. (iv) Enhancement factor E versus the applied pressures, with the corresponding output currents to image the illumination distributions at the illumination intensity of 1.38 mW cm^{-2}. Reproduced with permission [127]. Copyright 2015, Wiley-VCH GmbH. (d) Flexible polymer/Si/ZnO LED array device for image sensing via piezo-phototronic effect: (i) Schematic diagram of the transferred flexible LED array device and the Si substrate. (ii) The reverse side of the polymer/Si MW array composite film. (iii) SEM image of Si substrate after the transfer process. (iv) An optical image of an LED array device bias voltages of 10 V. (v) Working mechanism of the pressure distribution function of the flexible LED array device. (vi) A patterned sapphire stamp shaped to read "NANO" with a scale bar of 150 μm. (vii) Mapping of pressure distribution by using an LED array to represent the word "NANO". (viii) Pressure distribution mapping under different pressures by the LEDs array intensity image. Reproduced with permission [126]. Copyright 2017, American Chemical Society. (e) Tactile imaging and memory capabilities of the 6 × 6 HPPMS. (i) Sensing and memorizing force distribution data schematics from AFM tip writing. Insets are a SEM (left top) and an AFM topography (right bottom) image of the fabricated high-resolution HPPMS. Statistical distribution of pixel currents with the integrated 6 × 6 HPPMS under non-force (ii) and 300 nN force (iii). ((iv) Schematic diagram of the neuromorphic tactile system composed of human skin and brain. Reproduced with permission [132]. Copyright 2021, Elsevier.

et al. demonstrated a LED-based pressure/strain sensor array that offered a spatial resolution of 2.7 μm for multipixel parallel mapping of strain, corresponding to a pixel density of 6350 dpi [136]. Each pixel was composed of a single n-ZnO NW/p-GaN light-emitting diode, the emission intensity of which was dependent on the local strain owing to the piezo-phototronic effect [136]. R. Bao et al. fabricated a flexible LED array composed of PEDOT:PSS and patterned ZnO NWs with a spatial resolution of 7 μm (~3628 dpi) for mapping of spatial pressure distributions [135]. Pressure distribution was acquired by parallel-reading the illumination intensities of LED arrays which was modulated by the strain-induced polarization charges in the vicinity of local interface [135]. Y. Peng et al. demonstrated a flexible and stable p-n junction LED-based pressure sensor array composed of p-GaN/n-ZnO NW HS having a high spatial resolution of 2.6 μm (~9769 dpi) (much better than human skin resolution of 50 μm) and a fast response time of 180 ms to map pressure distributions [128]. X. Han et al. demonstrated an addressable device array consisting of 32 × 40 pixels based on vertically aligned ZnO NWs (Fig. 14(c)) [127]. Each pixel was composed of ZnO NWs and Au nanopatterns to form a Schottky-contacted UV photodetector with spatial resolution of 100 μm (254 dpi). By introducing the piezo-phototronic effect, the strain-induced piezoelectric polarization charges substantially improved the performance of the UV photodetector array by 700% in photoresponsivity, 600% in sensitivity, and 280% in detection limit [127]. Flexible polymer/Si/ZnO LED pressure-distribution mapping sensors were demonstrated by X. Li et al. (Fig. 14(d)) [126]. They reported p-n junction HS LEDs consisting of Si MP obtained by inductively coupled plasma (ICP) etching and ZnO films through low-temperature hydrothermal method [126]. Based on piezo-phototronic effect, the intensity of the flexible LED array was enhanced by more than 3 times (under 60 MPa compressive strains) [126]. Additionally, the device was stable and energy saving. The flexible device could still work well after 1000 bending cycles or 6 months placed in the atmosphere. The spatial resolution was 4300 dpi [126]. Furthermore, they were able to achieve a resolution of 2 μm of the LED array without observing any cross-talk of the adjacent pixels which was promising for an ultra-high resolution LED array-based image sensor. C. Jiang et al. demonstrated an e-skin from dimension- and position-controlled ZnO NW arrays with a pixel-size of 60 nm and achieved an ultra-high resolution of ~ 195000 dpi in tactile imaging [132]. The device structure and the subsequent fabrication process are shown in Fig. 4(d). The ultrahigh-resolution 6 × 6 piezo-memory pixel arrays successfully produced the force image of 300 nN force as shown in Fig. 14(e(iii, iv)). The system could achieve the external pressure sensing and signal storage functionalities by connecting piezo-memory pixel arrays in series with the piezoelectric ZnO NW and MoO_3 resistive-memristor components. Finally, the HPPMS was utilized as a neuromorphic tactile sensor as shown in Fig. 14(e(iv)) [132].

6.3. Human activity and health monitoring

Continuous health monitoring using implantable and wearable medical devices is attracting profound interest nowadays both from academic researchers as well as healthcare industries. With the advancement of biomedical sensors and low-power electronics, wireless sensor networks (WSNs) which are commonly known as the IoT, are rapidly expanding in the advanced healthcare sectors [1–8,10–13,16,17,20–22,28–31,37,49–52,97–99,131,153,230–232,387,402–405]. Flexible piezotronic sensors composed of 1D ZnO nanostructure arrays can be an ideal candidate for the active sensor in e-skins for real-time monitoring of human health continually without interfering with daily activities. These piezotronic sensors are capable of performing a variety of health monitoring tasks, such as continuous home monitoring of vulnerable patients, accurate and effective vital sign monitoring, tracking of chronic diseases, maintaining personal wellness, and injury detection, particularly in the case of young children and the elderly people. With the rapid development of society in recent decades, wearable piezoelectric tactile sensors have attracted attentions for motion sensing-based health care and artificial intelligence. S. Lee et al. reported ZnO NW array-based super flexible PNG which had been demonstrated as an active sensor for monitoring tiny skin deformation (Fig. 15(a)) [406,407]. As shown in Fig. 15(a(i)), it was constructed utilizing arrays of ZnO NWs on an ultrathin Al foil substrate that was only 18 μm thick. The total thickness of the device was 25 μm, and the device dimension was 5 × 13 mm^2 [406]. A prototype sensor, mounted to the eye-lids as shown in Fig. 15(a(iii)), was utilized to detect minute skin deformations caused by eye blinking. The device generated currents of 2 nA and easily measurably voltages of 0.2 V (Fig. 15(a(iii))) [406]. They further developed a flexible, ultrathin, highly sensitive NG composed of aligned ZnO NW compacted arrays that were utilized for monitoring the eye-ball motion and thus demonstrated the potentiality of intensive care of sleep pattern, tiredness and possible brain activity (Fig. 15(a(iv–vi))) [407]. A vital sign monitoring system was developed by J. B. Park and co-workers using flexible pressure sensor arrays made of site-controlled ZnO NT arrays on Gr [131]. By mounting a sensor on the wrist and philtrum (Fig. 15(b(ii)) of a person, the sensors were able to volunteer the individual's breathing and pulse. As shown in Fig. 15(b

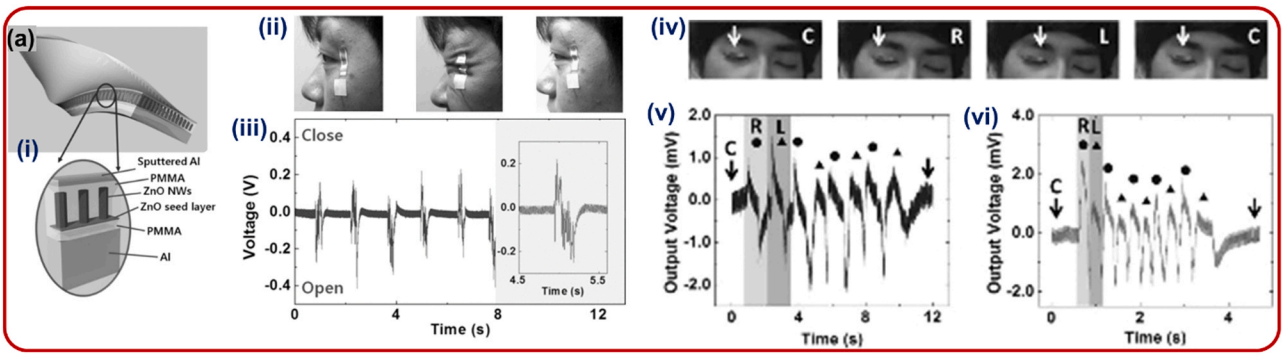

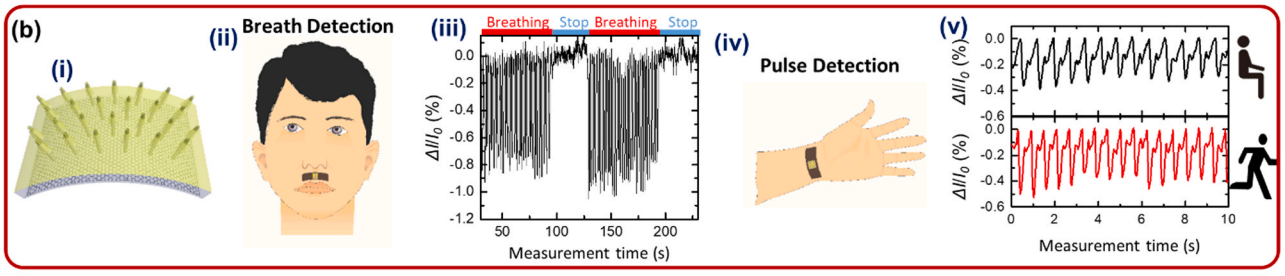

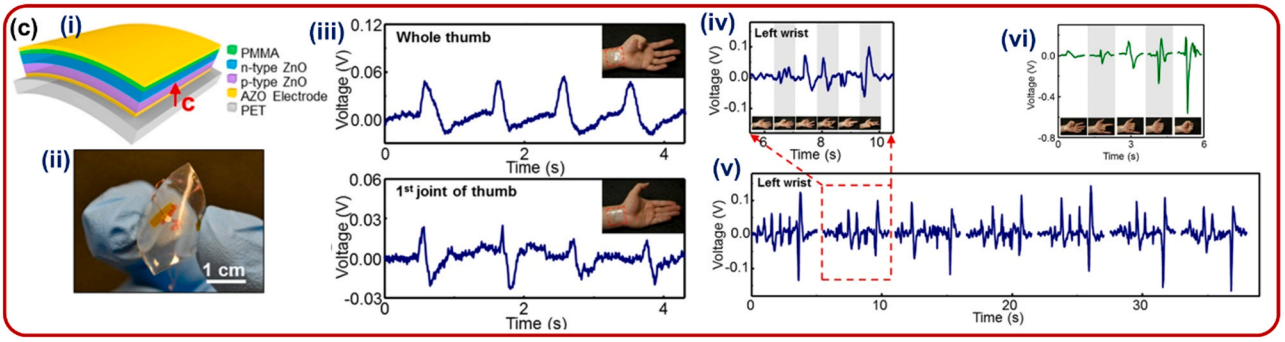

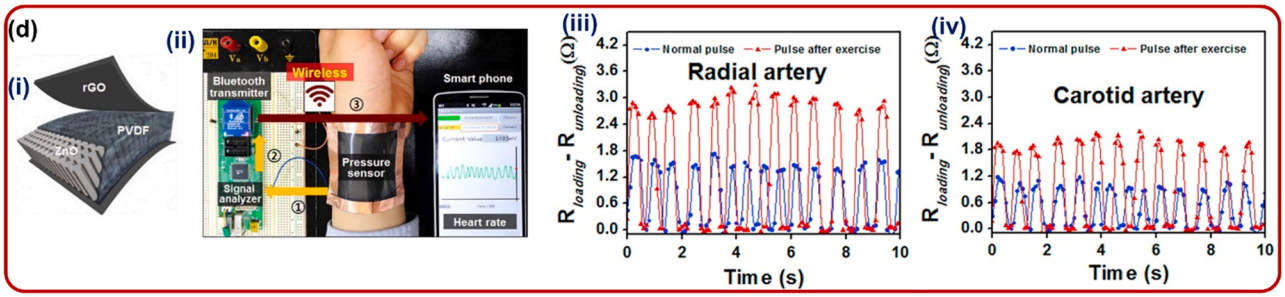

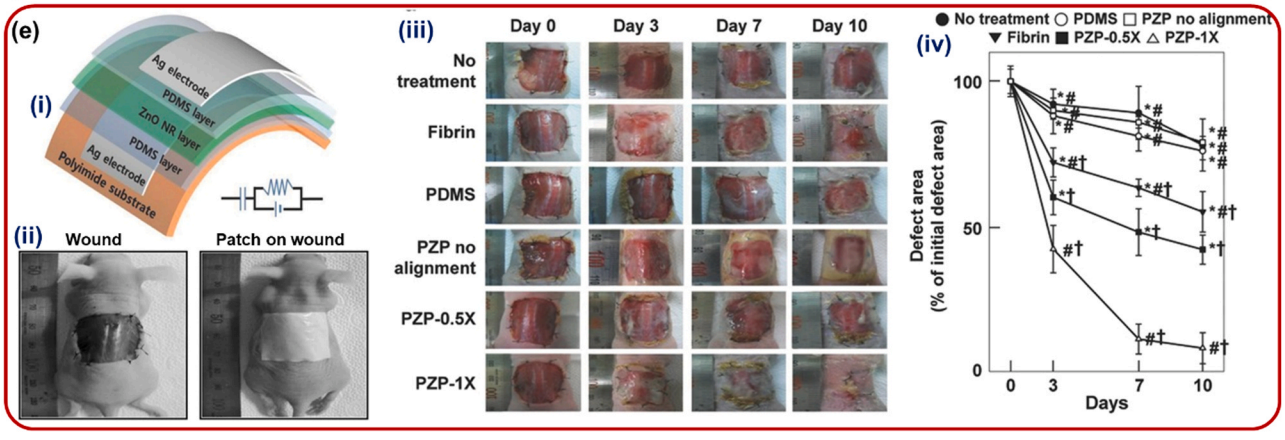

(caption on next page)

Fig. 15. Human activity and health monitoring devices. (a) Super-flexible NG as an active sensor under skin movement: (i) Schematic illustration of the super-flexible NG on ultrathin Al foil. An enhanced image of a device cross-section is displayed in the bottom panel. (ii) Photographs of NG mounted to the skin, ready (on the left), wrinkled (in the middle), and unwrinkled (on the right). (iii) Output of the NG driven by blinking of one eye. Reproduced with permission [406]. Copyright 2013, Wiley-VCH GmbH. (iv) The NG attached to the right eye-lid driven by moving the eye-ball in right (R) → center (C) → left (L) or L → C → R directions. Output voltage measured under (v) slow, and (vi) rapid eye movement. Reproduced with permission [407]. Copyright 2014, Wiley-VCH GmbH. (b) Vital sign detection from ZnO NT-based pressure sensors: (i) Schematic representation of a pressure sensor using dimension- and position-controlled ZnO NT arrays heteroepitaxially grown on Gr layers. (ii) Schematic illustration of constructed pressure sensor for breath detection when the sensor was directly attached to volunteer's philtrum. (iii) Real-time current response of the ZnO pressure sensor during breath monitoring. (iv) A schematic illustration of the pressure sensor that was made to detect pulses while being directly attached to a volunteer's wrist. (v) Real-time current response of the ZnO pressure sensor during pulse monitoring before and after running. Reproduced with permission [131]. Copyright 2021, Springer Nature. (c) Homojunction PNG grown in the p-n configuration on Si rubber for gesture recognition by the measurement of flexor movement: (i) Schematic illustration, and (ii) photograph of the homojunction PNG. (iii) The output of the device calculated as a function of the variation in thumb flexion. (iv) Measured signals by the gadget when the left wrist was used to individually flex and extend each finger. (v) The stability of the device demonstrated by making the identical gestures with the left hand repeatedly. (vi) The device's capacity to recognize more complicated motions demonstrated by using the multifinger gestures. In order, the patterns were thumb; middle and ring; index, middle, and ring; index, middle, ring, and little; and all five fingers. Reproduced with permission [208]. Copyright 2014, American Chemical Society. (d) Pressure sensor using free standing ZnO/PVDF for heart rate monitoring: (i) schematic of the pressure sensor. (ii) Photograph of a wearable and wireless pressure sensor. The difference between the electrical resistance of ZnO NN/PVDF film-based wireless pressure sensor as a function of time for measuring the pulse on the (iii) carotid artery, and the (iv) radial artery of a human object. The heart rate was 88 bpm for 10 s during the usual pulse and 121 bpm after exercise. Reproduced with permission [153]. Copyright 2016, Elsevier. (e) ZnO NR-based piezoelectric patch (PZP) for wound healing: (i) An illustration of the PZP modified with Ag electrodes to measure the piezoelectric voltage and current density generated by mechanical bending. (ii) Photographs of the skin wound on the back of a mouse (left), and a nine-layered PZP placed on the wound by covering the PZP with a transparent film (right). (iii) Photographs of a representative skin wound taken at 0, 3, 7, and 10 days following therapy. (iv) Wound closure rates. Reproduced with permission [408]. Copyright 2017, Wiley-VCH GmbH.

(ii)), the sensors effectively detected a simple pause in regular breathing, which is symptomatic of sleep apnea. Additionally, the monitoring of heartbeat rates was conducted on a volunteer, both at rest and during a brief workout (running). The corresponding pulse waveforms are shown in Fig. 15(b(v)). At rest, there were 13 pulses per 10 s, and after exercising, there were 16 pulses per 10 s. Due to the faster heartbeat caused by running, the depth of pulse climbed up to 25%, indicating the potential use of these pressure sensors as a workout partner in daily life, particularly for elderly people [131].

By measuring flexor movement, K. C. Pradel et al. demonstrated homojunction NG formed in the ZnO p-n configuration on Si rubber for gesture recognition (as depicted in Fig. 15(c)) [208]. The piezoelectric output was greatly increased in the p-n configuration as compared to a single layer device. The improvement was ascribed to the formation of the depletion zone at the p-n homojunction, which significantly reduced the internal screening of strain-induced polarization charges by free carriers in both n-ZnO and Sb-doped p-ZnO. As a result, the PNG could effectively translate the flexor tendon movements into distinct electrical signals for gesture identification [208]. Free-standing ZnO NN/PVDF hybrid thin film was developed by K. Y. Shin et al. to demonstrate a highly sensitive, wearable, and wireless pressure sensor for heart rate monitoring (Fig. 15(d)) [153]. The physical pulse pressure was measured in real time after mounting the sensor directly to the wrist (Fig. 15(d(ii))), where the radial artery is closest to the surface and a neck over the carotid artery. After integrating the sensor with a smart phone, the heart rate was monitored via smart phone screen. The sensor was utilized to investigate the effect of exercise (cycle pedalling) on heart rate. The post-exercise pulse was 121 bpm as compared to the usual pulse of 88 bpm. Due to the comparatively thin scarfskin, which could put the more intense pressure on the device, the normal and post-exercise heartbeat was monitored more sensitively on the radial artery [153]. 1D ZnO nanostructures and their well-ordered arrays.

The PNG-generated electric field, when placed to a wound, can mimic the endogenous electric field and promote in wound healing [408]. S. H. Bhang et al. designed a piezoelectric patch (PZP) composed of bidirectionally grown ZnO NRs and demonstrated its therapeutic efficacy in dermal wound healing [408]. The PZP was fabricated by aligned ZnO NRs embedded in a PDMS matrix as shown schematically in the Fig. 15(e(i)). The average voltage and current density generated on the PZP surface upon bending it with a 5 mm bending radius were $\approx$ 1.8 V and 85 nA cm^{-2}, respectively. By Applying the PZP to an animal's skin wound (Fig. 15(e(ii))), it generated an electric field upon animal motion and piezoelectric potentials to be induced at the site of wound for enabling wound healing. As shown in Fig. 15(e(iii, iv)), the wounds with PZP-1X (9 layers of PZP, the filling rate is 95.2%) were almost healed completely after 10 days, which suggested that the designed PNG had the best effect on promoting wound closure and skin regeneration [408].

One of the most serious metabolic diseases in the world has traditionally been regarded to be diabetes. One of the key requirements for diabetic patients is to constantly and everywhere check their blood glucose levels [409]. Thus, a novel skin-like glucose sensor that is integrated with the body, has a sustainable energy power source, is non-toxic, biocompatible, and affordable would be extremely beneficial to diabetes patients [267,378,410–413]. A self-powered closed-loop brain-machine interface system with biosensing-piezoelectric coupling was developed for real-time monitoring and rapid blood glucose concentration adjustments [412]. A flexible glucose sensor, a ZnO NW array-based energy harvester, and a micro-control unit were used to build the wearable and implantable device. The real-time monitoring of the saliva glucose levels and signal transmission to the micro-control unit were done using the flexible glucose sensor. After producing energy from bodily motion, the piezoelectric energy harvester converted it into electrical power for the micro-controller and brain stimulator. The micro-control unit was used to monitor the blood glucose level and, if necessary, send a stimulation current to the brain stimulator electrode to rapidly increase it. Based on the piezo-enzymatic reaction coupling mechanism of the glucose oxidase/ZnO NW array that can operate in liquid solution, a novel e-skin has been engineered by X. Xue et al [411]. The glucose concentration in the body fluids (tear, saliva, urine, and blood) had a substantial impact on the piezoelectric output voltage, which served as the device's biosensing signal and electrical power source [411]. On the basis of an enzyme/ZnO nanoarray piezo-biosensing unit matrix, a self-powered wearable noninvasive e-skin for perspiration analysis has also been developed [410]. The sweat-based e-skin was effective at identifying lactate, glucose, uric acid, and urea. Such an e-skin functioned as a workout monitor by constantly and in real-time tracking a runner's physiological state by examining the perspiration on his skin [410].

The von Neuman bottleneck, which restricts the performance of most contemporary computers, may be overcome by newly emerging brain-inspired neuromorphic computing systems [414]. Artificial synapses that imitate neural transmission and physical information sensing could be used to create extremely reliable and effective computing systems that are reminiscent of human brain. Different hybrid systems have been researched recently in order to create artificial synapse-based neuromorphic devices with multi-level sensory stimuli beyond light and electricity [132,171,342,414–416]. Two-terminal piezo-phototronic synapses array based on 1D ZnO nanostructures and their regularly

ordered arrays have secured their place to fabricate artificial synapse-based neuromorphic devices [132,171,342]. The utilization of piezopotential-induced modulation of channel conductance in a two-terminal device significantly reduced the complicacy of using three-terminal devices with transistor geometry. C. Jiang et al. demonstrated a bio-inspired e-skin structure with neuromorphic tactile sensing and memory functions based on site- and morphology-controlled ZnO NW arrays [132]. In addition to demonstrating functions beyond those of conventional e-skins and human skins, the device could imitate the neuromorphic tactile behavior of humans. It also exhibited nanoscale force perception and signal memory [132]. G. Hu et al. demonstrated a transparent and adaptable photonic synapse based on a single ZnO NW that resulted in multi-level modification of synaptic plasticity behavior and beneficial in constructing a multi-sensory neuromorphic system [171]. Furthermore, the piezo-phototronic effect induced in the ZnO NW allowed for efficient modulation of the synaptic weight change by applying compressive strains. Under a UV light pulse of 4.2 mW cm^{-2}, the weight change was decreased from 1437.5% to 191.4% with a compressive strain change from 0.00% to 0.28% [171]. Recently, X. Han et al. showed a optoelectronic synapses array based on ZnO NW/A-l_2O_3/CdS heterojunction that has potential applications in autonomous vision, neuromorphic computing, adaptive visual-perception systems, etc [342].

The piezotronic devices demonstrated their potential to be one of the key elements of a fully-fledged Internet of Medical Things (IoMT) system with the recent advances of implanted and wearable medical devices constructed by 1D ZnO nanostructures. In order to build a IoMT paradigm for the next generation of personalized healthcare for remote health mentoring and disease diagnostics, W. Deng et al. designed a PNG-based intelligent closed-loop system [1]. This smart system worked in three steps. 1st step involved the piezoelectric response of signals from a variety of physiological parameters such as physical motion, pulse, respiration, temperature, sweat, bio/organic compounds in the blood, etc. The integrated wireless network was used in the 2nd step to transfer directly these physiological data to the hospital or medical facility. In the final step, the transmitted data was examined by the experienced clinicians and doctors who then provided feedback to the patient, and thereby the closed-loop personalized healthcare was realized [1].

In addition to the physical health monitoring, 1D ZnO nanostructure and its HS-based piezotronic sensors are utilized for the detection and monitoring of different environmental phenomena, which are vital to maintain human health, updating personalized gadgets, bringing daily use tools for smooth life, and keeping our environment safe. These include pH sensor;[417] ascorbic acid sensing from sweat, tears, and saliva;[402] glucose sensor;[267,411] sweat sensor;[418] lactate, glucose, uric acid, and urea sensor for workout monitoring;[410] urea/uric-acid sensor for real-time kidney-disease diagnosis;[419] cancer therapy;[7,61] motion sensor;[59,420–422] motion sensor towards the remote control of gestures;[208,423,424] temperature sensor;[425] ethanol sensor;[204] humidity sensor;[256,426,427] heart rate monitoring and critical care; [153] muscle activity detection and gait monitoring;[428] protein sensor;[177] sensor for detecting protein kinases activity;[429] flammable/toxic gas detector;[176] H_2 sensor;[386] oxygen sensor;[430] footstep sensor;[431] transportation monitoring from vehicle motion; [432] LPG sensor;[433] triethylamine sensor;[434] H_2S sensor;[435, 436] logic computation;[368] wireless data transmission;[437] vibration sensor;[438] photonic synapse;[171] vehicle sensor;[439] piezo-induced photo/electrocatalysis;[440,441] piezo photo-transistor;[442] logic nanodevices;[369] resistive switches as programmable electromechanical memories;[443] photodetectors;[444–447] etc.

7. Conclusions and outlook

Herein, a detailed review on the recent developments of aligned 1D ZnO nanostructures and its regularly ordered arrays are presented for their applications in multifunctional piezotronic sensors. From a material standpoint, substantial effort is made on the fundamental research executed on 1D ZnO nanomaterials organized in the form of a regular array, leading to revolutionary manufacturing techniques to construct smart and intelligent, functional units with advanced performances in prospective piezotronic applications. In the light of piezoelectric properties and prospective applications, well-ordered 1D ZnO nanostructures are compared with individual 1D components, irregular 1D ZnO arrays and their random alignment, patterned bundles of nanostructures, and thin films to determine their potentiality as one of the most suitable active components for a multifunctional piezotronic sensor. As an introductory part, the important aspects of 1D ZnO nanomaterials and its arrays are explored for improving/controlling their piezoelectric properties and associated piezotronic device performances, which include nanostructure aspect ratio, alignment, arial density, shape, doping, surface functionalization, integrating materials and HS approach, 1D/2D combination of materials, device contact type, substrate flexibility, hybridization of mechano-electric properties, integration of piezoelectricity with photonics, etc. This review covered the well-established synthesis techniques for high-quality, controllable 1D ZnO nanostructures, the rational design, piezoelectric performance, the utilization of HSs for improved performance and incorporation of multifunctionalities, fabrication of piezotronic devices, and their integration with a flexible substrate/supported matrix for flexible and wearable applications. A detailed discussion on the pressure sensing, strain detection, and the piezopotential-gated transistors are made which are the main principles for piezotronic sensors. Furthermore, an overview of the latest progress in practical applications of piezotronic sensors in unconventional power sources, self-powered sensors, high-resolution image sensors, and personalized healthcare devices is provided.

With the recent developments of implantable and wearable medical devices made by 1D ZnO nanostructures, the piezotronic devices demonstrated their promising application to be one of the core components of a closed-loop IoMT system for the next-generation personalized healthcare for remote health mentoring and diagnosis of diseases. A schematic of prospective physical/physiological sensing applications of 1D ZnO-based piezotronic sensors are shown in Fig. 16. Despite the intriguing developments that have been achieved for 1D ZnO-based piezotronics, there are still a number of issues that need to be resolved.

- *Large-scale production:* It is generally convenient to fabricate well-ordered nanostructures on a small scale. The majority of practical applications for piezotronic technology, however, require the production of active materials in large quantities with high levels of homogeneity and reproducibility. Furthermore, the yield of high-quality, ordered arrays of 1D ZnO nanostructures is considerably insufficient for the fabrication and integration of scalable devices. Therefore, the development of a low-cost, scalable, and reproducible fabrication technique is greatly desired, especially for high aspect ratio ZnO nanoarchitectures organized in a regular array. Apart from the design of nano/microstructured sensing materials, the macrostructural design of these functional materials is also crucial from the prospect of practical applications.
- *Cost-effective manufacturing:* For small-powered daily-use personalized gadgets, cost reduction is one of the main future goals. The need for cost-effective personalized healthcare devices has sparked a great deal of research interest due to the economic limits associated with devices based on 1D ZnO nanostructure arrays. These constraints have presented a significant challenge to both academics and companies.
- *Stability of the nanoarchitectures and long lifetime of the associated devices:* For reliable use in various domains, the active material for the piezotronic devices as well as the devices themselves should not be too fragile upon mechanical stress. Consideration should be given to maintain the stability of devices in the harsh environments, including atmospheric conditions, humidity, heating, light exposure, and chemical strength. To maintain consistent device performance

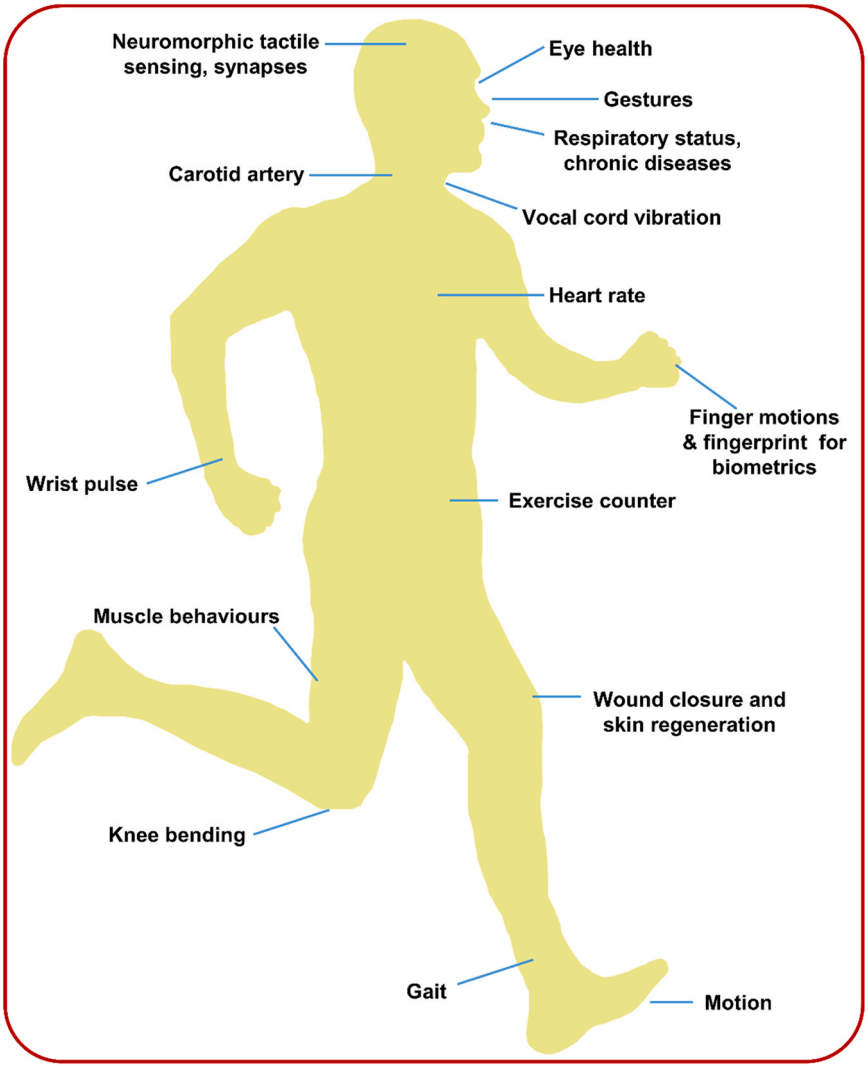

Fig. 16. Schematic illustration of prospective physical/physiological sensing applications of 1D ZnO-based piezotronic sensors.

throughout time, research attention must be paid to encapsulation technologies.

- *Selective and specific detection for the piezoelectric sensor:* Due to signal interference from the capacitive, resistive, and photon-induced responses, it may be difficult to recognize the piezoelectric response in a complex matrix. It follows that the active piezoelectric matrices should respond to mechanical stimuli without interference from external sources, which can be achieved by creating the appropriate heterostructure/functionalization. Such tactics can lead to the progress of 1D ZnO nanostructures in the direction of the reliable piezoelectric sensor.
- *Extension of applications through interface engineering:* With the integration of various metallic, semiconducting, and other optoelectronic functionalities, numerous directions in device application can be created, opening up a wide range of opportunities for interface engineering. For instance, 1D ZnO-based vdW HSs can offer more novel interaction modes with external stimuli, and hence the study of these HSs and their interface engineering will continue to be one of the frontier subjects in the coming years [448].

- *Modification strategies for appropriate utilization of the active material system:* Despite the availability of large materials and structures today, it is difficult to balance all of the critical factors that affect sensing performance. For instance, sensors with great sensitivity typically have lower stability or a smaller working range. However, the actual use of flexible piezotronic sensors calls for balanced performance. Thus, the development of a reliable strategy for figuring out the modification process of active is crucial. Over the past years, there has been substantial research on doping, surface modification, organic-inorganic hybrids, and the development of multiple compounds or heterojunctions. Yet, an effective modification technique would need that will take into account a number of variables, including surface states, defects, traps, contamination caused by catalysts (during synthesis), orientation, and polarization of 1D ZnO nanostructures.
- *Doping in a controlled way:* Controlled doping in ZnO at the nanoscale level for functional nanodevices is still challenging and demands research attention as it is regarded as one of the primary methods for adjusting piezoelectric characteristics. Moreover, not only doping components, levels, and processes but also all the induced electrical and structural changes to the materials that come along with doping need to be properly characterized and regulated for this approach.
- *Development of decoupling techniques in device output to avoid crosstalk and maintain accuracy:* In the case of piezoelectric sensors, it is desirable to detect multiple stimuli by a single device, which may cause an overlapping response. In addition to that interference in response from a specific stimulus can originate from the surrounding environment. A pressure sensor, for instance, may detect disturbances caused by sound, light, temperature, wind, and a range of other stimuli that might cause strain in ZnO at the nanoscale.

Decoupling the output requires significant attention in order to prevent crosstalk and enable precise detection and pattern recognition [449–451]. Successful decomposition of the in-plane flexoelectric contribution to electromechanical responses from a ZnO NR-based PNG revealed that it contributed 12–20% of overall NG output [449].

- *Integration of piezoelectricity with other mechano-electric qualities for synergistic use:* Along with piezoelectricity, different other effects, including piezoresistive, triboelectric, flexoelectric, magnetoelastic effects can also convert mechanical energy into electrical energy. Thus, successful integration between piezoelectricity with these effects can enhance the device's performance significantly and introduce multifunctionalities. For example, the potential from a ZnO NR-based NG that integrated triboelectric and piezoelectric effects was enhanced by 21.8 V as compared to that of pure triboelectric effects [91]. Thus, plenty of research opportunities are lying in this field.
- *Appropriate electrode material for flexible and wearable applications:* Development of extremely flexible and wearable piezotronic devices depends on the design and fabrication of electrodes with high conductivity, low fatigue, and great stretchability. Considering the scalability, reliability, and compatibility with the active materials and substrates utilized for the respective devices, soft metal electrodes (SMEs) can play a crucial role and serve as the foundation of these devices [452]. SMEs offer important advantages of simplicity, cost effectiveness, and compatibility to the mass manufacturing of flexible piezotronic devices in contrast to traditional microfabrication technologies that have migrated from silicon technology. SME must therefore undergo significant development for their successful implementation in piezotronics.
- *Environment-friendly devices:* Different types of plastics and other nonbiodegradable polymers are typically employed as a substrate, insulating filler or host matrix for piezotronic devices in order to fabricate flexible and wearable applications. Sometimes, soft polymers are also used for lamination/encapsulation of the devices to protect device performance from interfering substances. The widespread use of these nonbiodegradable products has detrimental effects on both human and environmental health. The goal of the future research should be to examine alternate flexible materials those have least effect in device output while conserving the biocompatibility as well as the environment-friendly nature of the devices.
- *Implantable medical applications:* The delivery of highly specific treatments and on-organ monitoring will be made possible by appropriate implantation of sensing and stimulating devices, without harming the healthy operation of the surrounding organs and tissues. As a result, this area offers a wealth of research possibilities from both a scientific and an industrial perspective.

Piezotronics of 1D ZnO nanostructures have attracted people enormously from both academia as well as industrial bodies. Based on the multi-disciplinary perspective combining physics, materials, electronics, biology, computer science, and other disciplines, piezotronics is going to transform our daily life by developing next-generation smart devices, AI, IoT, IoMT, advanced healthcare, robotics, and energy technologies.

CRediT authorship contribution statement

Ramesh Ghosh: Writing – original draft, Writing – review & editing, Conceptualization, Methodology, Investigation, Data curation, Formal analysis.

Declaration of Competing Interest

The author declare that they have no known competing financial interests or personal relationships that could have appeared to influence the work reported in this paper.

Data availability

Data will be made available on request.

References

[1] W. Deng, Y. Zhou, A. Libanori, G. Chen, W. Yang, J. Chen, Piezoelectric nanogenerators for personalized healthcare, Chem. Soc. Rev. 51 (2022) 3380–3435.
[2] C. Steiger, A. Abramson, P. Nadeau, A.P. Chandrakasan, R. Langer, G. Traverso, Ingestible electronics for diagnostics and therapy, Nat. Rev. Mater. 4 (2019) 83–98.
[3] C.T. Lim, Future of health diagnostics, VIEW 1 (2020), e3.
[4] Y. Yang, W. Gao, Wearable and flexible electronics for continuous molecular monitoring, Chem. Soc. Rev. 48 (2019) 1465–1491.
[5] R. Ghosh, M.S. Song, J. Park, Y. Tchoe, P. Guha, W. Lee, Y. Lim, B. Kim, S.-W. Kim, M. Kim, G.-C. Yi, Fabrication of piezoresistive Si nanorod-based pressure sensor arrays: A promising candidate for portable breath monitoring devices, Nano Energy 80 (2021), 105537.
[6] W. Gao, S. Emaminejad, H.Y.Y. Nyein, S. Challa, K. Chen, A. Peck, H.M. Fahad, H. Ota, H. Shiraki, D. Kiriya, D.-H. Lien, G.A. Brooks, R.W. Davis, A. Javey, Fully integrated wearable sensor arrays for multiplexed in situ perspiration analysis, Nature 529 (2016) 509–514.
[7] Q. Truong Hoang, V. Ravichandran, T.G. Nguyen Cao, J.H. Kang, Y.T. Ko, T. I. Lee, M.S. Shim, Piezoelectric Au-decorated ZnO nanorods: Ultrasound-triggered generation of ROS for piezocatalytic cancer therapy, Chem. Eng. J. 435 (2022), 135039.
[8] S. Chen, J. Qi, S. Fan, Z. Qiao, J.C. Yeo, C.T. Lim, Flexible Wearable Sensors for Cardiovascular Health Monitoring, Adv. Healthc. Mater. 10 (2021) 2100116.
[9] Chen S., Zhu P., Mao L., Wu W., Lin H., Xu D., Lu X., Shi J., Piezocatalytic Medicine: An Emerging Frontier Using Piezoelectric Materials for Biomedical Applications, Advanced Materials n/a 2208256.
[10] S. Pyo, J. Lee, K. Bae, S. Sim, J. Kim, Recent Progress in Flexible Tactile Sensors for Human-Interactive Systems: From Sensors to Advanced Applications, Adv. Mater. 33 (2021) 2005902.
[11] T.R. Ray, J. Choi, A.J. Bandodkar, S. Krishnan, P. Gutruf, L. Tian, R. Ghaffari, J. A. Rogers, Bio-Integrated Wearable Systems: A Comprehensive Review, Chem. Rev. 119 (2019) 5461–5533.
[12] D. Chen, Q. Pei, Electronic muscles and skins: a review of soft sensors and actuators, Chem. Rev. 117 (2017) 11239–11268.
[13] S. Shrivastava, T.Q. Trung, N.-E. Lee, Recent progress, challenges, and prospects of fully integrated mobile and wearable point-of-care testing systems for self-testing, Chem. Soc. Rev. 49 (2020) 1812–1866.
[14] M. Tan, Y. Xu, Z. Gao, T. Yuan, Q. Liu, R. Yang, B. Zhang, L. Peng, Recent advances in intelligent wearable medical devices integrating biosensing and drug delivery, Adv. Mater. 34 (2022) 2108491.
[15] Y. Wang, H. Haick, S. Guo, C. Wang, S. Lee, T. Yokota, T. Someya, Skin bioelectronics towards long-term, continuous health monitoring, Chem. Soc. Rev. 51 (2022) 3759–3793.
[16] K. Meng, S. Zhao, Y. Zhou, Y. Wu, S. Zhang, Q. He, X. Wang, Z. Zhou, W. Fan, X. Tan, J. Yang, J. Chen, A. Wireless, Textile-Based Sensor System for Self-Powered Personalized Health Care, Matter 2 (2020) 896–907.
[17] K. Meng, X. Xiao, W. Wei, G. Chen, A. Nashalian, S. Shen, X. Xiao, J. Chen, Wearable pressure sensors for pulse wave monitoring, Adv. Mater. 34 (2022) 2109357.
[18] X. Wang, Z. Liu, T. Zhang, Flexible sensing electronics for wearable/attachable health monitoring, Small 13 (2017) 1602790.
[19] M. Zarei, G. Lee, S.G. Lee, K. Cho, Advances in Biodegradable Electronic Skin: Material Progress and Recent Applications in Sensing, Robotics, and Human–Machine Interfaces, Adv. Mater. 35 (2023) 2203193.
[20] Z.L. Wang, Progress in Piezotronics and Piezo-Phototronics, Adv. Mater. 24 (2012) 4632–4646.
[21] X. Cao, X. Cao, H. Guo, T. Li, Y. Jie, N. Wang, Z.L. Wang, Piezotronic Effect Enhanced Label-Free Detection of DNA Using a Schottky-Contacted ZnO Nanowire Biosensor, ACS Nano 10 (2016) 8038–8044.
[22] N. Wang, C. Gao, F. Xue, Y. Han, T. Li, X. Cao, X. Zhang, Y. Zhang, Z.L. Wang, Piezotronic-Effect Enhanced Drug Metabolism and Sensing on a Single ZnO Nanowire Surface with the Presence of Human Cytochrome P450, ACS Nano 9 (2015) 3159–3168.
[23] X. Wen, W. Wu, C. Pan, Y. Hu, Q. Yang, Lin, Z. Wang, Development and progress in piezotronics, Nano Energy 14 (2015) 276–295.
[24] Y. Zhang, Z.L. Wang, Theory of piezo-phototronics for light-emitting diodes, Adv. Mater. 24 (2012) 4712–4718.
[25] Z.L. Wang, W. Wu, Piezotronics and piezo-phototronics: fundamentals and applications, Natl. Sci. Rev. 1 (2013) 62–90.
[26] Z. Xu, C. Zhang, W. Wang, Y. Bando, X. Bai, D. Golberg, Lateral piezopotential-gated field-effect transistor of ZnO nanowires, Nano Energy 13 (2015) 233–239.
[27] Y. Liu, Y. Zhang, Q. Yang, S. Niu, Z.L. Wang, Fundamental theories of piezotronics and piezo-phototronics, Nano Energy 14 (2015) 257–275.
[28] K. Gupta, S. Brahma, J. Dutta, B. Rao, C.-P. Liu, Recent progress in microstructure development of inorganic one-dimensional nanostructures for enhancing performance of piezotronics and piezoelectric nanogenerators, Nano Energy 55 (2019) 1–21.

[29] Y. Wang, P. Zang, D. Yang, R. Zhang, S. Gai, P. Yang, The fundamentals and applications of piezoelectric materials for tumor therapy: recent advances and outlook, Mater. Horiz. (2023).
[30] X. Cao, Y. Xiong, J. Sun, X. Zhu, Q. Sun, Z.L. Wang, Piezoelectric Nanogenerators Derived Self-Powered Sensors for Multifunctional Applications and Artificial Intelligence, Adv. Funct. Mater. 31 (2021) 2102983.
[31] Z.L. Wang, On Maxwell's displacement current for energy and sensors: the origin of nanogenerators, Mater. Today 20 (2017) 74–82.
[32] L. Zhao, H. Li, J. Meng, Z. Li, The recent advances in self-powered medical information sensors, InfoMat 2 (2020) 212–234.
[33] Q. Zheng, Q. Tang, Z.L. Wang, Z. Li, Self-powered cardiovascular electronic devices and systems, Nat. Rev. Cardiol. 18 (2021) 7–21.
[34] F.R. Fan, W. Tang, Z.L. Wang, Flexible nanogenerators for energy harvesting and self-powered electronics, Adv. Mater. 28 (2016) 4283–4305.
[35] C. Dagdeviren, Z. Li, Z.L. Wang, Energy harvesting from the animal/human body for self-powered electronics, Annu. Rev. Biomed. Eng. 19 (2017) 85–108.
[36] Z.L. Wang, Towards self-powered nanosystems: from nanogenerators to nanopiezotronics, Adv. Funct. Mater. 18 (2008) 3553–3567.
[37] A.T. Le, M. Ahmadipour, S.-Y. Pung, A review on ZnO-based piezoelectric nanogenerators: Synthesis, characterization techniques, performance enhancement and applications, J. Alloy. Compd. 844 (2020), 156172.
[38] L. Liu, X. Guo, C. Lee, Promoting smart cities into the 5G era with multi-field Internet of Things (IoT) applications powered with advanced mechanical energy harvesters, Nano Energy 88 (2021), 106304.
[39] S. Panda, S. Hajra, K. Mistewicz, P. In-na, M. Sahu, P.M. Rajaitha, H.J. Kim, Piezoelectric energy harvesting systems for biomedical applications, Nano Energy 100 (2022), 107514.
[40] H. Askari, N. Xu, B.H. Groenner Barbosa, Y. Huang, L. Chen, A. Khajepour, H. Chen, Z.L. Wang, Intelligent systems using triboelectric, piezoelectric, and pyroelectric nanogenerators, Mater. Today 52 (2022) 188–206.
[41] P. Sun, S. Jiang, Y. Huang, Nanogenerator as self-powered sensing microsystems for safety monitoring, Nano Energy 81 (2021), 105646.
[42] Z.L. Wang, G. Zhu, Y. Yang, S. Wang, C. Pan, Progress in nanogenerators for portable electronics, Mater. Today 15 (2012) 532–543.
[43] Z. Yang, S. Zhou, J. Zu, D. Inman, High-Performance Piezoelectric Energy Harvesters and Their Applications, Joule 2 (2018) 642–697.
[44] E.S. Nour, M.O. Sandberg, M. Willander, O. Nur, Handwriting enabled harvested piezoelectric power using ZnO nanowires/polymer composite on paper substrate, Nano Energy 9 (2014) 221–228.
[45] B. Shi, Z. Li, Y. Fan, Implantable energy-harvesting devices, Adv. Mater. 30 (2018) 1801511.
[46] D.Y. Kim, S. Lee, Z.-H. Lin, K.H. Choi, S.G. Doo, H. Chang, J.-Y. Leem, Z.L. Wang, S.-O. Kim, High temperature processed ZnO nanorods using flexible and transparent mica substrates for dye-sensitized solar cells and piezoelectric nanogenerators, Nano Energy 9 (2014) 101–111.
[47] M. Zhou, M.S.H. Al-Furjan, J. Zou, W. Liu, A review on heat and mechanical energy harvesting from human – Principles, prototypes and perspectives, Renew. Sustain. Energy Rev. 82 (2018) 3582–3609.
[48] X. Wang, J. Song, J. Liu, Z.L. Wang, Direct-Current Nanogenerator Driven by Ultrasonic Waves, Science 316 (2007) 102–105.
[49] S.D. Mahapatra, P.C. Mohapatra, A.I. Aria, G. Christie, Y.K. Mishra, S. Hofmann, V.K. Thakur, Piezoelectric Materials for Energy Harvesting and Sensing Applications: Roadmap for Future Smart Materials, Adv. Sci. 8 (2021) 2100864.
[50] X. Li, M. Sun, X. Wei, C. Shan, Q. Chen, 1D Piezoelectric Material Based Nanogenerators: Methods, Mater. Prop. Optim. 8 (2018).
[51] Y. Wu, Y. Ma, H. Zheng, S. Ramakrishna, Piezoelectric materials for flexible and wearable electronics: A review, Mater. Des. 211 (2021), 110164.
[52] M. Safaei, H.A. Sodano, S.R. Anton, A review of energy harvesting using piezoelectric materials: state-of-the-art a decade later (2008–2018), Smart Mater. Struct. 28 (2019), 113001.
[53] Y. Hu, C. Pan, Z.L. Wang, Recent progress in piezo-phototronics with extended materials, application areas and understanding, Semicond. Sci. Technol. 32 (2017), 053002.
[54] H. Liu, J. Zhong, C. Lee, S.-W. Lee, L. Lin, A comprehensive review on piezoelectric energy harvesting technology: Materials, mechanisms, and applications, Appl. Phys. Rev. 5 (2018), 041306.
[55] F. Invernizzi, S. Dulio, M. Patrini, G. Guizzetti, P. Mustarelli, Energy harvesting from human motion: materials and techniques, Chem. Soc. Rev. 45 (2016) 5455–5473.
[56] F. Zhang, S. Niu, W. Guo, G. Zhu, Y. Liu, X. Zhang, Z.L. Wang, Piezo-phototronic Effect Enhanced Visible/UV Photodetector of a Carbon-Fiber/ZnO-CdS Double-Shell Microwire, ACS Nano 7 (2013) 4537–4544.
[57] Z. Guo, H. Li, L. Zhou, D. Zhao, Y. Wu, Z. Zhang, W. Zhang, C. Li, J. Yao, Large-Scale Horizontally Aligned ZnO Microrod Arrays with Controlled Orientation, Periodic Distribution as Building Blocks for Chip-in Piezo-Phototronic LEDs, Small 11 (2015) 438–445.
[58] K.C. Pradel, W. Wu, Y. Zhou, X. Wen, Y. Ding, Z.L. Wang, Piezotronic Effect in Solution-Grown p-Type ZnO Nanowires and Films, Nano Lett. 13 (2013) 2647–2653.
[59] Y. Tan, K. Yang, B. Wang, H. Li, L. Wang, C. Wang, High-performance textile piezoelectric pressure sensor with novel structural hierarchy based on ZnO nanorods array for wearable application, Nano Res. 14 (2021) 3969–3976.
[60] S. Xu, Y. Wei, J. Liu, R. Yang, Z.L. Wang, Integrated Multilayer Nanogenerator Fabricated Using Paired Nanotip-to-Nanowire Brushes, Nano Lett. 8 (2008) 4027–4032.
[61] B. Ortiz-Casas, A. Galdámez-Martínez, J. Gutiérrez-Flores, A. Baca Ibañez, P. Kumar Panda, G. Santana, H.A. de la Vega, M. Suar, C. Gutiérrez Rodelo, A. Kaushik, Y. Kumar Mishra, A. Dutt, Bio-acceptable 0D and 1D ZnO nanostructures for cancer diagnostics and treatment, Mater. Today 50 (2021) 533–569.
[62] Z. Lou, L. Wang, K. Jiang, Z. Wei, G. Shen, Reviews of wearable healthcare systems: Materials, devices and system integration, Mater. Sci. Eng.: R: Rep. 140 (2020), 100523.
[63] S. Zhang, C. Liu, X. Sun, W. Huang, Current development of materials science and engineering towards epidermal sensors, Prog. Mater. Sci. 128 (2022), 100962.
[64] W. Wu, Z.L. Wang, Piezotronics and piezo-phototronics for adaptive electronics and optoelectronics, Nat. Rev. Mater. 1 (2016) 16031.
[65] V. Consonni, A.M. Lord, Polarity in ZnO nanowires: A critical issue for piezotronic and piezoelectric devices, Nano Energy 83 (2021), 105789.
[66] W. Wu, C. Pan, Y. Zhang, X. Wen, Z.L. Wang, Piezotronics and piezo-phototronics – From single nanodevices to array of devices and then to integrated functional system, Nano Today 8 (2013) 619–642.
[67] J. Yu, X. Yang, Q. Sun, Piezo/tribotronics toward smart flexible sensors, Adv. Intell. Syst. 2 (2020) 1900175.
[68] C. Pan, M. Chen, R. Yu, Q. Yang, Y. Hu, Y. Zhang, Z.L. Wang, Progress in piezo-phototronic-effect-enhanced light-emitting diodes and pressure imaging, Adv. Mater. 28 (2016) 1535–1552.
[69] L. Wang, Z.L. Wang, Advances in piezotronic transistors and piezotronics, Nano Today 37 (2021), 101108.
[70] Z.L. Wang, Nanogenerators, self-powered systems, blue energy, piezotronics and piezo-phototronics – A recall on the original thoughts for coining these fields, Nano Energy 54 (2018) 477–483.
[71] H. Askari, A. Khajepour, M.B. Khamesee, Z. Saadatnia, Z.L. Wang, Piezoelectric and triboelectric nanogenerators: Trends and impacts, Nano Today 22 (2018) 10–13.
[72] B. Yin, H. Zhang, Y. Qiu, Y. Chang, J. Lei, D. Yang, Y. Luo, Y. Zhao, L. Hu, Piezo-phototronic effect enhanced pressure sensor based on ZnO/NiO core/shell nanorods array, Nano Energy 21 (2016) 106–114.
[73] J. Sun, X. Zhang, Y. Lang, J. Bian, R. Gao, P. Li, Y. Wang, C. Li, Piezo-phototronic effect improved performance of n-ZnO nano-arrays/p-Cu2O film based pressure sensor synthesized on flexible Cu foil, Nano Energy 32 (2017) 96–104.
[74] S. Pal, S. Bayan, D.K. Goswami, S.K. Ray, Superior Performance Self-Powered Photodetectors Utilizing the Piezo-Phototronic Effect in SnO Nanosheet/ZnO Nanorod Hybrid Heterojunctions, ACS Appl. Electron. Mater. 2 (2020) 1716–1723.
[75] X. Yang, L. Dong, C. Shan, J. Sun, N. Zhang, S. Wang, M. Jiang, B. Li, X. Xie, D. Shen, Piezophototronic-Effect-Enhanced Electrically Pumped Lasing, Adv. Mater. 29 (2017) 1602832.
[76] K. Kim, Y. Jeon, K. Cho, S. Kim, Enhancement of Trap-Assisted Green Electroluminescence Efficiency in ZnO/SiO2/Si Nanowire Light-Emitting Diodes on Bendable Substrates by Piezophototronic Effect, ACS Appl. Mater. Interfaces 8 (2016) 2764–2773.
[77] S. Liu, Q. Liao, Z. Zhang, X. Zhang, S. Lu, L. Zhou, M. Hong, Z. Kang, Y. Zhang, Strain modulation on graphene/ZnO nanowire mixed-dimensional van der Waals heterostructure for high-performance photosensor, Nano Res. 10 (2017) 3476–3485.
[78] Y. Zhang, M. Xie, V. Adamaki, H. Khanbareh, C.R. Bowen, Control of electro-chemical processes using energy harvesting materials and devices, Chem. Soc. Rev. 46 (2017) 7757–7786.
[79] L. Dong, C. Jin, A.B. Closson, I. Trase, H.C. Richards, Z. Chen, J.X.J. Zhang, Cardiac energy harvesting and sensing based on piezoelectric and triboelectric designs, Nano Energy 76 (2020), 105076.
[80] S.C. Rai, K. Wang, Y. Ding, J.K. Marmon, M. Bhatt, Y. Zhang, W. Zhou, Z.L. Wang, Piezo-phototronic Effect Enhanced UV/Visible Photodetector Based on Fully Wide Band Gap Type-II ZnO/ZnS Core/Shell Nanowire Array, ACS Nano 9 (2015) 6419–6427.
[81] F. Zhang, Y. Ding, Y. Zhang, X. Zhang, Z.L. Wang, Piezo-phototronic Effect Enhanced Visible and Ultraviolet Photodetection Using a ZnO–CdS Core–Shell Micro/nanowire, ACS Nano 6 (2012) 9229–9236.
[82] Z. Wang, R. Yu, C. Pan, Y. Liu, Y. Ding, Z.L. Wang, Piezo-Phototronic UV/Visible Photosensing with Optical-Fiber–Nanowire Hybridized Structures, Adv. Mater. 27 (2015) 1553–1560.
[83] S. Yan, S.C. Rai, Z. Zheng, F. Alqarni, M. Bhatt, M.A. Retana, W. Zhou, Piezophototronic Effect Enhanced UV/Visible Photodetector Based on ZnO/ZnSe Heterostructure Core/Shell Nanowire Array and Its Self-Powered Performance, Adv. Electron. Mater. 2 (2016) 1600242.
[84] M. Chen, B. Zhao, G. Hu, X. Fang, H. Wang, L. Wang, J. Luo, X. Han, X. Wang, C. Pan, Z.L. Wang, Piezo-Phototronic Effect Modulated Deep UV Photodetector Based on ZnO-Ga2O3 Heterojuction Microwire, Adv. Funct. Mater. 28 (2018) 1706379.
[85] W. Peng, X. Wang, R. Yu, Y. Dai, H. Zou, A.C. Wang, Y. He, Z.L. Wang, Enhanced Performance of a Self-Powered Organic/Inorganic Photodetector by Pyro-Phototronic and Piezo-Phototronic Effects, Adv. Mater. 29 (2017) 1606698.
[86] Q. Yang, Y. Liu, C. Pan, J. Chen, X. Wen, Z.L. Wang, Largely Enhanced Efficiency in ZnO Nanowire/p-Polymer Hybridized Inorganic/Organic Ultraviolet Light-Emitting Diode by Piezo-Phototronic Effect, Nano Lett. 13 (2013) 607–613.
[87] B. Dai, G.M. Biesold, M. Zhang, H. Zou, Y. Ding, Z.L. Wang, Z. Lin, Piezo-phototronic effect on photocatalysis, solar cells, photodetectors and light-emitting diodes, Chem. Soc. Rev. 50 (2021) 13646–13691.

[88] Y. Hu, Y. Chang, P. Fei, R.L. Snyder, Z.L. Wang, Designing the Electric Transport Characteristics of ZnO Micro/Nanowire Devices by Coupling Piezoelectric and Photoexcitation Effects, ACS Nano 4 (2010) 1234–1240.
[89] Y.Y. Broza, R. Vishinkin, O. Barash, M.K. Nakhleh, H. Haick, Synergy between nanomaterials and volatile organic compounds for non-invasive medical evaluation, Chem. Soc. Rev. 47 (2018) 4781–4859.
[90] X. Li, J. Wang, One-dimensional and two-dimensional synergized nanostructures for high-performing energy storage and conversion, InfoMat 2 (2020) 3–32.
[91] X. Yang, W.A. Daoud, Triboelectric and Piezoelectric Effects in a Combined Tribo-Piezoelectric Nanogenerator Based on an Interfacial ZnO Nanostructure, Adv. Funct. Mater. 26 (2016) 8194–8201.
[92] S. Wang, Z.L. Wang, Y. Yang, A One-Structure-Based Hybridized Nanogenerator for Scavenging Mechanical and Thermal Energies by Triboelectric–Piezoelectric–Pyroelectric Effects, Adv. Mater. 28 (2016) 2881–2887.
[93] Y.P. Lim, J.S.C. Koay, J. Zhao, S. Huang, B.T. Goh, K.C. Aw, B. Chen, C.Y. Haw, W.C. Gan, Modulating ZnO growth structures for maximum power output of hybrid piezo/triboelectric nanogenerator, Adv. Funct. Mater. 32 (2022) 2206750.
[94] C. Jirayupat, W. Wongwiriyapan, P. Kasamechonchung, T. Wutikhun, K. Tantisantisom, Y. Rayanasukha, T. Jiemsakul, C. Tansarawiput, M. Liangruksa, P. Khanchaitit, M. Horprathum, S. Porntheeraphat, A. Klamchuen, Piezoelectric-Induced Triboelectric Hybrid Nanogenerators Based on the ZnO Nanowire Layer Decorated on the Au/polydimethylsiloxane–Al Structure for Enhanced Triboelectric Performance, ACS Appl. Mater. Interfaces 10 (2018) 6433–6440.
[95] R. Yu, S. Niu, C. Pan, Z.L. Wang, Piezotronic effect enhanced performance of Schottky-contacted optical, gas, chemical and biological nanosensors, Nano Energy 14 (2015) 312–339.
[96] Y. Yang, Z.L. Wang, Hybrid energy cells for simultaneously harvesting multi-types of energies, Nano Energy 14 (2015) 245–256.
[97] Y. Liu, M. Pharr, G.A. Salvatore, Lab-on-Skin: A Review of Flexible and Stretchable Electronics for Wearable Health Monitoring, ACS Nano 11 (2017) 9614–9635.
[98] Y. Gao, L. Yu, J.C. Yeo, C.T. Lim, Flexible Hybrid Sensors for Health Monitoring: Materials and Mechanisms to Render Wearability, Adv. Mater. 32 (2020) 1902133.
[99] T.Q. Trung, N.-E. Lee, Flexible and Stretchable Physical Sensor Integrated Platforms for Wearable Human-Activity Monitoringand Personal Healthcare, Adv. Mater. 28 (2016) 4338–4372.
[100] L.-s Zhang, J. Li, F. Wang, J.-d Shi, W. Chen, X.-m Tao, Flexible stimuli-responsive materials for smart personal protective equipment, Mater. Sci. Eng.: R: Rep. 146 (2021), 100629.
[101] R. Agrawal, B. Peng, E.E. Gdoutos, H.D. Espinosa, Elasticity Size Effects in ZnO Nanowires—A Combined Experimental-Computational Approach, Nano Lett. 8 (2008) 3668–3674.
[102] J. Li, S. Ma, X. Liu, Z. Zhou, C.Q. Sun, ZnO Meso-Mechano-Thermo Physical Chemistry, Chem. Rev. 112 (2012) 2833–2852.
[103] X. Wang, W. Peng, C. Pan, Z. Lin Wang, Piezotronics and piezo-phototronics based ona-axis nano/microwires: fundamentals and applications, Semicond. Sci. Technol. 32 (2017), 043005.
[104] J. Nie, G. Hu, L. Li, Y. Zhang, Piezotronic analog-to-digital converters based on strain-gated transistors, Nano Energy 46 (2018) 423–427.
[105] R.K. Pandey, J. Dutta, S. Brahma, B. Rao, C.-P. Liu, Review on ZnO-based piezotronics and piezoelectric nanogenerators: aspects of piezopotential and screening effect, J. Phys.: Mater. 4 (2021), 044011.
[106] S. Liu, Z.-R. Tang, Y. Sun, J.C. Colmenares, Y.-J. Xu, One-dimension-based spatially ordered architectures for solar energy conversion, Chem. Soc. Rev. 44 (2015) 5053–5075.
[107] S.-H. Bae, H. Kum, W. Kong, Y. Kim, C. Choi, B. Lee, P. Lin, Y. Park, J. Kim, Integration of bulk materials with two-dimensional materials for physical coupling and applications, Nat. Mater. 18 (2019) 550–560.
[108] C. Liu, A. Yu, M. Peng, M. Song, W. Liu, Y. Zhang, J. Zhai, Improvement in the Piezoelectric Performance of a ZnO Nanogenerator by a Combination of Chemical Doping and Interfacial Modification, J. Phys. Chem. C. 120 (2016) 6971–6977.
[109] P. Ghamgosar, F. Rigoni, M.G. Kohan, S. You, E.A. Morales, R. Mazzaro, V. Morandi, N. Almqvist, I. Concina, A. Vomiero, Self-Powered Photodetectors Based on Core–Shell ZnO–Co3O4 Nanowire Heterojunctions, ACS Appl. Mater. Interfaces 11 (2019) 23454–23462.
[110] T. Zhang, M. Li, J. Chen, Y. Wang, L. Miao, Y. Lu, Y. He, Multi-component ZnO alloys: Bandgap engineering, hetero-structures, and optoelectronic devices, Mater. Sci. Eng.: R: Rep. 147 (2022), 100661.
[111] A. Mahmud, A.A. Khan, P. Voss, T. Das, E. Abdel-Rahman, D. Ban, A. High, Performance and Consolidated Piezoelectric Energy Harvester Based on 1D/2D Hybrid Zinc Oxide Nanostructures, Adv. Mater. Interfaces 5 (2018) 1801167.
[112] Y.-S. Chen, G.-W. Hsieh, S.-P. Chen, P.-Y. Tseng, C.-W. Wang, Zinc Oxide Nanowire-Poly(Methyl Methacrylate) Dielectric Layers for Polymer Capacitive Pressure Sensors, ACS Appl. Mater. Interfaces 7 (2015) 45–50.
[113] D.-M. Shin, E.L. Tsege, S.H. Kang, W. Seung, S.-W. Kim, H.K. Kim, S.W. Hong, Y.-H. Hwang, Freestanding ZnO nanorod/graphene/ZnO nanorod epitaxial double heterostructure for improved piezoelectric nanogenerators, Nano Energy 12 (2015) 268–277.
[114] H. Zhang, G. Tian, D. Xiong, T. Yang, S. Zhong, L. Jin, B. Lan, L. Deng, S. Wang, Y. Sun, W. Yang, W. Deng, Understanding the Enhancement Mechanism of ZnO Nanorod-based Piezoelectric Devices through Surface Engineering, ACS Appl. Mater. Interfaces 14 (2022) 29061–29069.
[115] A. Waseem, M.A. Johar, A. Abdullah, I.V. Bagal, J.-S. Ha, J.K. Lee, S.-W. Ryu, Enhanced performance of a flexible and wearable piezoelectric nanogenerator using semi-insulating GaN:Mg/ZnO coaxial nanowires, Nano Energy 90 (2021), 106552.
[116] H.J. Fan, W. Lee, R. Hauschild, M. Alexe, G. Le Rhun, R. Scholz, A. Dadgar, K. Nielsch, H. Kalt, A. Krost, M. Zacharias, U. Gösele, Template-Assisted Large-Scale Ordered Arrays of ZnO Pillars for Optical and Piezoelectric Applications, Small 2 (2006) 561–568.
[117] Y.J. Hong, S.J. An, H.S. Jung, C.-H. Lee, G.-C. Yi, Position-Controlled Selective Growth of ZnO Nanorods on Si Substrates Using Facet-Controlled GaN Micropatterns, Adv. Mater. 19 (2007) 4416–4419.
[118] W.Z. Wu, X.N. Wen, Z.L. Wang, Taxel-Addressable Matrix of Vertical-Nanowire Piezotronic Transistors for Active and Adaptive Tactile Imaging, Science 340 (2013) 952–957.
[119] D. Yang, Y. Qiu, Q. Jiang, Z. Guo, W. Song, J. Xu, Y. Zong, Q. Feng, X. Sun, Patterned growth of ZnO nanowires on flexible substrates for enhanced performance of flexible piezoelectric nanogenerators, Appl. Phys. Lett. 110 (2017), 063901.
[120] G. Tian, D. Xiong, Y. Su, T. Yang, Y. Gao, C. Yan, W. Deng, L. Jin, H. Zhang, X. Fan, C. Wang, W. Deng, W. Yang, Understanding the Potential Screening Effect through the Discretely Structured ZnO Nanorods Piezo Array, Nano Lett. 20 (2020) 4270–4277.
[121] Y. Zhang, J. Zhai, Z.L. Wang, Piezo-phototronic matrix via a nanowire array, Small 13 (2017) 1702377.
[122] H. Yin, K. Xing, Y. Zhang, D.M.A.S. Dissanayake, Z. Lu, H. Zhao, Z. Zeng, J.-H. Yun, D.-C. Qi, Z. Yin, Periodic nanostructures: preparation, properties and applications, Chem. Soc. Rev. 50 (2021) 6423–6482.
[123] V. Schmidt, J.V. Wittemann, U. Gösele, Growth, Thermodynamics, and Electrical Properties of Silicon Nanowires, Chem. Rev. 110 (2010) 361–388.
[124] Y.-F. Yao, C.-H. Shen, W.-F. Chen, P.-Y. Shih, W.-H. Chou, C.-Y. Su, H.-S. Chen, C.-H. Liao, W.-M. Chang, Y.-W. Kiang, C.C. Yang, Void Structures in Regularly Patterned ZnO Nanorods Grown with the Hydrothermal Method, J. Nanomater. 2014 (2014), 756401.
[125] H. Oh, J. Park, W. Choi, H. Kim, Y. Tchoe, A. Agrawal, G.-C. Yi, Vertical ZnO Nanotube Transistor on a Graphene Film for Flexible Inorganic Electronics, Small 14 (2018) 1800240.
[126] X. Li, R. Liang, J. Tao, Z. Peng, Q. Xu, X. Han, X. Wang, C. Wang, J. Zhu, C. Pan, Z. L. Wang, Flexible Light Emission Diode Arrays Made of Transferred Si Microwires-ZnO Nanofilm with Piezo-Phototronic Effect Enhanced Lighting, ACS Nano 11 (2017) 3883–3889.
[127] X. Han, W. Du, R. Yu, C. Pan, Z.L. Wang, Piezo-Phototronic Enhanced UV Sensing Based on a Nanowire Photodetector Array, Adv. Mater. 27 (2015) 7963–7969.
[128] Y. Peng, M. Que, H.E. Lee, R. Bao, X. Wang, J. Lu, Z. Yuan, X. Li, J. Tao, J. Sun, J. Zhai, K.J. Lee, C. Pan, Achieving high-resolution pressure mapping via flexible GaN/ ZnO nanowire LEDs array by piezo-phototronic effect, Nano Energy 58 (2019) 633–640.
[129] Y.J. Hong, R.K. Saroj, W.I. Park, G.-C. Yi, One-dimensional semiconductor nanostructures grown on two-dimensional nanomaterials for flexible device applications, APL Mater. 9 (2021), 060907.
[130] C. Jiang, Q. Li, N. Sun, J. Huang, S. Bi, R. Ji, Q. Guo, J. Song, High-Dynamic-Range Pressure Mapping Interactions by Dual Piezo-Phototronic Transistor with Piezo-Nanowire Channels and Piezo-OLED Gates, Adv. Funct. Mater. 30 (2020) 2004724.
[131] J.B. Park, M.S. Song, R. Ghosh, R.K. Saroj, Y. Hwang, Y. Tchoe, H. Oh, H. Baek, Y. Lim, B. Kim, S.-W. Kim, G.-C. Yi, Highly sensitive and flexible pressure sensors using position- and dimension-controlled ZnO nanotube arrays grown on graphene films, NPG Asia Mater. 13 (2021) 57.
[132] C. Jiang, D. Tan, N. Sun, J. Huang, R. Ji, Q. Li, S. Bi, Q. Guo, X. Wang, J. Song, 60 nm Pixel-size pressure piezo-memory system as ultrahigh-resolution neuromorphic tactile sensor for in-chip computing, Nano Energy 87 (2021), 106190.
[133] W.G. Hu, C. Zhang, Z.L. Wang, Recent progress in piezotronics and tribotronics, Nanotechnology 30 (2019).
[134] Y. Tchoe, M.S. Song, H. Kim, H. Baek, J.Y. Park, H. Oh, K. Lee, K. Chung, J. K. Hyun, G.-C. Yi, Individually addressable, high-density vertical nanotube Schottky diode crossbar array, Nano Energy 76 (2020), 104955.
[135] R. Bao, C. Wang, L. Dong, R. Yu, K. Zhao, Z.L. Wang, C. Pan, Flexible and Controllable Piezo-Phototronic Pressure Mapping Sensor Matrix by ZnO NW/p-Polymer LED Array, Adv. Funct. Mater. 25 (2015) 2884–2891.
[136] C. Pan, L. Dong, G. Zhu, S. Niu, R. Yu, Q. Yang, Y. Liu, Z.L. Wang, High-resolution electroluminescent imaging of pressure distribution using a piezoelectric nanowire LED array, Nat. Photonics 7 (2013) 752–758.
[137] R. Bao, J. Tao, C. Pan, Z.L. Wang, Piezophototronic effect in nanosensors, Small Sci. 1 (2021) 2000060.
[138] L. Zhu, L. Wang, C. Pan, L. Chen, F. Xue, B. Chen, L. Yang, L. Su, Z.L. Wang, Enhancing the efficiency of silicon-based solar cells by the piezo-phototronic effect, ACS Nano 11 (2017) 1894–1900.
[139] C. Pan, J. Zhai, Z.L. Wang, Piezotronics and Piezo-phototronics of Third Generation Semiconductor Nanowires, Chem. Rev. 119 (2019) 9303–9359.
[140] A. Fraleoni-Morgera, I. Cesini, P. Kumar, C.M. Oddo, Hydrothermally Grown ZnO Nanorods as Promising Materials for Low Cost Electronic Skin, ChemNanoMat 6 (2020) 15–31.
[141] T. Vijayakanth, D.J. Liptrot, E. Gazit, R. Boomishankar, C.R. Bowen, Recent Advances in Organic and Organic–Inorganic Hybrid Materials for Piezoelectric Mechanical Energy Harvesting, Adv. Funct. Mater. 32 (2022) 2109492.
[142] R. Liu, Z.L. Wang, K. Fukuda, T. Someya, Flexible self-charging power sources, Nat. Rev. Mater. 7 (2022) 870–886.

[143] Y. Wang, W. Xie, W. Peng, F. Li, Y. He, Fundamentals and Applications of ZnO-Nanowire-Based Piezotronics and Piezo-Phototronics, Micromachines 14 (2023) 47.
[144] Y. Hu, Z.L. Wang, Recent progress in piezoelectric nanogenerators as a sustainable power source in self-powered systems and active sensors, Nano Energy 14 (2015) 3–14.
[145] F. Narita, Z. Wang, H. Kurita, Z. Li, Y. Shi, Y. Jia, C. Soutis, A Review of Piezoelectric and Magnetostrictive Biosensor Materials for Detection of COVID-19 and Other Viruses, Adv. Mater. 33 (2021) 2005448.
[146] Z.L. Wang, From nanogenerators to piezotronics—A decade-long study of ZnO nanostructures, MRS Bull. 37 (2012) 814–827.
[147] B. Nikoobakht, X. Wang, A. Herzing, J. Shi, Scalable synthesis and device integration of self-registered one-dimensional zinc oxide nanostructures and related materials, Chem. Soc. Rev. 42 (2013) 342–365.
[148] J. Park, R. Ghosh, M.S. Song, Y. Hwang, Y. Tchoe, R.K. Saroj, A. Ali, P. Guha, B. Kim, S.-W. Kim, M. Kim, G.-C. Yi, Individually addressable and flexible pressure sensor matrixes with ZnO nanotube arrays on graphene, NPG Asia Mater. 14 (2022) 40.
[149] S. Stassi, V. Cauda, C. Ottone, A. Chiodoni, C.F. Pirri, G. Canavese, Flexible piezoelectric energy nanogenerator based on ZnO nanotubes hosted in a polycarbonate membrane, Nano Energy 13 (2015) 474–481.
[150] W. Liu, M. Lee, L. Ding, J. Liu, Z.L. Wang, Piezopotential gated nanowire−nanotube hybrid field-effect transistor, Nano Lett. 10 (2010) 3084–3089.
[151] Y. Xi, J. Song, S. Xu, R. Yang, Z. Gao, C. Hu, Z.L. Wang, Growth of ZnO nanotube arrays and nanotube based piezoelectric nanogenerators, J. Mater. Chem. 19 (2009) 9260–9264.
[152] R. Araneo, G. Lovat, P. Burghignoli, C. Falconi, Piezo-Semiconductive Quasi-1D Nanodevices with or without Anti-Symmetry, Adv. Mater. 24 (2012) 4719–4724.
[153] K.Y. Shin, J.S. Lee, J. Jang, Highly sensitive, wearable and wireless pressure sensor using free-standing ZnO nanoneedle/PVDF hybrid thin film for heart rate monitoring, Nano Energy 22 (2016) 95–104.
[154] A. Rinaldi, R. Araneo, S. Celozzi, M. Pea, A. Notargiacomo, The Clash of Mechanical and Electrical Size-Effects in ZnO Nanowires and a Double Power Law Approach to Elastic Strain Engineering of Piezoelectric and Piezotronic Devices, Adv. Mater. 26 (2014) 5976–5985.
[155] C. Periasamy, P. Chakrabarti, Time-dependent degradation of Pt/ZnO nanoneedle rectifying contact based piezoelectric nanogenerator, J. Appl. Phys. 109 (2011), 054306.
[156] Z.L. Wang, R. Yang, J. Zhou, Y. Qin, C. Xu, Y. Hu, S. Xu, Lateral nanowire/nanobelt based nanogenerators, piezotronics and piezo-phototronics, Mater. Sci. Eng.: R: Rep. 70 (2010) 320–329.
[157] H.D. Espinosa, R.A. Bernal, M. Minary-Jolandan, A Review of Mechanical and Electromechanical Properties of Piezoelectric Nanowires, Adv. Mater. 24 (2012) 4656–4675.
[158] J.Y. Huang, H. Zheng, S.X. Mao, Q. Li, G.T. Wang, In Situ Nanomechanics of GaN Nanowires, Nano Lett. 11 (2011) 1618–1622.
[159] X. Li, X. Wang, Q. Xiong, P.C. Eklund, Mechanical Properties of ZnS Nanobelts, Nano Lett. 5 (2005) 1982–1986.
[160] G.R. Yazdi, P.O.Å. Persson, D. Gogova, R. Fornari, L. Hultman, M. Syväjärvi, R. Yakimova, Aligned AlN nanowires by self-organized vapor–solid growth, Nanotechnology 20 (2009), 495304.
[161] C.-C. Röhlig, M. Niebelschütz, K. Brueckner, K. Tonisch, O. Ambacher, V. Cimalla, Elastic properties of nanowires, Phys. Status Solidi (b) 247 (2010) 2557–2570.
[162] C. Du, W. Hu, Z.L. Wang, Recent Progress on Piezotronic and Piezo-Phototronic Effects in III-Group Nitride Devices and Applications, Adv. Eng. Mater. 20 (2018) 1700760.
[163] Z.L. Wang, Piezopotential gated nanowire devices: Piezotronics and piezo-phototronics, Nano Today 5 (2010) 540–552.
[164] X. Wang, Piezoelectric nanogenerators—Harvesting ambient mechanical energy at the nanometer scale, Nano Energy 1 (2012) 13–24.
[165] X. Wang, J. Zhou, J. Song, J. Liu, N. Xu, Z.L. Wang, Piezoelectric Field Effect Transistor and Nanoforce Sensor Based on a Single ZnO Nanowire, Nano Lett. 6 (2006) 2768–2772.
[166] Z.L. Wang, Nanopiezotronics, Adv. Mater. 19 (2007) 889–892.
[167] Y. Zhang, Y. Liu, Z.L. Wang, Fundamental theory of piezotronics, Adv. Mater. 23 (2011) 3004–3013.
[168] Z.L. Wang, The new field of nanopiezotronics, Mater. Today 10 (2007) 20–28.
[169] Y. Gao, Z.L. Wang, Electrostatic Potential in a Bent Piezoelectric Nanowire. The Fundamental Theory of Nanogenerator and Nanopiezotronics, Nano Lett. 7 (2007) 2499–2505.
[170] J. Zhou, Y. Gu, P. Fei, W. Mai, Y. Gao, R. Yang, G. Bao, Z.L. Wang, Flexible Piezotronic Strain Sensor, Nano Lett. 8 (2008) 3035–3040.
[171] G. Hu, H. An, J. Xi, J. Lu, Q. Hua, Z. Peng, A. ZnO, micro/nanowire-based photonic synapse with piezo-phototronic modulation, Nano Energy 89 (2021), 106282.
[172] S. Liu, L. Wang, X. Feng, Z. Wang, Q. Xu, S. Bai, Y. Qin, Z.L. Wang, Ultrasensitive 2D ZnO Piezotronic Transistor Array for High Resolution Tactile Imaging, Adv. Mater. 29 (2017) 1606346.
[173] M. Song, Y. Liu, A. Yu, Y. Zhang, J. Zhai, Z.L. Wang, Flexible Li-doped ZnO piezotronic transistor array for in-plane strain mapping, Nano Energy 55 (2019) 341–347.
[174] L. Chen, F. Xue, X. Li, X. Huang, L. Wang, J. Kou, Z.L. Wang, Strain-Gated Field Effect Transistor of a MoS2–ZnO 2D–1D Hybrid Structure, ACS Nano 10 (2016) 1546–1551.
[175] W. Han, Y. Zhou, Y. Zhang, C.-Y. Chen, L. Lin, X. Wang, S. Wang, Z.L. Wang, Strain-Gated Piezotronic Transistors Based on Vertical Zinc Oxide Nanowires, ACS Nano 6 (2012) 3760–3766.
[176] R. Zhou, G. Hu, R. Yu, C. Pan, Z.L. Wang, Piezotronic effect enhanced detection of flammable/toxic gases by ZnO micro/nanowire sensors, Nano Energy 12 (2015) 588–596.
[177] R. Yu, C. Pan, Z.L. Wang, High performance of ZnO nanowire protein sensors enhanced by the piezotronic effect, Energy Environ. Sci. 6 (2013) 494–499.
[178] X. Chen, J. Shao, H. Tian, X. Li, C. Wang, Y. Luo, S. Li, Scalable Imprinting of Flexible Multiplexed Sensor Arrays with Distributed Piezoelectricity-Enhanced Micropillars for Dynamic Tactile Sensing, Adv. Mater. Technol. 5 (2020) 2000046.
[179] R. Agrawal, H.D. Espinosa, Giant piezoelectric size effects in zinc oxide and gallium nitride nanowires. a first principles investigation, Nano Lett. 11 (2011) 786–790.
[180] H.J. Xiang, J. Yang, J.G. Hou, Q. Zhu, Piezoelectricity in ZnO nanowires: A first-principles study, Appl. Phys. Lett. 89 (2006), 223111.
[181] F. Glas, Critical dimensions for the plastic relaxation of strained axial heterostructures in free-standing nanowires, Phys. Rev. B 74 (2006), 121302.
[182] R. Tao, M. Mouis, G. Ardila, Unveiling the Influence of Surface Fermi Level Pinning on the Piezoelectric Response of Semiconducting Nanowires, Adv. Electron. Mater. 4 (2018) 1700299.
[183] J. Zhang, T. Sun, Y. Chen, L. Liu, H. Zhao, C. Zhang, X. Meng, D. Wang, Z. Hu, H. Zhang, B. Li, S. Niu, Z. Han, L. Ren, Q. Lin, Nanowires in Flexible Sensors: Structure is Becoming a Key in Controlling the Sensing Performance, Adv. Mater. Technol. 7 (2022) 2200163.
[184] Y. Ma, Y. Zhang, S. Cai, Z. Han, X. Liu, F. Wang, Y. Cao, Z. Wang, H. Li, Y. Chen, X. Feng, Flexible Hybrid Electronics for Digital Healthcare, Adv. Mater. 32 (2020) 1902062.
[185] Z. Jiang, M.O.G. Nayeem, K. Fukuda, S. Ding, H. Jin, T. Yokota, D. Inoue, D. Hashizume, T. Someya, Highly Stretchable Metallic Nanowire Networks Reinforced by the Underlying Randomly Distributed Elastic Polymer Nanofibers via Interfacial Adhesion Improvement, Adv. Mater. 31 (2019) 1903446.
[186] T. Yang, D. Xie, Z. Li, H. Zhu, Recent advances in wearable tactile sensors: Materials, sensing mechanisms, and device performance, Mater. Sci. Eng.: R: Rep. 115 (2017) 1–37.
[187] M. Riaz, O. Nur, M. Willander, P. Klason, Buckling of ZnO nanowires under uniaxial compression, Appl. Phys. Lett. 92 (2008), 103118.
[188] C. Cheng, M. Lei, L. Feng, T.L. Wong, K.M. Ho, K.K. Fung, M.M.T. Loy, D. Yu, N. Wang, High-Quality ZnO Nanowire Arrays Directly Fabricated from Photoresists, ACS Nano 3 (2009) 53–58.
[189] D.S. Kim, R. Ji, H.J. Fan, F. Bertram, R. Scholz, A. Dadgar, K. Nielsch, A. Krost, J. Christen, U. Gösele, M. Zacharias, Laser-Interference Lithography Tailored for Highly Symmetrically Arranged ZnO Nanowire Arrays, Small 3 (2007) 76–80.
[190] D. Yuan, R. Guo, Y. Wei, W. Wu, Y. Ding, Z.L. Wang, S. Das, Heteroepitaxial Patterned Growth of Vertically Aligned and Periodically Distributed ZnO Nanowires on GaN Using Laser Interference Ablation, Adv. Funct. Mater. 20 (2010) 3484–3489.
[191] M. Ha, S. Lim, J. Park, D.S. Um, Y. Lee, H. Ko, Bioinspired Interlocked and Hierarchical Design of ZnO Nanowire Arrays for Static and Dynamic Pressure-Sensitive Electronic Skins, Adv. Funct. Mater. 25 (2015) 2841–2849.
[192] M. Parmar, E.A.A. Leon Perez, G. Ardila, E. Saoutieff, E. Pauliac-Vaujour, M. Mouis, A demonstration of the mechanical sensing capability of individually contacted vertical piezoelectric nanowires arranged in matrices, Nano Energy 56 (2019) 859–867.
[193] B. Xiang, P. Wang, X. Zhang, S.A. Dayeh, D.P.R. Aplin, C. Soci, D. Yu, D. Wang, Rational Synthesis of p-Type Zinc Oxide Nanowire Arrays Using Simple Chemical Vapor Deposition, Nano Lett. 7 (2007) 323–328.
[194] X. Chen, X. Yan, Z. Bai, Y. Shen, Z. Wang, X. Dong, X. Duan, Y. Zhang, High-throughput fabrication of large-scale highly ordered ZnO nanorod arrays via three-beam interference lithography, CrystEngComm 15 (2013) 8416–8421.
[195] J.M. Lee, Y.-S. No, S. Kim, H.-G. Park, W.I. Park, Strong interactive growth behaviours in solution-phase synthesis of three-dimensional metal oxide nanostructures, Nat. Commun. 6 (2015) 6325.
[196] Y.J. Hong, H.S. Jung, J. Yoo, Y.-J. Kim, C.-H. Lee, M. Kim, G.-C. Yi, Shape-Controlled Nanoarchitectures Using Nanowalls, Adv. Mater. 21 (2009) 222–226.
[197] H.T. Ng, J. Han, T. Yamada, P. Nguyen, Y.P. Chen, M. Meyyappan, Single Crystal Nanowire Vertical Surround-Gate Field-Effect Transistor, Nano Lett. 4 (2004) 1247–1252.
[198] B. Su, Y. Wu, L. Jiang, The art of aligning one-dimensional (1D) nanostructures, Chem. Soc. Rev. 41 (2012) 7832–7856.
[199] Y. Li, Z. Çelik-Butler, D.P. Butler, An integrated piezoelectric zinc oxide nanowire micro-energy harvester, Nano Energy 26 (2016) 456–465.
[200] X. Han, W. Du, M. Chen, X. Wang, X. Zhang, X. Li, J. Li, Z. Peng, C. Pan, Z. L. Wang, Visualization Recording and Storage of Pressure Distribution through a Smart Matrix Based on the Piezotronic Effect, Adv. Mater. 29 (2017) 1701253.
[201] M. Chen, C. Pan, T. Zhang, X. Li, R. Liang, Z.L. Wang, Tuning Light Emission of a Pressure-Sensitive Silicon/ZnO Nanowires Heterostructure Matrix through Piezo-phototronic Effects, ACS Nano 10 (2016) 6074–6079.
[202] J. Yoo, Y.J. Hong, H.S. Jung, Y.-J. Kim, C.-H. Lee, J. Cho, Y.-J. Doh, L.S. Dang, K. H. Park, G.-C. Yi, Fabrication and Optical Characteristics of Position-Controlled ZnO Nanotubes and ZnO/Zn0.8Mg0.2O Coaxial Nanotube Quantum Structure Arrays, Adv. Funct. Mater. 19 (2009) 1601–1608.
[203] B. Yadian, H. Liu, Y. Wei, J. Wu, S. Zhang, L. Sun, C. Zhao, Q. Liu, R. V. Ramanujan, K. Zhou, C.L. Gan, Y. Huang, Towards Perfectly Ordered Novel ZnO/Si Nano-Heterojunction Arrays, Small 10 (2014) 344–348.

[204] Y. Lin, P. Deng, Y. Nie, Y. Hu, L. Xing, Y. Zhang, X. Xue, Room-temperature self-powered ethanol sensing of a Pd/ZnO nanoarray nanogenerator driven by human finger movement, Nanoscale 6 (2014) 4604–4610.
[205] M. Lee, C.-Y. Chen, S. Wang, S.N. Cha, Y.J. Park, J.M. Kim, L.-J. Chou, Z.L. Wang, A hybrid piezoelectric structure for wearable nanogenerators, Adv. Mater. 24 (2012) 1759–1764.
[206] G. Liu, Y. Tang, A.M. Soomro, P. Shen, S. Lu, Y. Cai, H. Wang, Q. Yang, H. Chen, Y. Shi, C. Lin, F. Xu, F. Xu, Z. Wu, X. Chen, D. Cai, J. Kang, Vertically aligned ZnO nanoarray directly orientated on Cu paper by h-BN monolayer for flexible and transparent piezoelectric nanogenerator, Nano Energy 109 (2023), 108265.
[207] J. Shi, M.B. Starr, X. Wang, Band structure engineering at heterojunction interfaces via the piezotronic effect, Adv. Mater. 24 (2012) 4683–4691.
[208] K.C. Pradel, W. Wu, Y. Ding, Z.L. Wang, Solution-Derived ZnO Homojunction Nanowire Films on Wearable Substrates for Energy Conversion and Self-Powered Gesture Recognition, Nano Lett. 14 (2014) 6897–6905.
[209] S. Lu, Q. Liao, J. Qi, S. Liu, Y. Liu, Q. Liang, G. Zhang, Y. Zhang, The enhanced performance of piezoelectric nanogenerator via suppressing screening effect with Au particles/ZnO nanoarrays Schottky junction, Nano Res. 9 (2016) 372–379.
[210] S. Vishniakou, R. Chen, Y.G. Ro, C.J. Brennan, C. Levy, E.T. Yu, S.A. Dayeh, Improved Performance of Zinc Oxide Thin Film Transistor Pressure Sensors and a Demonstration of a Commercial Chip Compatibility with the New Force Sensing Technology, Adv. Mater. Technol. 3 (2018) 1700279.
[211] M.R. Hasan, S.-H. Baek, K.S. Seong, J.H. Kim, I.-K. Park, Hierarchical ZnO Nanorods on Si Micropillar Arrays for Performance Enhancement of Piezoelectric Nanogenerators, ACS Appl. Mater. Interfaces 7 (2015) 5768–5774.
[212] N. Jalali, P. Woolliams, M. Stewart, P.M. Weaver, M.G. Cain, S. Dunn, J. Briscoe, Improved performance of p–n junction-based ZnO nanogenerators through CuSCN-passivation of ZnO nanorods, J. Mater. Chem. A 2 (2014) 10945–10951.
[213] A.S. Dahiya, F. Morini, S. Boubenia, K. Nadaud, D. Alquier, G. Poulin-Vittrant, Organic/Inorganic Hybrid Stretchable Piezoelectric Nanogenerators for Self-Powered Wearable Electronics, Adv. Mater. Technol. 3 (2018) 1700249.
[214] H.-R. Lim, H.S. Kim, R. Qazi, Y.-T. Kwon, J.-W. Jeong, W.-H. Yeo, Advanced Soft Materials, Sensor Integrations, and Applications of Wearable Flexible Hybrid Electronics in Healthcare, Energy, and Environment, Adv. Mater. 32 (2020) 1901924.
[215] J.I. Sohn, S.N. Cha, B.G. Song, S. Lee, S.M. Kim, J. Ku, H.J. Kim, Y.J. Park, B. L. Choi, Z.L. Wang, J.M. Kim, K. Kim, Engineering of efficiency limiting free carriers and an interfacial energy barrier for an enhancing piezoelectric generation, Energy Environ. Sci. 6 (2013) 97–104.
[216] H. Kum, D. Lee, W. Kong, H. Kim, Y. Park, Y. Kim, Y. Baek, S.-H. Bae, K. Lee, J. Kim, Epitaxial growth and layer-transfer techniques for heterogeneous integration of materials for electronic and photonic devices, Nat. Electron. 2 (2019) 439–450.
[217] H. Kim, C.S. Chang, S. Lee, J. Jiang, J. Jeong, M. Park, Y. Meng, J. Ji, Y. Kwon, X. Sun, W. Kong, H.S. Kum, S.-H. Bae, K. Lee, Y.J. Hong, J. Shi, J. Kim, Remote epitaxy, Nat. Rev. Methods Prim. 2 (2022) 40.
[218] H. Ryu, H. Park, J.-H. Kim, F. Ren, J. Kim, G.-H. Lee, S.J. Pearton, Two-dimensional material templates for van der Waals epitaxy, remote epitaxy, and intercalation growth, Appl. Phys. Rev. 9 (2022), 031305.
[219] Z. Zhang, P. Lin, Q. Liao, Z. Kang, H. Si, Y. Zhang, Graphene-Based Mixed-Dimensional van der Waals Heterostructures for Advanced Optoelectronics, Adv. Mater. 31 (2019) 1806411.
[220] M. Panth, B. Cook, Y. Zhang, D. Ewing, A. Tramble, A. Wilson, J. Wu, High-Performance Strain Sensors Based on Vertically Aligned Piezoelectric Zinc Oxide Nanowire Array/Graphene Nanohybrids, ACS Appl. Nano Mater. 3 (2020) 6711–6718.
[221] D. Choi, M.-Y. Choi, W.M. Choi, H.-J. Shin, H.-K. Park, J.-S. Seo, J. Park, S.-M. Yoon, S.J. Chae, Y.H. Lee, S.-W. Kim, J.-Y. Choi, S.Y. Lee, J.M. Kim, Fully Rollable Transparent Nanogenerators Based on Graphene Electrodes, Adv. Mater. 22 (2010) 2187–2192.
[222] Y. Chen, Y.-Y. Yue, S.-R. Wang, N. Zhang, J. Feng, H.-B. Sun, Graphene as a Transparent and Conductive Electrode for Organic Optoelectronic Devices, Adv. Electron. Mater. 5 (2019) 1900247.
[223] K.S. Kim, Y. Zhao, H. Jang, S.Y. Lee, J.M. Kim, K.S. Kim, J.-H. Ahn, P. Kim, J.-Y. Choi, B.H. Hong, Large-scale pattern growth of graphene films for stretchable transparent electrodes, Nature 457 (2009) 706–710.
[224] Y. Wang, L. Zhu, C. Du, Flexible Difunctional (Pressure and Light) Sensors Based on ZnO Nanowires/Graphene Heterostructures, Adv. Mater. Interfaces 7 (2020) 1901932.
[225] R.K.L. Tan, S.P. Reeves, N. Hashemi, D.G. Thomas, E. Kavak, R. Montazami, N. N. Hashemi, Graphene as a flexible electrode: review of fabrication approaches, J. Mater. Chem. A 5 (2017) 17777–17803.
[226] H. Jang, Y.J. Park, X. Chen, T. Das, M.-S. Kim, J.-H. Ahn, Graphene-based flexible and stretchable electronics, Adv. Mater. 28 (2016) 4184–4202.
[227] J.A. Rogers, T. Someya, Y. Huang, Materials and mechanics for stretchable electronics, Science 327 (2010) 1603–1607.
[228] Y. Geng, J. Xu, M.A. Bin Che Mahzan, P. Lomax, M.M. Saleem, E. Mastropaolo, R. Cheung, Mixed Dimensional ZnO/WSe2 Piezo-gated Transistor with Active Millinewton Force Sensing, ACS Appl. Mater. Interfaces 14 (2022) 49026–49034.
[229] R.K. Joshi, J.J. Schneider, Assembly of one dimensional inorganic nanostructures into functional 2D and 3D architectures. Synthesis, arrangement and functionality, Chem. Soc. Rev. 41 (2012) 5285–5312.
[230] J. Li, R. Bao, J. Tao, Y. Peng, C. Pan, Recent progress in flexible pressure sensor arrays: from design to applications, J. Mater. Chem. C. 6 (2018) 11878–11892.
[231] F. Xu, X. Li, Y. Shi, L. Li, W. Wang, L. He, R. Liu, Recent developments for flexible pressure sensors: a review, Micromachines 9 (2018) 580.
[232] Y. Wan, Y. Wang, C.F. Guo, Recent progresses on flexible tactile sensors, Mater. Today Phys. 1 (2017) 61–73.
[233] B.C.-K. Tee, A. Chortos, R.R. Dunn, G. Schwartz, E. Eason, Z. Bao, Tunable Flexible Pressure Sensors using Microstructured Elastomer Geometries for Intuitive Electronics, Adv. Funct. Mater. 24 (2014) 5427–5434.
[234] Y. Gao, T. Xiao, Q. Li, Y. Chen, X. Qiu, J. Liu, Y. Bian, F. Xuan, Flexible microstructured pressure sensors: design, fabrication and applications, Nanotechnology 33 (2022), 322002.
[235] C.H. Hu, C.H. Liu, L.Z. Chen, Y.C. Peng, S.S. Fan, Resistance-pressure sensitivity and a mechanism study of multiwall carbon nanotube networks/poly (dimethylsiloxane) composites, Appl. Phys. Lett. 93 (2008), 033108.
[236] S. Gong, W. Schwalb, Y. Wang, Y. Chen, Y. Tang, J. Si, B. Shirinzadeh, W. Cheng, A wearable and highly sensitive pressure sensor with ultrathin gold nanowires, Nature, Communications 5 (2014) 3132.
[237] B.C.K. Tee, C. Wang, R. Allen, Z. Bao, An electrically and mechanically self-healing composite with pressure- and flexion-sensitive properties for electronic skin applications, Nat. Nanotechnol. 7 (2012) 825.
[238] C.-Y. Chen, J.-H. Huang, J. Song, Y. Zhou, L. Lin, P.-C. Huang, Y. Zhang, C.-P. Liu, J.-H. He, Z.L. Wang, Anisotropic Outputs of a Nanogenerator from Oblique-Aligned ZnO Nanowire Arrays, ACS Nano 5 (2011) 6707–6713.
[239] N.-J. Ku, G. Liu, C.-H. Wang, K. Gupta, W.-S. Liao, D. Ban, C.-P. Liu, Optimal geometrical design of inertial vibration DC piezoelectric nanogenerators based on obliquely aligned InN nanowire arrays, Nanoscale 9 (2017) 14039–14046.
[240] G. Zhu, R. Yang, S. Wang, Z.L. Wang, Flexible High-Output Nanogenerator Based on Lateral ZnO Nanowire Array, Nano Lett. 10 (2010) 3151–3155.
[241] S. Xu, Y. Qin, C. Xu, Y. Wei, R. Yang, Z.L. Wang, Self-powered nanowire devices, Nat. Nanotechnol. 5 (2010) 366–373.
[242] R. Yang, Y. Qin, L. Dai, Z.L. Wang, Power generation with laterally packaged piezoelectric fine wires, Nat. Nanotechnol. 4 (2009) 34–39.
[243] S. Jeong, M.W. Kim, Y.-R. Jo, Y.-C. Leem, W.-K. Hong, B.-J. Kim, S.-J. Park, High-performance photoresponsivity and electrical transport of laterally-grown ZnO/ZnS core/shell nanowires by the piezotronic and piezo-phototronic effect, Nano Energy 30 (2016) 208–216.
[244] M.-H. Seo, J.-Y. Yoo, M.-S. Jo, J.-B. Yoon, Geometrically Structured Nanomaterials for Nanosensors, NEMS, and Nanosieves, Adv. Mater. 32 (2020) 1907082.
[245] Y. Wang, X. Guo, L.H. Li, J. Zhang, G.K. Li, A. Zavabeti, Y. Li, Enhanced Piezoelectric Properties Enabled by Engineered Low-Dimensional Nanomaterials, ACS Appl. Nano Mater. 5 (2022) 12126–12142.
[246] M.-P. Lu, M.-Y. Lu, L.-J. Chen, p-Type ZnO nanowires: From synthesis to nanoenergy, Nano Energy 1 (2012) 247–258.
[247] Z. Huo, X. Wang, Y. Zhang, B. Wan, W. Wu, J. Xi, Z. Yang, G. Hu, X. Li, C. Pan, High-performance Sb-doped p-ZnO NW films for self-powered piezoelectric strain sensors, Nano Energy 73 (2020), 104744.
[248] Y.-T. Chang, J.-Y. Chen, T.-P. Yang, C.-W. Huang, C.-H. Chiu, P.-H. Yeh, W.-W. Wu, Excellent piezoelectric and electrical properties of lithium-doped ZnO nanowires for nanogenerator applications, Nano Energy 8 (2014) 291–296.
[249] S.-H. Shin, Y.-H. Kim, M.H. Lee, J.-Y. Jung, J.H. Seol, J. Nah, Lithium-doped zinc oxide nanowires–polymer composite for high performance flexible piezoelectric nanogenerator, ACS Nano 8 (2014) 10844–10850.
[250] A.R. Chowdhury, A.M. Abdullah, I. Hussain, J. Lopez, D. Cantu, S.K. Gupta, Y. Mao, S. Danti, M.J. Uddin, Lithium doped zinc oxide based flexible piezoelectric-triboelectric hybrid nanogenerator, Nano Energy 61 (2019) 327–336.
[251] K. Batra, N. Sinha, B. Kumar, Tb-doped ZnO:PDMS based flexible nanogenerator with enhanced piezoelectric output performance by optimizing nanofiller concentration, Ceram. Int. 46 (2020) 24120–24128.
[252] Y. Zhang, C. Liu, J. Liu, J. Xiong, J. Liu, K. Zhang, Y. Liu, M. Peng, A. Yu, A. Zhang, Y. Zhang, Z. Wang, J. Zhai, Z.L. Wang, Lattice Strain Induced Remarkable Enhancement in Piezoelectric Performance of ZnO-Based Flexible Nanogenerators, ACS Appl. Mater. Interfaces 8 (2016) 1381–1387.
[253] N. Mufti, H. Ali, A.S.P. Dewi, H. Pujiarti, Sunaryono, Aripriharta, Enhanced piezoelectric nanogenerator performance with AZO/NiO heterojunction, Mater. Sci. Energy Technol. 6 (2023) 81–88.
[254] M.-S. Suen, Y.-C. Lin, R. Chen, A flexible multifunctional tactile sensor using interlocked zinc oxide nanorod arrays for artificial electronic skin, Sens. Actuators A: Phys. 269 (2018) 574–584.
[255] Y.-L. Chu, S.-J. Young, H.-C. Chang, S. Arya, Y.-H. Liu, T.-T. Chu, Enhanced Nanogenerator Performances of 1-D Al-Doped ZnO Nanorod Arrays through Ultrasonic Wave Systems, ACS Appl. Electron. Mater. (2023).
[256] D. Zhu, T. Hu, Y. Zhao, W. Zang, L. Xing, X. Xue, High-performance self-powered/active humidity sensing of Fe-doped ZnO nanoarray nanogenerator, Sens. Actuators B: Chem. 213 (2015) 382–389.
[257] Y. Sun, S. Shen, W. Deng, G. Tian, D. Xiong, H. Zhang, T. Yang, S. Wang, J. Chen, W. Yang, Suppressing piezoelectric screening effect at atomic scale for enhanced piezoelectricity, Nano Energy 105 (2023), 108024.
[258] V.F. Rivera, F. Auras, P. Motto, S. Stassi, G. Canavese, E. Celasco, T. Bein, B. Onida, V. Cauda, Length-Dependent Charge Generation from Vertical Arrays of High-Aspect-Ratio ZnO Nanowires, Chem. – A Eur. J. 19 (2013) 14665–14674.
[259] R. Hinchet, S. Lee, G. Ardila, L. Montès, M. Mouis, Z.L. Wang, Performance Optimization of Vertical Nanowire-based Piezoelectric Nanogenerators, Adv. Funct. Mater. 24 (2014) 971–977.
[260] M. Riaz, J. Song, O. Nur, Z.L. Wang, M. Willander, Study of the Piezoelectric Power Generation of ZnO Nanowire Arrays Grown by Different Methods, Adv. Funct. Mater. 21 (2011) 628–633.

[261] C. Pan, R. Yu, S. Niu, G. Zhu, Z.L. Wang, Piezotronic Effect on the Sensitivity and Signal Level of Schottky Contacted Proactive Micro/Nanowire Nanosensors, ACS Nano 7 (2013) 1803–1810.
[262] K. Jenkins, V. Nguyen, R. Zhu, R. Yang, Piezotronic Effect: An Emerging Mechanism for Sensing Applications, Sensors 15 (2015) 22914–22940.
[263] J. Meng, Z. Li, Schottky-Contacted Nanowire Sensors, Adv. Mater. 32 (2020) 2000130.
[264] J. Zhou, P. Fei, Y. Gu, W. Mai, Y. Gao, R. Yang, G. Bao, Z.L. Wang, Piezoelectric-Potential-Controlled Polarity-Reversible Schottky Diodes and Switches of ZnO Wires, Nano Lett. 8 (2008) 3973–3977.
[265] T.-Y. Wei, P.-H. Yeh, S.-Y. Lu, Z.L. Wang, Gigantic enhancement in sensitivity using schottky contacted nanowire nanosensor, J. Am. Chem. Soc. 131 (2009) 17690–17695.
[266] Y. Hu, J. Zhou, P.-H. Yeh, Z. Li, T.-Y. Wei, Z.L. Wang, Supersensitive, Fast-Response Nanowire Sensors by Using Schottky Contacts, Adv. Mater. 22 (2010) 3327–3332.
[267] R. Yu, C. Pan, J. Chen, G. Zhu, Z.L. Wang, Enhanced Performance of a ZnO Nanowire-Based Self-Powered Glucose Sensor by Piezotronic Effect, Adv. Funct. Mater. 23 (2013) 5868–5874.
[268] S.M.A.Z. Shawon, A.X. Sun, V.S. Vega, B.D. Chowdhury, P. Tran, Z.D. Carballo, J. A. Tolentino, J. Li, M.S. Rafaqut, S. Danti, M.J. Uddin, Piezo-tribo dual effect hybrid nanogenerators for health monitoring, Nano Energy 82 (2021), 105691.
[269] B.-C. Kang, S.-J. Park, T.-J. Ha, Wearable Pressure/Touch Sensors Based on Hybrid Dielectric Composites of Zinc Oxide Nanowires/Poly(dimethylsiloxane) and Flexible Electrodes of Immobilized Carbon Nanotube Random Networks, ACS Appl. Mater. Interfaces 13 (2021) 42014–42023.
[270] C. Yoon, S. Ippili, V. Jella, A.M. Thomas, J.-S. Jung, Y. Han, T.-Y. Yang, S.-G. Yoon, G. Yoon, Synergistic contribution of flexoelectricity and piezoelectricity towards a stretchable robust nanogenerator for wearable electronics, Nano Energy 91 (2022), 106691.
[271] J. Zhang, Y. He, C. Boyer, K. Kalantar-Zadeh, S. Peng, D. Chu, C.H. Wang, Recent developments of hybrid piezo–triboelectric nanogenerators for flexible sensors and energy harvesters, Nanoscale Adv. 3 (2021) 5465–5486.
[272] Y. Geng, M.A. Bin Che Mahzan, K. Jeronimo, M.M. Saleem, P. Lomax, E. Mastropaolo, R. Cheung, Integration of ZnO nanorods with MOS capacitor for self-powered force sensors and nanogenerators, Nanotechnology 32 (2021), 455502.
[273] Y. Yang, H. Zhang, G. Zhu, S. Lee, Z.-H. Lin, Z.L. Wang, Flexible Hybrid Energy Cell for Simultaneously Harvesting Thermal, Mechanical, and Solar Energies, ACS Nano 7 (2013) 785–790.
[274] A. Mahmud, A.A. Khan, S. Islam, P. Voss, D. Ban, Integration of organic/inorganic nanostructured materials in a hybrid nanogenerator enables efficacious energy harvesting via mutual performance enhancement, Nano Energy 58 (2019) 112–120.
[275] H. Ryu, H.-J. Yoon, S.-W. Kim, Hybrid energy harvesters: toward sustainable energy harvesting, Adv. Mater. 31 (2019) 1802898.
[276] S. Yan, Z. Zheng, S. Rai, M.A. Retana, M. Bhatt, L. Malkinski, W. Zhou, Coupling Effect of Magnetic Fields on Piezotronic and Piezophototronic Properties of ZnO and ZnO/Co3O4 Core/Shell Nanowire Arrays, ACS Appl. Nano Mater. 1 (2018) 6897–6903.
[277] J. Liu, Z. Liang, J. Chen, S. Wang, C. Pan, S. Qiao, A. New, Strategy of Coupling Pyroelectric and Piezoelectric Effects for Photoresponse Enhancement of a Cu(In, Ga)Se2 Heterojunction Photodetector, Adv. Funct. Mater. 32 (2022) 2208658.
[278] Y. Zhang, L. Yang, Y. Zhang, Z. Ding, M. Wu, Y. Zhou, C. Diao, H. Zheng, X. Wang, Z.L. Wang, Enhanced Photovoltaic Performances of La-Doped Bismuth Ferrite/Zinc Oxide Heterojunction by Coupling Piezo-Phototronic Effect and Ferroelectricity, ACS Nano 14 (2020) 10723–10732.
[279] A.J. Lopez Garcia, M. Mouis, V. Consonni, G. Ardila, Dimensional Roadmap for Maximizing the Piezoelectrical Response of ZnO Nanowire-Based Transducers: Impact of Growth Method, Nanomaterials 11 (2021) 941.
[280] J.-J. Wu, S.-C. Liu, Low-Temperature Growth of Well-Aligned ZnO Nanorods by Chemical Vapor Deposition, Adv. Mater. 14 (2002) 215–218.
[281] Wang Wang, Song, P. Li, J.H. Ryou, R.D. Dupuis, C.J. Summers, Z.L. Wang, Growth of Uniformly Aligned ZnO Nanowire Heterojunction Arrays on GaN, AlN, and Al0.5Ga0.5N Substrates, J. Am. Chem. Soc. 127 (2005) 7920–7923.
[282] D.F. Liu, Y.J. Xiang, X.C. Wu, Z.X. Zhang, L.F. Liu, L. Song, X.W. Zhao, S.D. Luo, W.J. Ma, J. Shen, W.Y. Zhou, G. Wang, C.Y. Wang, S.S. Xie, Periodic ZnO Nanorod Arrays Defined by Polystyrene Microsphere Self-Assembled Monolayers, Nano Lett. 6 (2006) 2375–2378.
[283] X.X. Zhang, D. Zhao, M. Gao, H.B. Dong, W.Y. Zhou, S.S. Xie, Site-specific multi-stage CVD of large-scale arrays of ultrafine ZnO nanorods, Nanotechnology 22 (2011), 135603.
[284] M. Malekzadeh, M.T. Swihart, Vapor-phase production of nanomaterials, Chem. Soc. Rev. 50 (2021) 7132–7249.
[285] H.J. Fan, W. Lee, R. Scholz, A. Dadgar, A. Krost, K. Nielsch, M. Zacharias, Arrays of vertically aligned and hexagonally arranged ZnO nanowires: a new template-directed approach, Nanotechnology 16 (2005) 913.
[286] M.H. Huang, S. Mao, H. Feick, H. Yan, Y. Wu, H. Kind, E. Weber, R. Russo, P. Yang, Room-Temperature Ultraviolet Nanowire Nanolasers, Science 292 (2001) 1897–1899.
[287] D. Alameri, L.E. Ocola, I. Kuljanshvili, Controlled Selective CVD Growth of ZnO Nanowires Enabled by Mask-Free Fabrication Approach using Aqueous Fe Catalytic Inks, Adv. Mater. Interfaces 4 (2017) 1700950.
[288] B. Kumar, K.Y. Lee, H.-K. Park, S.J. Chae, Y.H. Lee, S.-W. Kim, Controlled Growth of Semiconducting Nanowire, Nanowall, and Hybrid Nanostructures on Graphene for Piezoelectric Nanogenerators, ACS Nano 5 (2011) 4197–4204.
[289] H. Oh, Y.J. Hong, K.-S. Kim, S. Yoon, H. Baek, S.-H. Kang, Y.-K. Kwon, M. Kim, G.-C. Yi, Architectured van der Waals epitaxy of ZnO nanostructures on hexagonal BN, NPG Asia, Materials 6 (2014) e145-e145.
[290] C.-H. Lee, Y.-J. Kim, Y.J. Hong, S.-R. Jeon, S. Bae, B.H. Hong, G.-C. Yi, Flexible Inorganic Nanostructure Light-Emitting Diodes Fabricated on Graphene Films, Adv. Mater. 23 (2011) 4614–4619.
[291] W.I. Park, D.H. Kim, S.-W. Jung, G.-C. Yi, Metalorganic vapor-phase epitaxial growth of vertically well-aligned ZnO nanorods, Appl. Phys. Lett. 80 (2002) 4232–4234.
[292] M.H. Huang, Y. Wu, H. Feick, N. Tran, E. Weber, P. Yang, Catalytic Growth of Zinc Oxide Nanowires by Vapor Transport, Adv. Mater. 13 (2001) 113–116.
[293] W.I. Park, G.-C. Yi, M. Kim, S.J. Pennycook, ZnO Nanoneedles Grown Vertically on Si Substrates by Non-Catalytic Vapor-Phase Epitaxy, Adv. Mater. 14 (2002) 1841–1843.
[294] J. Jo, H. Yoo, S.-I. Park, J.B. Park, S. Yoon, M. Kim, G.-C. Yi, High-Resolution Observation of Nucleation and Growth Behavior of Nanomaterials Using a Graphene Template, Adv. Mater. 26 (2014) 2011–2015.
[295] Y.-J. Kim, H. Yoo, C.-H. Lee, J.B. Park, H. Baek, M. Kim, G.-C. Yi, Position- and Morphology-Controlled ZnO Nanostructures Grown on Graphene Layers, Adv. Mater. 24 (2012) 5565–5569.
[296] K. Chung, C.-H. Lee, G.-C. Yi, Transferable GaN Layers Grown on ZnO-Coated Graphene Layers for Optoelectronic Devices, Science 330 (2010) 655–657.
[297] W.I. Park, C.-H. Lee, J.H. Chae, D.H. Lee, G.-C. Yi, Ultrafine ZnO nanowire electronic device arrays fabricated by selective metal–organic chemical vapor deposition, Small 5 (2009) 181–184.
[298] J.B. Park, H. Oh, J. Park, N.J. Kim, H. Yoon, G.C. Yi, Scalable ZnO nanotube arrays grown on CVD-graphene films, Apl. Mater. 4 (2016).
[299] S.B. Kim, W.W. Lee, J. Yi, W.I. Park, J.-S. Kim, W.T. Nichols, Simple, Large-Scale Patterning of Hydrophobic ZnO Nanorod Arrays, ACS Appl. Mater. Interfaces 4 (2012) 3910–3915.
[300] S. Xu, Y. Wei, M. Kirkham, J. Liu, W. Mai, D. Davidovic, R.L. Snyder, Z.L. Wang, Patterned Growth of Vertically Aligned ZnO Nanowire Arrays on Inorganic Substrates at Low Temperature without Catalyst, J. Am. Chem. Soc. 130 (2008) 14958–14959.
[301] Y. Wei, W. Wu, R. Guo, D. Yuan, S. Das, Z.L. Wang, Wafer-Scale High-Throughput Ordered Growth of Vertically Aligned ZnO Nanowire Arrays, Nano Lett. 10 (2010) 3414–3419.
[302] J. Volk, R. Erdélyi, Morphology and crystallinity control of wet chemically grown ZnO nanorods, Turk. J. Phys. 38 (2014) 391–398.
[303] H. Liu, H. Peng, K. Li, L. Lu, J. Deng, Y. Liu, C. Qiu, G. Li, X. Cheng, Transfer Printing of Solution-Processed 3D ZnO Nanostructures with Ultra-High Yield for Flexible Metasurface Color Filter, Adv. Mater. Interfaces 9 (2022) 2101963.
[304] S. Xu, N. Adiga, S. Ba, T. Dasgupta, C.F.J. Wu, Z.L. Wang, Optimizing and Improving the Growth Quality of ZnO Nanowire Arrays Guided by Statistical Design of Experiments, ACS Nano 3 (2009) 1803–1812.
[305] S. Zhang, Y. Shen, H. Fang, S. Xu, J. Song, Z.L. Wang, Growth and replication of ordered ZnO nanowire arrays on general flexible substrates, J. Mater. Chem. 20 (2010) 10606–10610.
[306] D.-b Zhang, S.-j Wang, K. Cheng, S.-x Dai, B.-b Hu, X. Han, Q. Shi, Z.-l Du, Controllable Fabrication of Patterned ZnO Nanorod Arrays: Investigations into the Impacts on Their Morphology, ACS Appl. Mater. Interfaces 4 (2012) 2969–2977.
[307] Z. Huang, Y. Huang, N. Xu, J. Chen, J. She, S. Deng, Band-to-Band Tunneling-Dominated Thermo-Enhanced Field Electron Emission from p-Si/ZnO Nanoemitters, ACS Appl. Mater. Interfaces 10 (2018) 21518–21526.
[308] S. Xu, Y. Ding, Y. Wei, H. Fang, Y. Shen, A.K. Sood, D.L. Polla, Z.L. Wang, Patterned Growth of Horizontal ZnO Nanowire Arrays, J. Am. Chem. Soc. 131 (2009) 6670–6671.
[309] Y. Qin, R. Yang, Z.L. Wang, Growth of horizonatal ZnO nanowire arrays on any substrate, J. Phys. Chem. C. 112 (2008) 18734–18736.
[310] K. Sun, H. Zhang, L. Hu, D. Yu, S. Qiao, J. Sun, J. Bian, X. Chen, L. Zhang, Q. Fu, Z. Zhao, Growth of ultralong ZnO microwire and its application in isolatable and flexible piezoelectric strain sensor, Phys. Status Solidi (a) 207 (2010) 488–492.
[311] V. Consonni, E. Sarigiannidou, E. Appert, A. Bocheux, S. Guillemin, F. Donatini, I.-C. Robin, J. Kioseoglou, F. Robaut, Selective Area Growth of Well-Ordered ZnO Nanowire Arrays with Controllable Polarity, ACS Nano 8 (2014) 4761–4770.
[312] A.M. Lord, V. Consonni, T. Cossuet, F. Donatini, S.P. Wilks, Schottky Contacts on Polarity-Controlled Vertical ZnO Nanorods, ACS Appl. Mater. Interfaces 12 (2020) 13217–13228.
[313] T. Cossuet, E. Appert, J.-L. Thomassin, V. Consonni, Polarity-Dependent Growth Rates of Selective Area Grown ZnO Nanorods by Chemical Bath Deposition, Langmuir 33 (2017) 6269–6279.
[314] H. Liu, D. Quan, K. Li, Y. Zheng, F. Lou, S. Liu, Y. Liu, A.K. Srivastava, G. Li, C. Qiu, Z. Liu, X. Cheng, Dielectric Metasurface from Solution-Phase Epitaxy of ZnO Nanorods for Subtractive Color Filter Application, Adv. Opt. Mater. 9 (2021) 2001670.
[315] M. de la Mata, R.R. Zamani, S. Martí-Sánchez, M. Eickhoff, Q. Xiong, A. Fontcuberta i Morral, P. Caroff, J. Arbiol, The Role of Polarity in Nonplanar Semiconductor Nanostructures, Nano Lett. 19 (2019) 3396–3408.
[316] J. Zúñiga-Pérez, V. Consonni, L. Lymperakis, X. Kong, A. Trampert, S. Fernández-Garrido, O. Brandt, H. Renevier, S. Keller, K. Hestroffer, M.R. Wagner, J. S. Reparaz, F. Akyol, S. Rajan, S. Rennesson, T. Palacios, G. Feuillet, Polarity in GaN and ZnO: Theory, measurement, growth, and devices, Appl. Phys. Rev. 3 (2016), 041303.
[317] Y. Leprince-Wang, S. Bouchaib, T. Brouri, M. Capo-Chichi, K. Laurent, J. Leopoldes, S. Tusseau-Nenez, L. Lei, Y. Chen, Fabrication of ZnO micro- and

nano-structures by electrodeposition using nanoporous and lithography defined templates, Mater. Sci. Eng. B 170 (2010) 107–112.
[318] S.K. Sharma, A. Rammohan, A. Sharma, Templated one step electrodeposition of high aspect ratio n-type ZnO nanowire arrays, J. Colloid Interface Sci. 344 (2010) 1–9.
[319] H.C.S. Gómez, F.A. Cataño, H. Altamirano, A. Burgos, Template assisted electrodeposition of highly oriented ZnO nanowire arrays and their integration in dye sensitized solar cells, J. Chil. Chem. Soc. 59 (2014) 2447–2450.
[320] G. Nagaraju, Y.H. Ko, J.S. Yu, Effect of diameter and height of electrochemically-deposited ZnO nanorod arrays on the performance of piezoelectric nanogenerators, Mater. Chem. Phys. 149–150 (2015) 393–399.
[321] M. Skompska, K. Zarębska, Electrodeposition of ZnO nanorod arrays on transparent conducting substrates–a review, Electrochim. Acta 127 (2014) 467–488.
[322] C. Liu, W. Zhang, J. Sun, J. Wen, Q. Yang, H. Cuo, X. Ma, M. Zhang, Piezoelectric nanogenerator based on a flexible carbon-fiber/ZnO–ZnSe bilayer structure wire, Appl. Surf. Sci. 322 (2014) 95–100.
[323] F.L. Boughey, T. Davies, A. Datta, R.A. Whiter, S.-L. Sahonta, S. Kar-Narayan, Vertically aligned zinc oxide nanowires electrodeposited within porous polycarbonate templates for vibrational energy harvesting, Nanotechnology 27 (2016) 28LT02.
[324] X. Zheng, K. Zhang, Y. Sun, S. Jin, Y. Li, H. Yu, H. Qin, Y. Ding, Tunable ZnO/NiO heterojunction interface for supercapacitors electrodes by piezoelectric modulation, J. Alloy. Compd. 851 (2021), 156902.
[325] N.S. Ayati, E. Akbari, S.P. Marashi, S. Saramad, Template Assisted Growth of Zinc Oxide-Based Nanowires and Piezoelectric Properties, Adv. Mater. Res. 829 (2014) 757–761.
[326] C.V. Manzano, L. Philippe, A. Serrà, Recent progress in the electrochemical deposition of ZnO nanowires: synthesis approaches and applications, Crit. Rev. Solid State Mater. Sci. 47 (2022) 772–805.
[327] H. Chik, J. Liang, S.G. Cloutier, N. Kouklin, J.M. Xu, Periodic array of uniform ZnO nanorods by second-order self-assembly, Appl. Phys. Lett. 84 (2004) 3376–3378.
[328] H. Zeng, X. Xu, Y. Bando, U.K. Gautam, T. Zhai, X. Fang, B. Liu, D. Golberg, Template Deformation-Tailored ZnO Nanorod/Nanowire Arrays: Full Growth Control and Optimization of Field-Emission, Adv. Funct. Mater. 19 (2009) 3165–3172.
[329] C. Li, G. Hong, P. Wang, D. Yu, L. Qi, Wet Chemical Approaches to Patterned Arrays of Well-Aligned ZnO Nanopillars Assisted by Monolayer Colloidal Crystals, Chem. Mater. 21 (2009) 891–897.
[330] J.J. Dong, X.W. Zhang, Z.G. Yin, S.G. Zhang, J.X. Wang, H.R. Tan, Y. Gao, F.T. Si, H.L. Gao, Controllable Growth of Highly Ordered ZnO Nanorod Arrays via Inverted Self-Assembled Monolayer Template, ACS Appl. Mater. Interfaces 3 (2011) 4388–4395.
[331] X. Xu, Q. Yang, N. Wattanatorn, C. Zhao, N. Chiang, S.J. Jonas, P.S. Weiss, Multiple-Patterning Nanosphere Lithography for Fabricating Periodic Three-Dimensional Hierarchical Nanostructures, ACS Nano 11 (2017) 10384–10391.
[332] J. Jeong, D.K. Jin, J. Cha, B.K. Kang, Q. Wang, J. Choi, S.W. Lee, V. Y. Mikhailovskii, V. Neplokh, N. Amador-Mendez, M. Tchernycheva, W.S. Yang, J. Yoo, M.J. Kim, S. Hong, Y.J. Hong, Selective-Area Remote Epitaxy of ZnO Microrods Using Multilayer–Monolayer-Patterned Graphene for Transferable and Flexible Device Fabrications, ACS Appl. Nano Mater. 3 (2020) 8920–8930.
[333] Y.-J. Kim, C.-H. Lee, Y.J. Hong, G.-C. Yi, S.S. Kim, H. Cheong, Controlled selective growth of ZnO nanorod and microrod arrays on Si substrates by a wet chemical method, Appl. Phys. Lett. 89 (2006), 163128.
[334] R. Bao, C. Wang, Z. Peng, C. Ma, L. Dong, C. Pan, Light-Emission Enhancement in a Flexible and Size-Controllable ZnO Nanowire/Organic Light-Emitting Diode Array by the Piezotronic Effect, ACS Photonics 4 (2017) 1344–1349.
[335] X. Li, M. Chen, R. Yu, T. Zhang, D. Song, R. Liang, Q. Zhang, S. Cheng, L. Dong, A. Pan, Z.L. Wang, J. Zhu, C. Pan, Enhancing Light Emission of ZnO-Nanofilm/Si-Micropillar Heterostructure Arrays by Piezo-Phototronic Effect, Adv. Mater. 27 (2015) 4447–4453.
[336] L. Zhang, Y. Fu, L. Xing, B. Liu, Y. Zhang, X. Xue, A self-powered flexible vision electronic-skin for image recognition based on a pixel-addressable matrix of piezophototronic ZnO nanowire arrays, J. Mater. Chem. C. 5 (2017) 6005–6013.
[337] J. Yeo, S. Hong, M. Wanit, H.W. Kang, D. Lee, C.P. Grigoropoulos, H.J. Sung, S. H. Ko, Rapid, One-Step, Digital Selective Growth of ZnO Nanowires on 3D Structures Using Laser Induced Hydrothermal Growth, Adv. Funct. Mater. 23 (2013) 3316–3323.
[338] J. Yeo, S. Hong, G. Kim, H. Lee, Y.D. Suh, I. Park, C.P. Grigoropoulos, S.H. Ko, Laser-Induced Hydrothermal Growth of Heterogeneous Metal-Oxide Nanowire on Flexible Substrate by Laser Absorption Layer Design, ACS Nano 9 (2015) 6059–6068.
[339] W. Liu, J. Wang, X. Xu, C. Zhao, X. Xu, P.S. Weiss, Single-Step Dual-Layer Photolithography for Tunable and Scalable Nanopatterning, ACS Nano 15 (2021) 12180–12188.
[340] Q. Ahsanulhaq, J.-H. Kim, Y.-B. Hahn, Controlled selective growth of ZnO nanorod arrays and their field emission properties, Nanotechnology 18 (2007), 485307.
[341] S.A. Morin, F.F. Amos, S. Jin, Biomimetic Assembly of Zinc Oxide Nanorods onto Flexible Polymers, J. Am. Chem. Soc. 129 (2007) 13776–13777.
[342] Han X., Zhang Y., Huo Z., Wang X., Hu G., Xu Z., Lu H., Lu Q., Sun X., Qiu L., Yan P., Pan C., A Two-Terminal Optoelectronic Synapses Array Based on the ZnO/Al2O3/CdS Heterojunction with Strain-Modulated Synaptic Weight, Advanced Electronic Materials n/a 2201068.
[343] X. Chen, X. Yan, Z. Bai, P. Lin, Y. Shen, X. Zheng, Y. Feng, Y. Zhang, Facile fabrication of large-scale patterned ZnO nanorod arrays with tunable arrangement, period and morphology, CrystEngComm 15 (2013) 8022–8028.
[344] P. Lin, X. Yan, F. Li, J. Du, J. Meng, Y. Zhang, Polarity-Dependent Piezotronic Effect and Controllable Transport Modulation of ZnO with Multifield Coupled Interface Engineering, Adv. Mater. Interfaces 4 (2017) 1600842.
[345] K.S. Kim, H. Jeong, M.S. Jeong, G.Y. Jung, Polymer-Templated Hydrothermal Growth of Vertically Aligned Single-Crystal ZnO Nanorods and Morphological Transformations Using Structural Polarity, Adv. Funct. Mater. 20 (2010) 3055–3063.
[346] B.P. Nabar, Z. Celik-Butler, D.P. Butler, Self-Powered Tactile Pressure Sensors Using Ordered Crystalline ZnO Nanorods on Flexible Substrates Toward Robotic Skin and Garments, IEEE Sens. J. 15 (2015) 63–70.
[347] M.-H. Jung, H. Lee, Selective patterning of ZnO nanorods on silicon substrates using nanoimprint lithography, Nanoscale Res. Lett. 6 (2011) 159.
[348] J.W.P. Hsu, Z.R. Tian, N.C. Simmons, C.M. Matzke, J.A. Voigt, J. Liu, Directed Spatial Organization of Zinc Oxide Nanorods, Nano Lett. 5 (2005) 83–86.
[349] H.-H. Park, X. Zhang, K.W. Lee, K.H. Kim, S.H. Jung, D.S. Park, Y.S. Choi, H.-B. Shin, H.K. Sung, K.H. Park, H.K. Kang, H.-H. Park, C.K. Ko, Position-controlled hydrothermal growth of ZnO nanorods on arbitrary substrates with a patterned seed layer via ultraviolet-assisted nanoimprint lithography, CrystEngComm 15 (2013) 3463–3469.
[350] D. Sakai, K. Nagashima, H. Yoshida, M. Kanai, Y. He, G. Zhang, X. Zhao, T. Takahashi, T. Yasui, T. Hosomi, Y. Uchida, S. Takeda, Y. Baba, T. Yanagida, Substantial Narrowing on the Width of "Concentration Window" of Hydrothermal ZnO Nanowires via Ammonia Addition, Sci. Rep. 9 (2019) 14160.
[351] O. Černohorský, J. Grym, H. Faitová, N. Bašinová, Š. Kučerová, R. Yatskiv, J. Veselý, Modeling of Solution Growth of ZnO Hexagonal Nanorod Arrays in Batch Reactors, Cryst. Growth Des. 20 (2020) 3347–3357.
[352] K. Diao, J. Zhang, M. Zhou, Y. Tang, S. Wang, X. Cui, Highly controllable and reproducible ZnO nanowire arrays growth with focused ion beam and low-temperature hydrothermal method, Appl. Surf. Sci. 317 (2014) 220–225.
[353] C. Ottone, K. Bejtka, A. Chiodoni, V. Farías, I. Roppolo, G. Canavese, S. Stassi, V. Cauda, Comprehensive study of the templating effect on the ZnO nanostructure formation within porous hard membranes, N. J. Chem. 38 (2014) 2058–2065.
[354] Y.H. Chen, Y.M. Shen, S.C. Wang, J.L. Huang, Fabrication of one-dimensional ZnO nanotube and nanowire arrays with an anodic alumina oxide template via electrochemical deposition, Thin Solid Films B 570 (2014) 303–309.
[355] C. Ou, P. Sanchez-Jimenez, A. Datta, F.L. Boughey, R.A. Whiter, SahontaS, S. Kar-Narayan, Template-assisted hydrothermal growth of aligned zinc oxide nanowires for piezoelectric energy harvesting applications, ACS Appl. Mater. Interfaces (2016).
[356] H.-N. Barad, H. Kwon, M. Alarcón-Correa, P. Fischer, Large Area Patterning of Nanoparticles and Nanostructures: Current Status and Future Prospects, ACS Nano 15 (2021) 5861–5875.
[357] Z. Wang, D. Cao, R. Xu, S. Qu, Z. Wang, Y. Lei, Realizing ordered arrays of nanostructures: A versatile platform for converting and storing energy efficiently, Nano Energy 19 (2016) 328–362.
[358] M.Y. Choi, D. Choi, M.J. Jin, I. Kim, S.H. Kim, J.Y. Choi, S.Y. Lee, J.M. Kim, S. W. Kim, Mechanically Powered Transparent Flexible Charge-Generating Nanodevices with Piezoelectric ZnO Nanorods, Adv. Mater. 21 (2009) 2185.
[359] Z. Liu, J. Xu, D. Chen, G. Shen, Flexible electronics based on inorganic nanowires, Chem. Soc. Rev. 44 (2015) 161–192.
[360] Nie Z., Kwak J.W., Han M., Rogers J.A., Mechanically Active Materials and Devices for Bio-Interfaced Pressure Sensors – A Review, Advanced Materials n/a 2205609.
[361] S. Xu, Y. Shen, Y. Ding, Z.L. Wang, Growth and transfer of monolithic horizontal ZnO nanowire superstructures onto flexible substrates, Adv. Funct. Mater. 20 (2010) 1493–1497.
[362] T. Shiosaki, T. Yamamoto, A. Kawabata, R.S. Muller, R.M. White, Fabrication and characterization of ZnO piezoelectric films for sensor devices, Int. Electron Devices Meet. 1979 (1979) 151–154.
[363] W. Zhang, R. Zhu, V. Nguyen, R. Yang, Highly sensitive and flexible strain sensors based on vertical zinc oxide nanowire arrays, Sens. Actuators A: Phys. 205 (2014) 164–169.
[364] Q. Yu, R. Ge, J. Wen, T. Du, J. Zhai, S. Liu, L. Wang, Y. Qin, Highly sensitive strain sensors based on piezotronic tunneling junction, Nat. Commun. 13 (2022) 778.
[365] N. Liu, G. Fang, W. Zeng, H. Long, L. Yuan, X. Zhao, Novel ZnO Nanorod Flexible Strain Sensor and Strain Driving Transistor with an Ultrahigh 107 Scale "On"–"Off" Ratio Fabricated by a Single-Step Hydrothermal Reaction, J. Phys. Chem. C. 115 (2011) 570–575.
[366] C.-T. Lee, Y.-S. Chiu, Piezoelectric ZnO-nanorod-structured pressure sensors using GaN-based field-effect-transistor, Appl. Phys. Lett. 106 (2015), 073502.
[367] F. Wang, J. Jiang, Q. Liu, Y. Zhang, J. Wang, S. Wang, L. Han, H. Liu, Y. Sang, Piezopotential gated two-dimensional InSe field-effect transistor for designing a pressure sensor based on piezotronic effect, Nano Energy 70 (2020), 104457.
[368] H. Li, N. Liu, X. Zhang, J. Su, L. Li, Y. Gao, Z.L. Wang, Piezotronic and piezo-phototronic logic computations using Au decorated ZnO microwires, Nano Energy 27 (2016) 587–594.
[369] W. Wu, Y. Wei, Z.L. Wang, Strain-Gated Piezotronic Logic Nanodevices, Adv. Mater. 22 (2010) 4711–4715.
[370] Z.L. Wang, Piezotronic Logic Circuits and Operations, in: Z.L. Wang (Ed.), Piezotronics and Piezo-Phototronics. Berlin, Heidelberg, Springer, Berlin Heidelberg, 2012, pp. 97–109.

[371] N. Liu, G. Fang, W. Zeng, H. Zhou, H. Long, X. Zou, Y. Liu, X. Zhao, High performance ZnO nanorod strain driving transistor based complementary metal-oxide-semiconductor logic gates, Appl. Phys. Lett. 97 (2010).
[372] J. Wang, S. Xu, C. Zhang, A. Yin, M. Sun, H. Yang, C. Hu, H. Liu, Field effect transistor-based tactile sensors: From sensor configurations to advanced applications, InfoMat 5 (2023), e12376.
[373] Z.L. Wang, J. Song, Piezoelectric Nanogenerators Based on Zinc Oxide Nanowire Arrays, Science 312 (2006) 242–246.
[374] D. Hu, M. Yao, Y. Fan, C. Ma, M. Fan, M. Liu, Strategies to achieve high performance piezoelectric nanogenerators, Nano Energy 55 (2019) 288–304.
[375] A. Anand, M.C. Bhatnagar, Role of vertically aligned and randomly placed zinc oxide (ZnO) nanorods in PVDF matrix: Used for energy harvesting, Mater. Today Energy 13 (2019) 293–301.
[376] Y. Sun, Y. Zheng, R. Wang, J. Fan, Y. Liu, Direct-current piezoelectric nanogenerator based on two-layer zinc oxide nanorod arrays with equal c-axis orientation for energy harvesting, Chem. Eng. J. 426 (2021), 131262.
[377] M. Lee, J. Bae, J. Lee, C.-S. Lee, S. Hong, Z.L. Wang, Self-powered environmental sensor system driven by nanogenerators, Energy Environ. Sci. 4 (2011) 3359–3363.
[378] C. Pan, Y. Fang, H. Wu, M. Ahmad, Z. Luo, Q. Li, J. Xie, X. Yan, L. Wu, Z.L. Wang, J. Zhu, Generating Electricity from Biofluid with a Nanowire-Based Biofuel Cell for Self-Powered Nanodevices, Adv. Mater. 22 (2010) 5388–5392.
[379] S.N. Cha, J.-S. Seo, S.M. Kim, H.J. Kim, Y.J. Park, S.-W. Kim, J.M. Kim, Sound-Driven Piezoelectric Nanowire-Based Nanogenerators, Adv. Mater. 22 (2010) 4726–4730.
[380] W. Deng, L. Jin, Y. Chen, W. Chu, B. Zhang, H. Sun, D. Xiong, Z. Lv, M. Zhu, W. Yang, An enhanced low-frequency vibration ZnO nanorod-based tuning fork piezoelectric nanogenerator, Nanoscale 10 (2018) 843–847.
[381] N. Cui, W. Wu, Y. Zhao, S. Bai, L. Meng, Y. Qin, Z.L. Wang, Magnetic force driven nanogenerators as a noncontact energy harvester and sensor, Nano Lett. 12 (2012) 3701–3705.
[382] N. Gogurla, B. Roy, S. Kim, Self-powered artificial skin made of engineered silk protein hydrogel, Nano Energy 77 (2020), 105242.
[383] Y. Qin, X. Wang, Z.L. Wang, Erratum: Microfibre–nanowire hybrid structure for energy scavenging, Nature 457 (2009) 340.
[384] Z. Li, G. Zhu, R. Yang, A.C. Wang, Z.L. Wang, Muscle-driven in vivo nanogenerator, Adv. Mater. 22 (2010) 2534–2537.
[385] R. Yang, Y. Qin, C. Li, G. Zhu, Z.L. Wang, Converting biomechanical energy into electricity by a muscle-movement-driven nanogenerator, Nano Lett. 9 (2009) 1201–1205.
[386] Y. Fu, W. Zang, P. Wang, L. Xing, X. Xue, Y. Zhang, Portable room-temperature self-powered/active H2 sensor driven by human motion through piezoelectric screening effect, Nano Energy 8 (2014) 34–43.
[387] Q. Zheng, B. Shi, Z. Li, Z.L. Wang, Recent progress on piezoelectric and triboelectric energy harvesters in biomedical systems, Adv. Sci. 4 (2017) 1700029.
[388] X. Xiao, L. Yuan, J. Zhong, T. Ding, Y. Liu, Z. Cai, Y. Rong, H. Han, J. Zhou, Z. L. Wang, High-Strain Sensors Based on ZnO Nanowire/Polystyrene Hybridized Flexible Films, Adv. Mater. 23 (2011) 5440–5444.
[389] Z. Zhao, Y. Dai, S.X. Dou, J. Liang, Flexible nanogenerators for wearable electronic applications based on piezoelectric materials, Mater. Today Energy 20 (2021), 100690.
[390] F. Ali, W. Raza, X. Li, H. Gul, K.-H. Kim, Piezoelectric energy harvesters for biomedical applications, Nano Energy 57 (2019) 879–902.
[391] S. Maiti, S.K. Karan, J.K. Kim, B.B. Khatua, Nature Driven Bio-Piezoelectric/Triboelectric Nanogenerator as Next-Generation Green Energy Harvester for Smart and Pollution Free Society, Adv. Energy Mater. 9 (2019) 1803027.
[392] W.F. Chen, X. Yan, Progress in achieving high-performance piezoresistive and capacitive flexible pressure sensors: A review, J. Mater. Sci. Technol. 43 (2020) 175–188.
[393] H. Oh, G.-C. Yi, M. Yip, S.A. Dayeh, Scalable tactile sensor arrays on flexible substrates with high spatiotemporal resolution enabling slip and grip for closed-loop robotics, Sci. Adv. 6 (2020) eabd7795.
[394] T. Yokota, K. Fukuda, T. Someya, Recent Progress of Flexible Image Sensors for Biomedical Applications, Adv. Mater. 33 (2021) 2004416.
[395] J.H. Lee, J.S. Heo, Y.-J. Kim, J. Eom, H.J. Jung, J.-W. Kim, I. Kim, H.-H. Park, H. S. Mo, Y.-H. Kim, S.K. Park, A Behavior-Learned Cross-Reactive Sensor Matrix for Intelligent Skin Perception, Adv. Mater. 32 (2020) 2000969.
[396] W. Zhong, C. Liu, Q. Liu, L. Piao, H. Jiang, W. Wang, K. Liu, M. Li, G. Sun, D. Wang, Ultrasensitive Wearable Pressure Sensors Assembled by Surface-Patterned Polyolefin Elastomer Nanofiber Membrane Interpenetrated with Silver Nanowires, ACS Appl. Mater. Interfaces 10 (2018) 42706–42714.
[397] X.-Z. Jiang, Y.-J. Sun, Z. Fan, T.-Y. Zhang, Integrated Flexible, Waterproof, Transparent, and Self-Powered Tactile Sensing Panel, ACS Nano 10 (2016) 7696–7704.
[398] J.C. Yang, J.-O. Kim, J. Oh, S.Y. Kwon, J.Y. Sim, D.W. Kim, H.B. Choi, S. Park, Microstructured Porous Pyramid-Based Ultrahigh Sensitive Pressure Sensor Insensitive to Strain and Temperature, ACS Appl. Mater. Interfaces 11 (2019) 19472–19480.
[399] J. Tao, R. Bao, X. Wang, Y. Peng, J. Li, S. Fu, C. Pan, Z.L. Wang, Self-Powered Tactile Sensor Array Systems Based on the Triboelectric Effect, Adv. Funct. Mater. 29 (2019) 1806379.
[400] W. Deng, L. Jin, B. Zhang, Y. Chen, L. Mao, H. Zhang, W. Yang, A flexible field-limited ordered ZnO nanorod-based self-powered tactile sensor array for electronic skin, Nanoscale 8 (2016) 16302–16306.
[401] L. Sun, N. Sun, T. Li, C. Jiang, Light Emission Enhancement of a ZnO/TAZ Heterostructure Piezo-OLED by Means of a Piezo-Phototronic Effect, ChemistrySelect 7 (2022), e202104353.
[402] N. Liu, R. Wang, S. Gao, R. Zhang, F. Fan, Y. Ma, X. Luo, D. Ding, W. Wu, High-Performance Piezo-Electrocatalytic Sensing of Ascorbic Acid with Nanostructured Wurtzite Zinc Oxide, Adv. Mater. 33 (2021) 2105697.
[403] S.C. Mukhopadhyay, Wearable Sensors for Human Activity Monitoring: A Review, IEEE Sens. J. 15 (2015) 1321–1330.
[404] K.S. Srikanth, A. Wazeer, P. Mathiyalagan, S. Vidya, K. Rajput, H.S. Kushwaha, 25 - Piezoelectric properties of ZnO, in: K. Awasthi (Ed.), Nanostructured Zinc Oxide, Elsevier, 2021, pp. 717–736.
[405] Advanced Materials n/a 2204964
[406] S. Lee, S.-H. Bae, L. Lin, Y. Yang, C. Park, S.-W. Kim, S.N. Cha, H. Kim, Y.J. Park, Z.L. Wang, Super-Flexible Nanogenerator for Energy Harvesting from Gentle Wind and as an Active Deformation Sensor, Adv. Funct. Mater. 23 (2013) 2445–2449.
[407] S. Lee, R. Hinchet, Y. Lee, Y. Yang, Z.-H. Lin, G. Ardila, L. Montès, M. Mouis, Z. L. Wang, Ultrathin Nanogenerators as Self-Powered/Active Skin Sensors for Tracking Eye Ball Motion, Adv. Funct. Mater. 24 (2014) 1163–1168.
[408] S.H. Bhang, W.S. Jang, J. Han, J.-K. Yoon, W.-G. La, E. Lee, Y.S. Kim, J.-Y. Shin, T.-J. Lee, H.K. Baik, B.-S. Kim, Zinc Oxide Nanorod-Based Piezoelectric Dermal Patch for Wound Healing, Adv. Funct. Mater. 27 (2017) 1603497.
[409] H. Teymourian, A. Barfidokht, J. Wang, Electrochemical glucose sensors in diabetes management: an updated review (2010–2020), Chem. Soc. Rev. 49 (2020) 7671–7709.
[410] W. Han, H. He, L. Zhang, C. Dong, H. Zeng, Y. Dai, L. Xing, Y. Zhang, X. Xue, A. Self-Powered, Wearable Noninvasive Electronic-Skin for Perspiration Analysis Based on Piezo-Biosensing Unit Matrix of Enzyme/ZnO Nanoarrays, ACS Appl. Mater. Interfaces 9 (2017) 29526–29537.
[411] X. Xue, Z. Qu, Y. Fu, B. Yu, L. Xing, Y. Zhang, Self-powered electronic-skin for detecting glucose level in body fluid basing on piezo-enzymatic-reaction coupling process, Nano Energy 26 (2016) 148–156.
[412] G. Yang, Y. Tang, T. Lin, T. Zhong, Y. Fan, Y. Zhang, L. Xing, X. Xue, Y. Zhan, A self-powered closed-loop brain-machine-interface system for real-time detecting and rapidly adjusting blood glucose concentration, Nano Energy 93 (2022), 106817.
[413] W. Zhang, L. Zhang, H. Gao, W. Yang, S. Wang, L. Xing, X. Xue, Self-Powered Implantable Skin-Like Glucometer for Real-Time Detection of Blood Glucose Level In Vivo, Nano-Micro Lett. 10 (2018) 32.
[414] J. Li, Z. Shen, Y. Cao, X. Tu, C. Zhao, Y. Liu, Z. Wen, Artificial synapses enabled neuromorphic computing: From blueprints to reality, Nano Energy 103 (2022), 107744.
[415] H. Han, H. Yu, H. Wei, J. Gong, W. Xu, Recent progress in three-terminal artificial synapses: from device to system, Small 15 (2019) 1900695.
[416] X. Liao, W. Song, X. Zhang, H. Jin, S. Liu, Y. Wang, A.V.-Y. Thean, Y. Zheng, An artificial peripheral neural system based on highly stretchable and integrated multifunctional sensors, Adv. Funct. Mater. 31 (2021) 2101107.
[417] B. Saravanakumar, S. Soyoon, S.-J. Kim, Self-Powered pH Sensor Based on a Flexible Organic–Inorganic Hybrid Composite Nanogenerator, ACS Appl. Mater. Interfaces 6 (2014) 13716–13723.
[418] W. Zhang, H. Guan, T. Zhong, T. Zhao, L. Xing, X. Xue, Wearable Battery-Free Perspiration Analyzing Sites Based on Sweat Flowing on ZnO Nanoarrays, Nano-Micro Lett. 12 (2020) 105.
[419] W. Yang, W. Han, H. Gao, L. Zhang, S. Wang, L. Xing, Y. Zhang, X. Xue, Self-powered implantable electronic-skin for in situ analysis of urea/uric-acid in body fluids and the potential applications in real-time kidney-disease diagnosis, Nanoscale 10 (2018) 2099–2107.
[420] X. Chang, S. Sun, S. Sun, T. Liu, X. Xiong, Y. Lei, L. Dong, Y. Yin, ZnO nanorods/carbon black-based flexible strain sensor for detecting human motions, J. Alloy. Compd. 738 (2018) 111–117.
[421] T. Lee, W. Lee, S.-W. Kim, J.J. Kim, B.-S. Kim, Flexible Textile Strain Wireless Sensor Functionalized with Hybrid Carbon Nanomaterials Supported ZnO Nanowires with Controlled Aspect Ratio, Adv. Funct. Mater. 26 (2016) 6206–6214.
[422] H. He, Y. Fu, W. Zang, Q. Wang, L. Xing, Y. Zhang, X. Xue, A flexible self-powered T-ZnO/PVDF/fabric electronic-skin with multi-functions of tactile-perception, atmosphere-detection and self-clean, Nano Energy 31 (2017) 37–48.
[423] W. Deng, T. Yang, L. Jin, C. Yan, H. Huang, X. Chu, Z. Wang, D. Xiong, G. Tian, Y. Gao, H. Zhang, W. Yang, Cowpea-structured PVDF/ZnO nanofibers based flexible self-powered piezoelectric bending motion sensor towards remote control of gestures, Nano Energy 55 (2019) 516–525.
[424] Y.-K. Fuh, H.-C. Ho, Highly flexible self-powered sensors based on printed circuit board technology for human motion detection and gesture recognition, Nanotechnology 27 (2016), 095401.
[425] F. Xue, L. Zhang, W. Tang, C. Zhang, W. Du, Z.L. Wang, Piezotronic Effect on ZnO Nanowire Film Based Temperature Sensor, ACS Appl. Mater. Interfaces 6 (2014) 5955–5961.
[426] D. Zhu, Y. Fu, W. Zang, Y. Zhao, L. Xing, X. Xue, Piezo/active humidity sensing of CeO2/ZnO and SnO2/ZnO nanoarray nanogenerators with high response and large detecting range, Sens. Actuators B: Chem. 205 (2014) 12–19.
[427] G. Hu, R. Zhou, R. Yu, L. Dong, C. Pan, Z.L. Wang, Piezotronic effect enhanced Schottky-contact ZnO micro/nanowire humidity sensors, Nano Res. 7 (2014) 1083–1091.
[428] T. Yang, H. Pan, G. Tian, B. Zhang, D. Xiong, Y. Gao, C. Yan, X. Chu, N. Chen, S. Zhong, L. Zhang, W. Deng, W. Yang, Hierarchically structured PVDF/ZnO core-

shell nanofibers for self-powered physiological monitoring electronics, Nano Energy 72 (2020), 104706.
[429] F. Lan, Y. Chen, J. Zhu, Q. Lu, C. Jiang, S. Hao, X. Cao, N. Wang, Z.L. Wang, Piezotronically enhanced detection of protein kinases at ZnO micro/nanowire heterojunctions, Nano Energy 69 (2020), 104330.
[430] S. Niu, Y. Hu, X. Wen, Y. Zhou, F. Zhang, L. Lin, S. Wang, Z.L. Wang, Enhanced Performance of Flexible ZnO Nanowire Based Room-Temperature Oxygen Sensors by Piezotronic Effect, Adv. Mater. 25 (2013) 3701–3706.
[431] E.S. Nour, A. Bondarevs, P. Huss, M. Sandberg, S. Gong, M. Willander, O. Nur, Low-Frequency Self-Powered Footstep Sensor Based on ZnO Nanowires on Paper Substrate, Nanoscale Res. Lett. 11 (2016) 156.
[432] L. Lin, Y. Hu, C. Xu, Y. Zhang, R. Zhang, X. Wen, Z. Lin Wang, Transparent flexible nanogenerator as self-powered sensor for transportation monitoring, Nano Energy 2 (2013) 75–81.
[433] Y. Fu, Y. Nie, Y. Zhao, P. Wang, L. Xing, Y. Zhang, X. Xue, Detecting Liquefied Petroleum Gas (LPG) at Room Temperature Using ZnSnO3/ZnO Nanowire Piezo-Nanogenerator as Self-Powered Gas Sensor, ACS Appl. Mater. Interfaces 7 (2015) 10482–10490.
[434] D. Ju, H. Xu, Z. Qiu, J. Guo, J. Zhang, B. Cao, Highly sensitive and selective triethylamine-sensing properties of nanosheets directly grown on ceramic tube by forming NiO/ZnO PN heterojunction, Sens. Actuators B: Chem. 200 (2014) 288–296.
[435] X. Xue, Y. Nie, B. He, L. Xing, Y. Zhang, Z.L. Wang, Surface free-carrier screening effect on the output of a ZnO nanowire nanogenerator and its potential as a self-powered active gas sensor, Nanotechnology 24 (2013), 225501.
[436] Z. Qu, Y. Fu, B. Yu, P. Deng, L. Xing, X. Xue, High and fast H2S response of NiO/ZnO nanowire nanogenerator as a self-powered gas sensor, Sens. Actuators B: Chem. 222 (2016) 78–86.
[437] Y. Hu, Y. Zhang, C. Xu, L. Lin, R.L. Snyder, Z.L. Wang, Self-powered system with wireless data transmission, Nano Lett. 11 (2011) 2572–2577.
[438] Z. Zhang, Q. Liao, X. Yan, Z.L. Wang, W. Wang, X. Sun, P. Lin, Y. Huang, Y. Zhang, Functional nanogenerators as vibration sensors enhanced by piezotronic effects, Nano Res. 7 (2014) 190–198.
[439] Y. Hu, C. Xu, Y. Zhang, L. Lin, R.L. Snyder, Z.L. Wang, A. Nanogenerator, for Energy Harvesting from a Rotating Tire and its Application as a Self-Powered Pressure/Speed Sensor, Adv. Mater. 23 (2011) 4068–4071.
[440] L. Pan, S. Sun, Y. Chen, P. Wang, J. Wang, X. Zhang, J.-J. Zou, Z.L. Wang, Advances in Piezo-Phototronic Effect Enhanced Photocatalysis and Photoelectrocatalysis, Adv. Energy Mater. 10 (2020) 2000214.
[441] Y. Wen, J. Chen, X. Gao, H. Che, P. Wang, B. Liu, Y. Ao, Piezo-enhanced photocatalytic performance of ZnO nanorod array for pollutants degradation in dynamic water: Insight into the effect of velocity and inner flow field, Nano Energy 101 (2022), 107614.
[442] S. Bi, Q. Li, Z. He, Q. Guo, K. Asare-Yeboah, Y. Liu, C. Jiang, Highly enhanced performance of integrated piezo photo-transistor with dual inverted OLED gate and nanowire array channel, Nano Energy 66 (2019), 104101.
[443] W. Wu, Z.L. Wang, Piezotronic Nanowire-Based Resistive Switches As Programmable Electromechanical Memories, Nano Lett. 11 (2011) 2779–2785.
[444] Z. Huo, Y. Zhang, X. Han, W. Wu, W. Yang, X. Wang, M. Zhou, C. Pan, Piezo-phototronic effect enhanced performance of a p-ZnO NW based UV–Vis–NIR photodetector, Nano Energy 86 (2021), 106090.
[445] Z. Zhang, Q. Liao, Y. Yu, X. Wang, Y. Zhang, Enhanced photoresponse of ZnO nanorods-based self-powered photodetector by piezotronic interface engineering, Nano Energy 9 (2014) 237–244.
[446] B. Yin, H. Zhang, Y. Qiu, Y. Luo, Y. Zhao, L. Hu, Piezo-phototronic effect enhanced self-powered and broadband photodetectors based on Si/ZnO/CdO three-component heterojunctions, Nano Energy 40 (2017) 440–446.
[447] X. Zhang, J. Zhang, B. Leng, J. Li, Z. Ma, W. Yang, F. Liu, B. Liu, Enhanced Performances of PVK/ZnO Nanorods/Graphene Heterostructure UV Photodetector via Piezo-Phototronic Interface Engineering, Adv. Mater. Interfaces 6 (2019) 1901365.
[448] X. Zhao, Q. Li, L. Xu, Z. Zhang, Z. Kang, Q. Liao, Y. Zhang, Interface Engineering in 1D ZnO-Based Heterostructures for Photoelectrical Devices, Adv. Funct. Mater. 32 (2022) 2106887.
[449] Y. Yan, X. Ma, T.M. Nguyen, S.-H. Ha, H. Ahn, D. Aben, K. Kim, J.-M. Kim, J.-W. Oh, D.-M. Shin, Y.-H. Hwang, Quadrant-electroded nanogenerators for decoupling piezoelectricity and flexoelectricity in the electromechanical outputs in flexible devices, Nano Energy 104 (2022), 107909.
[450] C. Chen, S. Zhao, C. Pan, Y. Zi, F. Wang, C. Yang, Z.L. Wang, A method for quantitatively separating the piezoelectric component from the as-received "Piezoelectric" signal, Nat. Commun. 13 (2022) 1391.
[451] A. Šutka, P.C. Sherrell, N.A. Shepelin, L. Lapčinskis, K. Mālnieks, A.V. Ellis, Measuring Piezoelectric Output—Fact or Friction? Adv. Mater. 32 (2020) 2002979.
[452] D. Wang, Y. Zhang, X. Lu, Z. Ma, C. Xie, Z. Zheng, Chemical formation of soft metal electrodes for flexible and wearable electronics, Chem. Soc. Rev. 47 (2018) 4611–4641.
[453] M.-P. Lu, J. Song, M.-Y. Lu, M.-T. Chen, Y. Gao, L.-J. Chen, Z.L. Wang, Piezoelectric Nanogenerator Using p-Type ZnO Nanowire Arrays, Nano Lett. 9 (2009) 1223–1227.
[454] D. Choi, M.-Y. Choi, H.-J. Shin, S.-M. Yoon, J.-S. Seo, J.-Y. Choi, S.Y. Lee, J. M. Kim, S.-W. Kim, Nanoscale Networked Single-Walled Carbon-Nanotube Electrodes for Transparent Flexible Nanogenerators, J. Phys. Chem. C. 114 (2010) 1379–1384.
[455] M.-Y. Choi, D. Choi, M.-J. Jin, I. Kim, S.-H. Kim, J.-Y. Choi, S.Y. Lee, J.M. Kim, S.-W. Kim, Mechanically powered transparent flexible charge-generating nanodevices with piezoelectric ZnO nanorods, Adv. Mater. 21 (2009) 2185–2189.
[456] Y. Peng, J. Lu, X. Wang, W. Ma, M. Que, Q. Chen, F. Li, X. Liu, W. Gao, C. Pan, Self-powered high-performance flexible GaN/ZnO heterostructure UV photodetectors with piezo-phototronic effect enhanced photoresponse, Nano Energy 94 (2022), 106945.
[457] Z. Zhang, Y. Chen, J. Guo, ZnO nanorods patterned-textile using a novel hydrothermal method for sandwich structured-piezoelectric nanogenerator for human energy harvesting, Phys. E: Low. -Dimens. Syst. Nanostruct. 105 (2019) 212–218.
[458] V. Quang Dang, D.-I. Kim, L. Thai Duy, B.-Y. Kim, B.-U. Hwang, M. Jang, K.-S. Shin, S.-W. Kim, N.-E. Lee, Piezoelectric coupling in a field-effect transistor with a nanohybrid channel of ZnO nanorods grown vertically on graphene, Nanoscale 6 (2014) 15144–15150.
[459] M.S. Al-Ruqeishi, T. Mohiuddin, B. Al-Habsi, F. Al-Ruqeishi, A. Al-Fahdi, A. Al-Khusaibi, Piezoelectric nanogenerator based on ZnO nanorods, Arab. J. Chem. 12 (2019) 5173–5179.
[460] C.-L. Hsu, K.-C. Chen, Improving Piezoelectric Nanogenerator Comprises ZnO Nanowires by Bending the Flexible PET Substrate at Low Vibration Frequency, J. Phys. Chem. C. 116 (2012) 9351–9355.
[461] S. Liu, Q. Liao, S. Lu, Z. Zhang, G. Zhang, Y. Zhang, Strain Modulation in Graphene/ZnO Nanorod Film Schottky Junction for Enhanced Photosensing Performance, Adv. Funct. Mater. 26 (2016) 1347–1353.
[462] D. Tamvakos, S. Lepadatu, V.-A. Antohe, A. Tamvakos, P.M. Weaver, L. Piraux, M. G. Cain, D. Pullini, Piezoelectric properties of template-free electrochemically grown ZnO nanorod arrays, Appl. Surf. Sci. 356 (2015) 1214–1220.
[463] M. Seifikar, B.P. Christian, J. Volk, J. Radó, I.E. Lukács, R. Dauksevicius, R. Gaidys, V. Lebedev, A. Viana, E.P. O'Reilly, Direct observation of spontaneous polarization induced electron charge transfer in stressed ZnO nanorods, Nano Energy 43 (2018) 376–382.
[464] B. Liu, Q. Liao, X. Zhang, J. Du, Y. Ou, J. Xiao, Z. Kang, Z. Zhang, Y. Zhang, Strain-Engineered van der Waals Interfaces of Mixed-Dimensional Heterostructure Arrays, ACS Nano 13 (2019) 9057–9066.
[465] J. Volk, T. Nagata, R. Erdélyi, I. Bársony, A.L. Tóth, I.E. Lukács, Z. Czigány, H. Tomimoto, Y. Shingaya, T. Chikyow, Highly Uniform Epitaxial ZnO Nanorod Arrays for Nanopiezotronics, Nanoscale Res. Lett. 4 (2009) 699.
[466] A. Bouvet-Marchand, A. Graillot, J. Volk, R. Dauksevicius, C. Sturm, M. Grundmann, E. Saoutieff, A. Viana, B. Christian, V. Lebedev, J. Radó, I.E., N.Q. K. Lukács, D. Grosso, C. Loubat, Design of UV-crosslinked polymeric thin layers for encapsulation of piezoelectric ZnO nanowires for pressure-based fingerprint sensors, J. Mater. Chem. C. 6 (2018) 605–613.
[467] E. Saoutieff, M. Allain, Y.R. Nowicki-Bringuier, A. Viana, E. Pauliac-Vaujour, Integration of Piezoelectric Nanowires Matrix onto a Microelectronics Chip, Procedia Eng. 168 (2016) 1638–1641.
[468] B. Christian, J. Volk, I.E. Lukàcs, E. Sautieff, C. Sturm, A. Graillot, R. Dauksevicius, E. O'Reilly, O. Ambacher, V. Lebedev, Piezo-force and Vibration Analysis of ZnO Nanowire Arrays for Sensor Application, Procedia Eng. 168 (2016) 1192–1195.
[469] D. Jiang, B. Shi, H. Ouyang, Y. Fan, Z.L. Wang, Z. Li, Emerging Implantable Energy Harvesters and Self-Powered Implantable Medical Electronics, ACS Nano 14 (2020) 6436–6448.
[470] R. Wang, S. Liu, C.R. Liu, W. Wu, Data-driven learning of process−property−performance relation in laser-induced aqueous manufacturing and integration of ZnO piezoelectric nanogenerator for self-powered nanosensors, Nano Energy 83 (2021), 105820.
[471] L. Hu, T. Zhong, Z. Long, S. Liang, L. Xing, X. Xue, A self-powered sound-driven humidity sensor for wearable intelligent dehydration monitoring system, Nanotechnology 34 (2023), 195501.
[472] T.I. Lee, W.S. Jang, E. Lee, Y.S. Kim, Z.L. Wang, H.K. Baik, J.M. Myoung, Ultrathin self-powered artificial skin, Energy Environ. Sci. 7 (2014) 3994–3999.
[473] S. Azimi, A. Golabchi, A. Nekookar, S. Rabbani, M.H. Amiri, K. Asadi, M. M. Abolhasani, Self-powered cardiac pacemaker by piezoelectric polymer nanogenerator implant, Nano Energy 83 (2021), 105781.
[474] Y. Fu, Y. Zhao, P. Wang, L. Xing, X. Xue, High response and selectivity of a Cu–ZnO nanowire nanogenerator as a self-powered/active H2S sensor, Phys. Chem. Chem. Phys. 17 (2015) 2121–2126.
[475] W. Zang, Y. Nie, D. Zhu, P. Deng, L. Xing, X. Xue, Core–Shell In2O3/ZnO Nanoarray Nanogenerator as a Self-Powered Active Gas Sensor with High H2S Sensitivity and Selectivity at Room Temperature, J. Phys. Chem. C. 118 (2014) 9209–9216.
[476] D. Zhu, Y. Fu, W. Zang, Y. Zhao, L. Xing, X. Xue, Room-temperature self-powered ethanol sensor based on the piezo-surface coupling effect of heterostructured α-Fe2O3/ZnO nanowires, Mater. Lett. 166 (2016) 288–291.
[477] L. Lin, Q. Jing, Y. Zhang, Y. Hu, S. Wang, Y. Bando, R.P.S. Han, Z.L. Wang, An elastic-spring-substrated nanogenerator as an active sensor for self-powered balance, Energy Environ. Sci. 6 (2013) 1164–1169.
[478] S. Vishniakou, B.W. Lewis, X. Niu, A. Kargar, K. Sun, M. Kalajian, N. Park, M. Yang, Y. Jing, P. Brochu, Z. Sun, C. Li, T. Nguyen, Q. Pei, D. Wang, Tactile Feedback Display with Spatial and Temporal Resolutions, Sci. Rep. 3 (2013) 2521.
[479] T. Cao, L. Luo, Y. Huang, B. Ye, J. She, S. Deng, J. Chen, N. Xu, Integrated ZnO Nano-Electron-Emitter with Self-Modulated Parasitic Tunneling Field Effect Transistor at the Surface of the p-Si/ZnO Junction, Sci. Rep. 6 (2016) 33983.